INVESTIGATING GROUNDWATER INPUTS TO MISSISSIPPI RIVER DELTAIC WETLANDS USING SPATIAL AND TEMPORAL RESPONSES OF THE GEOCHEMICAL TRACER, ^{222}Rn

Jihyuk Kim

A thesis submitted to the faculty at the University of North Carolina at Chapel Hill in partial fulfillment of the requirements for the degree of Master of Science in the Department of Marine Sciences in the College of Arts and Sciences.

Chapel Hill
2016

Approved by:

Jaye Cable

Brent McKee

Harvey Seim

ABSTRACT

Jihyuk Kim: Investigating groundwater inputs to Mississippi River Deltaic wetlands using spatial and temporal responses of the geochemical tracer, ^{222}Rn
(Under the direction of Jaye Cable)

Submarine groundwater discharge (SGD) has been recognized as a significant coastal process that transports terrestrial freshwater, nutrients, and anthropogenic contaminants to the ocean. Globally, total influxes of terrestrial SGD to the ocean are equal to 5 to 10% of the annual global river water discharge into the ocean. In particular, several recent SGD studies have reported significant SGD fluxes in global deltaic regions such as the Yellow River Delta and Ganges-Brahmaputra Delta. The Mississippi River Delta (MRD) is the seventh largest delta on Earth, and was formed by thick layers of sandy sediments that were transported and deposited by numerous ancient river channels. In particular, the point bar aquifer, characterized as having a high sediment permeability and porosity, has developed along the Mississippi River (MR) natural levee. Considering the increased difference of hydraulic head between the MR and nearby swamps at high flood stage of the MR, the point bar aquifer and buried paleo river channels may be a conduit for groundwater to the MRD. To understand the hydrologic interaction between the MR and nearby swamps, a natural radioisotope radon (^{222}Rn) was utilized as a groundwater tracer. In addition, dissolved organic carbon, total nitrogen, stable isotopes, and ^{222}Rn activities in surface waters were measured to understand the biogeochemical transports of SGD in the MRD. The average SGD seepage rate in MRD was found to be 2.1 cm/day, or 1.3×10^8 m^3 day^{-1} to the MRD. The source of the SGD in the MRD was a mixture of MR and precipitation based on stable isotope results. In addition, the concentration of

biogeochemical constituents in SGD was at maximum two orders of magnitude higher than in surface waters. The main control factor of SGD in the upper MRD was influenced by the seasonal MR water stage. Thus, SGD in the MRD is not only a significant biogeochemical source, but also contributes freshwater the wetland sustainability in the MRD.

To my family – for their love and support.

ACKNOWLEDGMENTS

This work would not have been possible without the many individuals who guided and supported me along the way. First, I would like to thank my amazing collaborators who supported me by collecting and analyzing water samples at the Mississippi River Delta area: Dr. Alexander Kolker, Alex Breaux, and Katherine Telfeyan. I would also like to express my sincere gratitude to my committee, Jaye Cable, Brent Mckee, and Harvey Seim, for their assistance and suggestions throughout the project. A very special thanks to my lab members, Jill Arriola, Kaylyn Gootman, and Maggie Esch, for their generous help in the lab and field, as well as being good friends. I also thank Carly Moreno and Caleb King, as well as all of my friends in the Department of Marine Sciences, for their awesome friendship and supports. Last, but not least, I would like to thank my beautiful family, my mom, dad, and sister, for their unwavering support and precious love.

TABLE OF CONTENTS

LIST OF TABLES

LIST OF FIGURES

Introduction

Globally, large rivers play a significant role in the transport of terrestrially derived materials, including sediments, freshwater, and nutrients, to the coastal ocean. Almost 50% of the total suspended particulate matter transferred to the ocean comes from the 21 largest worldwide rivers (Milliman and Mead, 1983). As a result, all global river deltas are composed of accumulated mineral and organic sediment derived from the vast watersheds that drain toward the coasts (Burdige, 2005). The Mississippi River Delta (MRD) was formed by small distributary channels that diverted off the main channel incising the thick sediment layers of fine-grained sand and by the consecutive main river channel avulsions that generated a new deltaic lobe as they abandoned their former distribution lobe (Coleman and Wright, 1975; Roberts, 1997). Over time these abandoned distributary channels fill-in with sediments, thus burying the original sandy channel bottom. These abandoned and buried sandy-bottom paleochannels now comprise a portion of the deltaic alluvial aquifer system. As such, these abandoned paleochannels represent a vast network of potential subterranean estuaries wherever they intersect saltwater intrusion from the Gulf of Mexico [Figure 1]. The subterranean estuary is defined as a dynamic reactive zone between freshwater and seawater chemical sources (Moore, 1999). In addition, the regional distribution of sandy sediment layers along the main river channel, point bar, are developed by the consecutive sediment deposition of river. These well sorted sediment layers are distributed subsurface between the main river channel and near by flood plain and compose a local shallow aquifer system, a part of alluvial aquifer. Therefore, the paleochannel and the local shallow aquifer such as point bar might paly a role as a groundwater conduit between the main river and nearby wetlands in the deltaic zone.

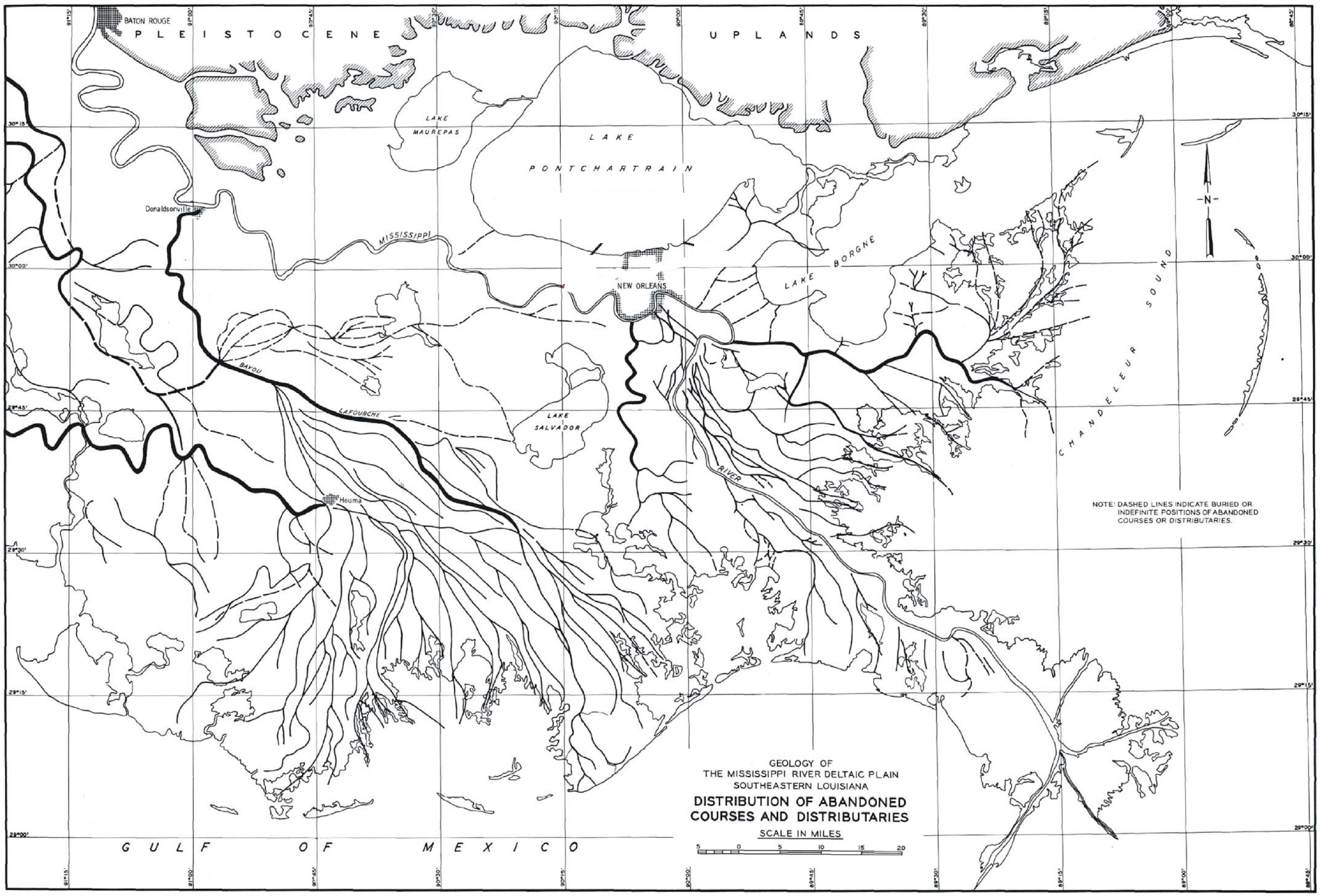

PLATE 5

Figure 1. The distribution of abandoned courses and distributaries in the Mississippi River Delta (Kolb and Van Lopik, 1958)

Recent research highlights submarine groundwater discharge (SGD) to marine systems might exceed global river water discharge (e.g. Zekster and Loaiciga, 1993; Moore, 1999, 2010; Burnett et al., 2001, 2003, 2006). These studies have shown as much as 80 to160% of river discharge is delivered into the Atlantic Ocean by SGD. In addition, the groundwater discharging from the world's large delta regions into coastal oceans has been increasingly recognized as a significant source of water and dissolved materials, including nutrients and other dissolved constituents (e.g. Moore, 1996; Burnett et al., 2003). For example, the significantly large volume of brackish groundwater fluxes on the western side of the MRD flow into the Gulf of Mexico at approximately 1000 $m^3\ s^{-1}$, or equal to 7% of the average Mississippi River discharge (Moore and Krest, 2004). The high groundwater flux entering along the Atchafalaya River side of the delta delivers high concentrations of radium (^{223}Ra, ^{224}Ra, ^{226}Ra, and ^{228}Ra) and the transportation of nutrients and other materials by groundwater was also considered important in this area (Krest and Moore, 1999; Moore and Krest, 2004). Recent research performed in Barataria Basin along the lower Mississippi River Delta shows that seasonal variations of groundwater discharge is related to Mississippi River stage (Kolker et al., 2013).

In eastern Asia, a large fresh groundwater flux is equivalent to 5 to 7% of the Yellow River discharge through the entire Yellow River Delta (Taniguchi, 2008). The groundwater flux in the Bay of Bengal, which is the receiving basin for the Ganges-Brahmaputra River and deltaic runoff, is approximately 19% of the total river flux (Basu et al., 2001). Although the literature recognizes the hydrological significance of SGD in coastal deltaic systems, relatively little is known about the internal mechanisms of groundwater flow in deltas.

Statement of Problem

Global deltas are generally characterized as extremely heterogeneous and anisotropic sediment deposition by the consecutive sediment transportation and its deposition. According to Martin and Whiteman 1999, the MRD consists of a complex sediment composition containing a variety of sand, silt, clay, and gravel. Thus, examining the groundwater flux in deltaic areas is challenging. On the other hand, highly permeable sediment layers with high hydraulic gradients play important roles as pathways of groundwater (Freeze and Witherspoon, 1967). Since deltas are dominantly built by sandy grain size sediments transported by past river channels, the deltaic aquifer has a high permeability (Colman and Prior, 1980). Additionally, the flood control levee system along the main river confines the river water to a smaller volume by preventing use of the floodplain. This levee construction of the river has caused the channel to incise deeper and also forced the water elevation much higher during flood stages because it can not flow into a floodplain. The greater water elevation in the main river channel during higher river discharge causes a higher hydraulic gradient by increasing the river water elevation relative to the adjacent wetlands behind the levees. Mississippi River paleochannels and other shallow aquifers including point bar are likely important hydraulic conduits between the river and nearby wetland aquatic system due to this higher hydraulic head during flood stage. The main question of this study is what the hydrologic connection between the Mississippi River and the adjacent deltaic wetlands in a levee-dominated flood control plan is. ***In this study, I hypothesize that the highly permeable sediment layers associated with lower Mississippi River Valley paleochannels and other sand deposits associated with the alluvial aquifer system play a significant role as a***

seasonal groundwater discharge link between the river and the nearby wetlands and subterranean estuary in the deltaic system.

Two specific research objectives are outlined to elucidate the hydraulic connection between the Mississippi River and adjacent deltaic wetlands:

1. Investigate the spatio-temporal variability of groundwater inputs to a sub-basin of the MRD at local and basin wide scales using a geochemical tracer, ^{222}Rn; and
2. Quantify the magnitude and seasonal responses of groundwater inputs to the Mississippi River water stage using a ^{222}Rn mass balance in Bayou Fortier.

Natural radioisotopes occurring as an indirect decay product of the uranium or thorium series are often used for understanding groundwater discharge to the ocean (e.g. Moore, 1996; Cable et al., 1996b). The noble and inert gas ^{222}Rn exists concentrations typically 3 to 4 orders of magnitude greater in groundwater than surface waters (e.g. Cable et al., 1996; Corbett et al., 1997; Burnett and Dulaiova, 2003; Burnett et al., 2010). Additionally, the relatively short half-life ($t_{1/2}$=3.83 days), water solubility, and conservative nature of radon under natural conditions have been used for understanding terrestrial and aquatic environmental mass interface exchange (e.g. Cable et al., 1996a; Cable et al., 1996b; Dulaiova et al., 2008; Martin et al., 2007). Applying a continuous radon analyzer, RAD7, for regional groundwater assessment at a high resolution of spatiotemporal sampling reduces errors in a groundwater mass balance approach (Burnett and Dulaiova, 2003). This sensitive real-time dissolved ^{222}Rn monitoring in the field has significantly contributed to increasing our ability to understand groundwater mechanisms in coastal environments (Santos et al., 2009; McCoy et al., 2011), rivers and estuaries (Dulaiova et al., 2006; Burnett et al., 2010; Peterson et al., 2010), and lakes (Dimova and Burnett, 2011; Dugan et al., 2012). In addition, the depth profile distribution of ^{222}Rn in sediment pore water has been used in a numerical model to understand groundwater flow in the subterranean estuary (Smith et al., 2008).

Field Site Description

The Mississippi River Delta (MRD) is a downstream landform that integrates the sediment loads from the largest watershed on the North American continent (approximately 3.2 million km^2). This delta formed in the Gulf of Mexico coastal zone due to the large volume of annual freshwater, sediment, and organic carbon discharge delivered by the Mississippi River (Milliman and Meade, 1983; Solis and Powell, 1999; Trefry et al., 1994; McKee et al., 2004). The Mississippi River water stage fluctuates seasonally increasing during the winter and decreasing during the summer, and typically has a higher water stage than sea level due to the surrounding natural or artificial levees. According to a 1990 USGS report, this deltaic aquifer is classified as a Coastal Lowland Aquifer System with 5 main permeable zones [Figure 2]. Total surface area of permeable zone A is 4×10^{10} km^2 and the average thickness is approximately 165 m. Additionally, this zone has an average sand content of about 65% and exceeds 80% of sand content in several area (Weiss, 1992; Grubb, 1998) [Figure 3]. The research area of this study, Barataria Basin, is located in the southern Mississippi River Delta and is surrounded by the Mississippi River to the east and Bayou Lafourche on the west [Figure 4]. Total basin area is approximately 6,300 km^2 with three main lakes, Lac des Allemands, Lake Cataouatche, and Lake Salvador, and includes numerous small bayous, marshes, and swamps that are characterized as estuarine wetlands (Inoue et al., 2008).

The major freshwater source into this region changed from river water to precipitation after the construction of the flood control levee along the modern Mississippi River channel in 1904 (Emad et al., 2007; www.Lacoast.gov; Stone et al., 1997). Only a small volume of

Mississippi River water occasionally flows into the lower part of the basin through three main freshwater diversions at Davis Pond (A), Naomi (B), and West Pointe a la Hache (C) (Inoue et al., 2008). All drainages are usually operated within the moderate range of their capacity in order to protect the saline environment in Barataria Basin. Highly variable spatiotemporal precipitation supplies a freshwater source with approximately 160 cm rainfall per year (Emad et al., 2007). Most of the upper basin water body is occupied by freshwater with a salinity range of about 0 to1, whereas the lower basin has a relatively high salinity (up to 20). Tidal range at mouth of Barataria Basin is about 50 cm and from 5 to 10 cm at Lac Des Allemands. A recent freshwater balance model applied for this wetland system suggested the existence of another freshwater input source was needed to balance the water budget (Inoue et al., 2008). Additionally, salt mass balance implies an approximate 1.5 x 10^3 m^3 s^{-1} groundwater source occurs in the upper basin (Kolker et al., 2013).

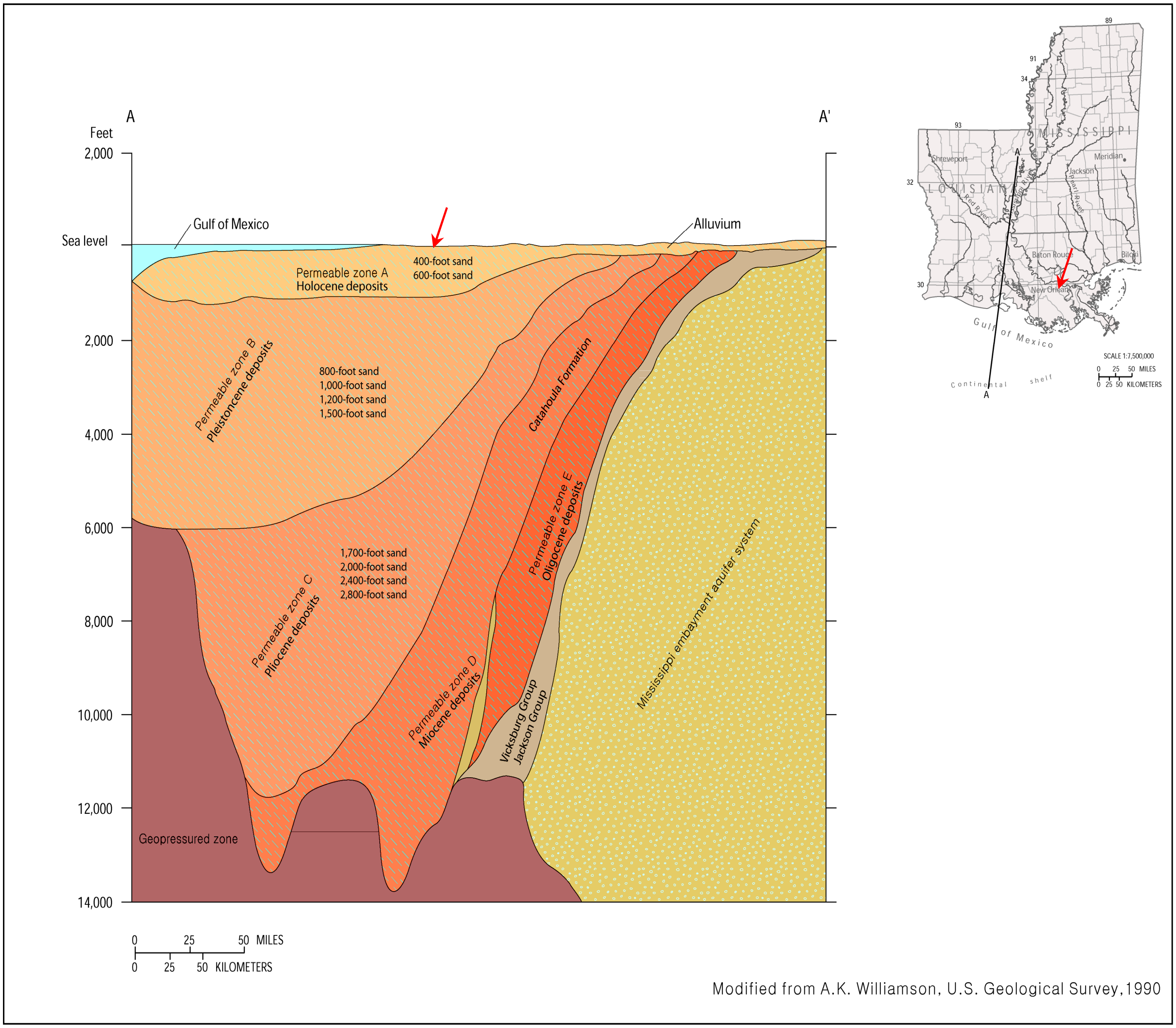

Figure 2. A to A' cross section of Coastal Lowland Aquifer system in Louisiana and vertical sand sediment layer (aquifer) distribution at each permeable zone (Permeable zone A to E). Each permeable zone has a different depth to the sandy sediment layer and they are connected to each other with numerous sporadic sandy layers (USGS, 1990). Note that red arrow indicates the location of this study area, Lac des Allemands.

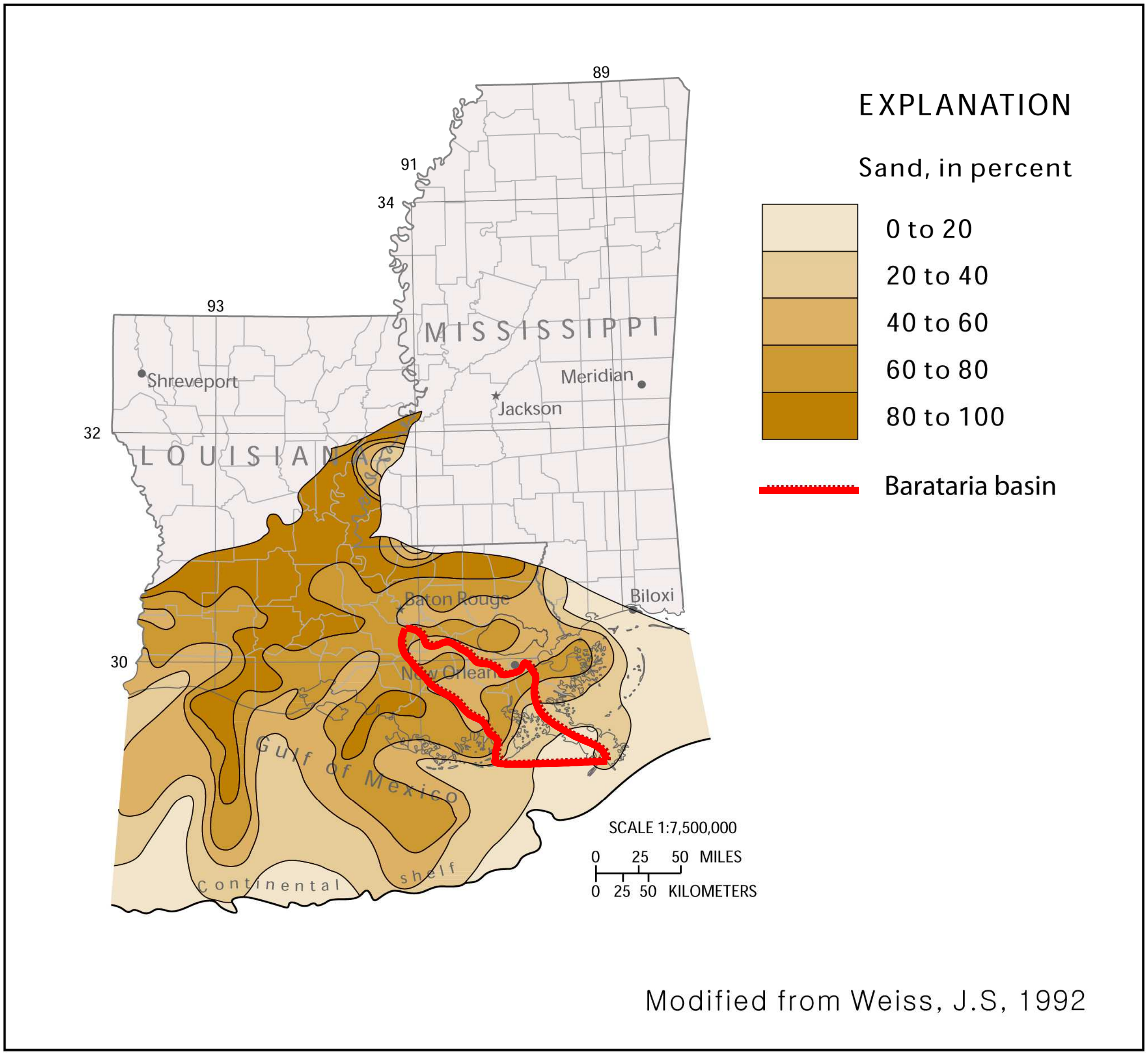

Figure 3. Horizontal sand content distribution along the Coastal Lowland Aquifer system in the Louisiana coastal area. The red line indicates the outline of the Barataria Basin study area (USGS, 1990).

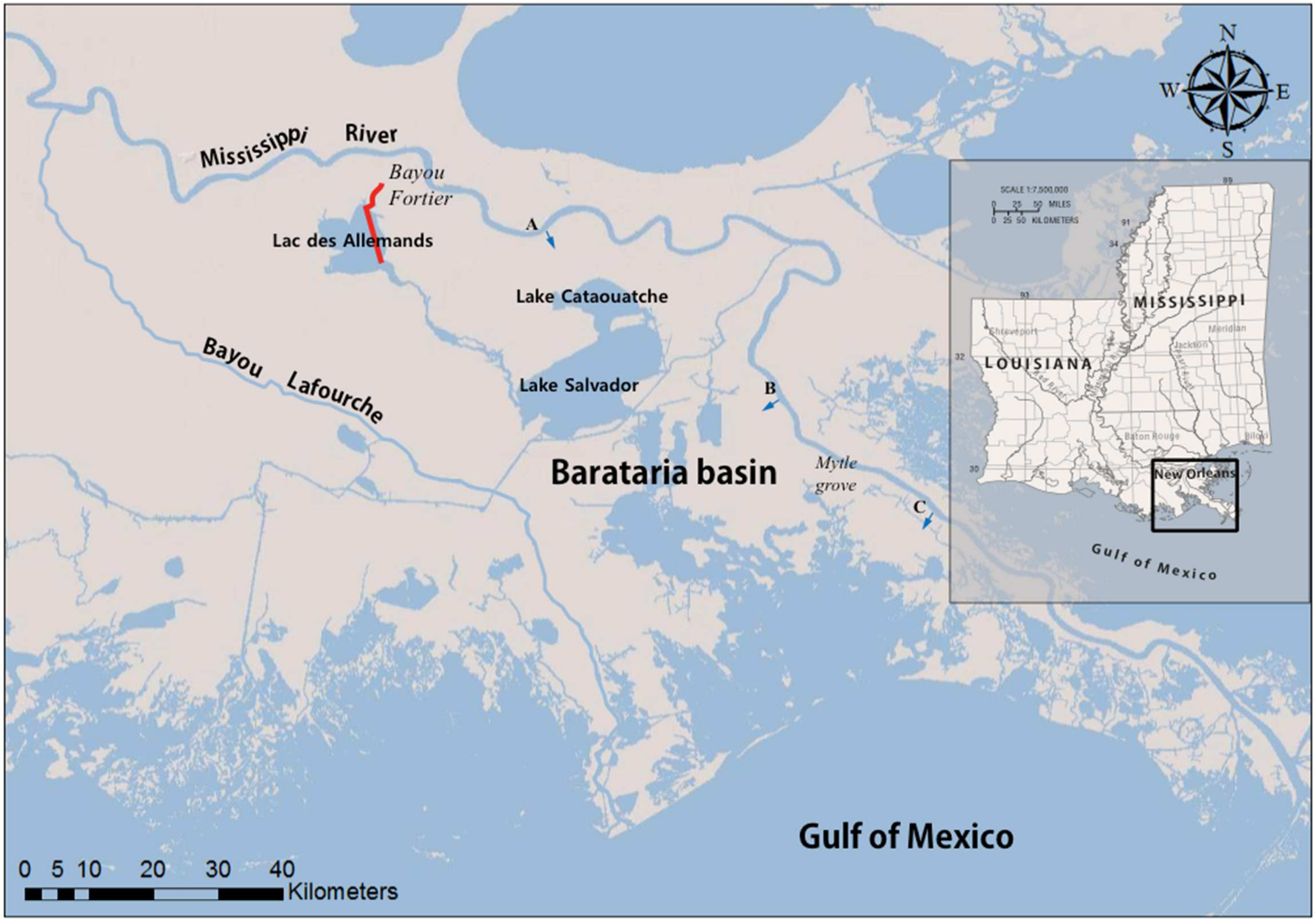

Figure 4. The study area is in Barataria Basin in the Mississippi River Delta, ^{222}Rn survey routes (a red line) and the Mississippi River diversion locations (A, B, and C blue arrows) are shown. Note that a red arrow indicates ^{222}Rn survey direction from mouth of the lake to the upper Bayou Fortier. *Mississippi River diversions - A: Davis pond; B: Naomi; C: West Pointe a la Hache

Local aquifer distribution

According to a U.S. Geological Survey (USGS), three different aquifers area distributed beneath the surface of St. John The Baptist Parish, Louisiana, which is located between the Mississippi River and Lac des Allemands (White and Prakken, 2015). The shallow aquifer, called the “Gramercy Aquifer”, is about 30 to 45 m thick and located at approximately 30 to 76 m below the National Geodetic Vertical Datum of 1929 (NGVD 29) (Hosman, 1972; Tomaszewski, 2003). The local ground water level in the Gramercy Aquifer seasonally corresponds to the Mississippi River water stage (Hosman, 1972). The Mississippi River point bar aquifer, which is located next to the Mississippi River channel bottom is approximately 30 to 45 m below the surface and contains fresh groundwater with a chloride concentration of 250 mg L^{-1} or less (approximately 0.5 salinity) (Sargent, 2011) [Figure 5]. This sandy sediment layer is also directly connected to the bottom of the Mississippi River channel as well as top of the local Gramercy Aquifer (Louisiana Department of Public Works, 1972). Thus, the hydraulic head change in the point bar is dynamic and based on the seasonal variation of the Mississippi River water stage. Consequently, this sandy point bar near the land surface may serve as a hydraulic connection between paleochannels and nearby bayou water bodies of the MRD [Figure 1].

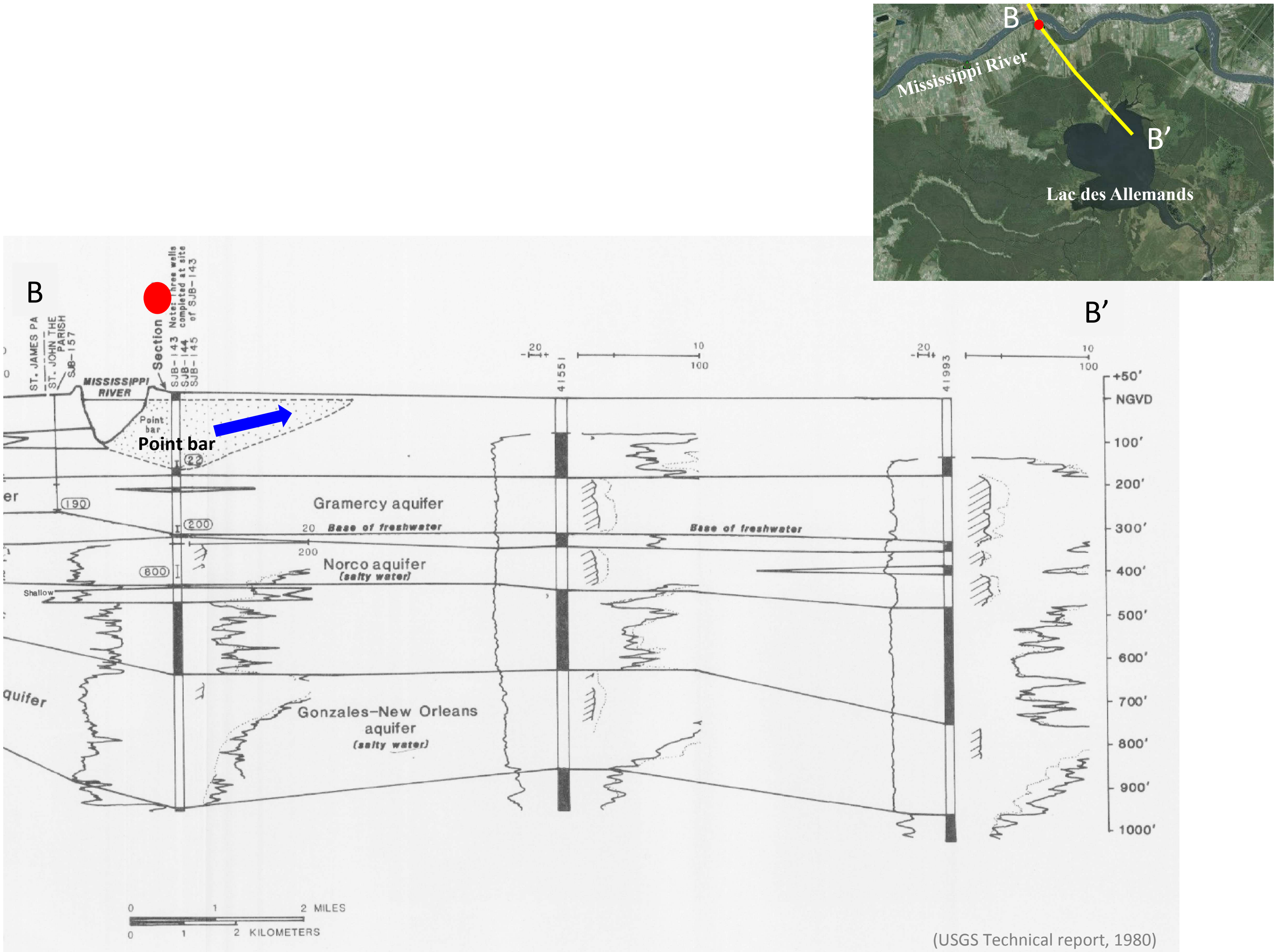

Figure 5. The vertical aquifer distribution in St. John The Baptist Parish Louisiana (USGS, 1980). Note that a blue arrow indicates a local groundwater flow direction in the subsurface area between the Mississippi River and Lac des Allemands.

Materials and Methods

Field Methods

Real-time ^{222}Rn surveys were conducted a total 10 times across Lac des Allemands and upstream on Bayou Fortier to capture the seasonal water stage variation in the Mississippi River. Six surveys occurred in 2013 (April 23, May 18, June 17, June 25, July 30, and September 29) and four surveys occurred in 2014 (April 17, June 17, June 18 and September 25). The route of the ^{222}Rn transect was always from the mouth of Bayou Fortier to the upper Bayou Fortier where the bayou transitioned into swamp forest and the depth became too shallow and vegetated for a boat to travel [Figure 6]. In addition, the bottom sediment and surface water were sampled at discrete stations during the ^{222}Rn survey from lakes, bayous, and the Mississippi River for ^{222}Rn diffusion sediment batch experiments.

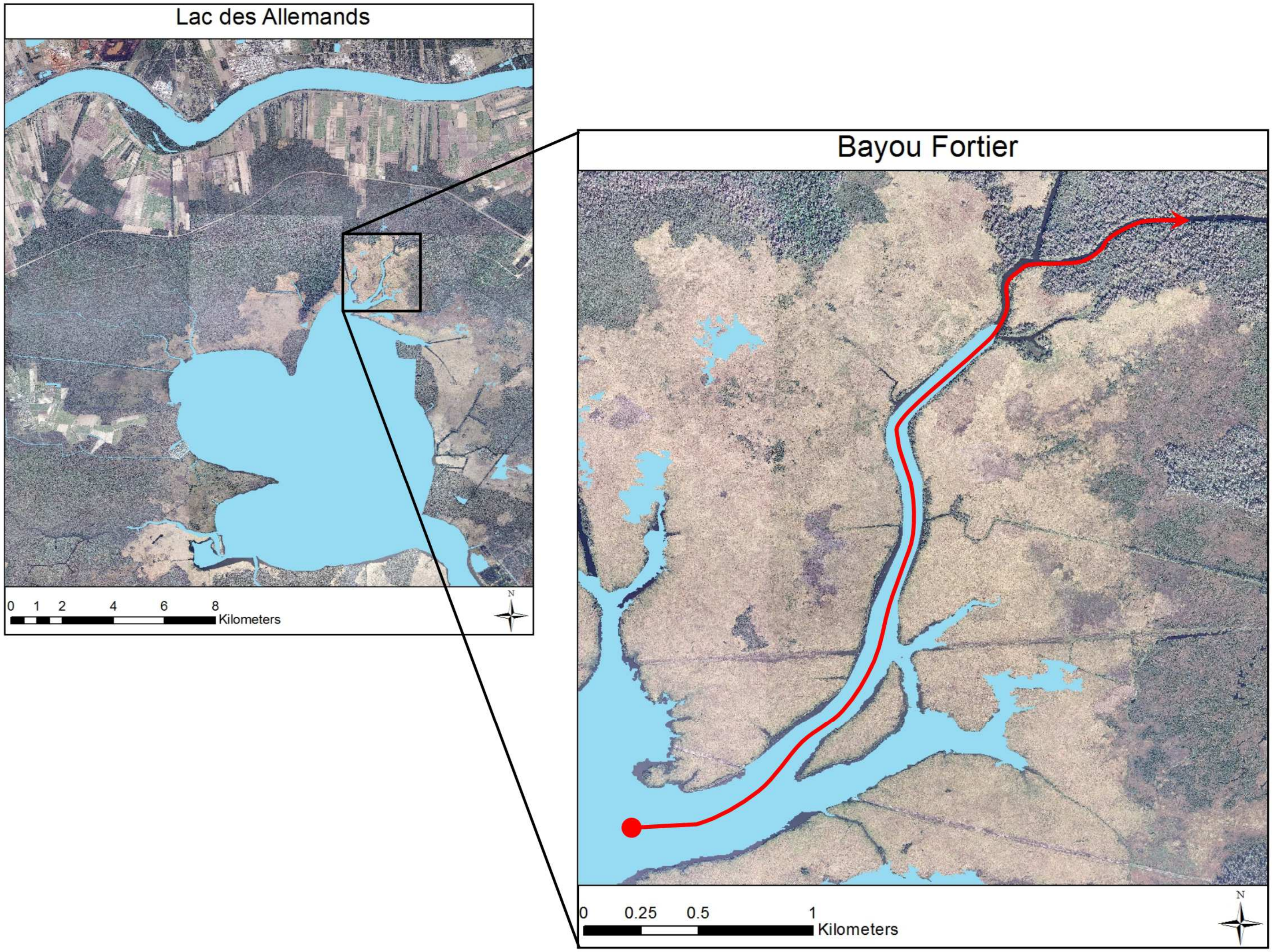

Figure. 6 A ^{222}Rn Transect route along the Bayou Fortier in Lac Des Allemands. Total ten times of ^{222}Rn real-time survey were performed from April, 2013 to September, 2014. The red dot indicates the start point of ^{222}Rn real-time monitoring. (*Figure generated by Katherine Telfeyan*)

^{222}Rn real-time monitoring and Calculation

A commercially available real-time ^{222}Rn detector, RAD7 (Durridge Co.), was used to measure water column ^{222}Rn ($t_{\frac{1}{2}} = 3.83$ days) concentrations *in situ*. This ^{222}Rn detector continuously measures the gas phase of ^{222}Rn decayed from its parent radioisotope, ^{226}Ra ($t_{\frac{1}{2}} = 1620$ years), with high efficiency and low background (Burnett and Dulaiova, 2003). The real-time ^{222}Rn monitoring system was installed with three RAD7 detectors in parallel and connected with an air-water equilibrium Radon-AQUA spray chamber [Figure 7]. The Radon-AQUA system was set up on a boat, and each RAD7 simultaneously reported accumulated ^{222}Rn concentration of air every 5 minutes. In order to decrease the ^{222}Rn equilibrium time between air and water phases in the closed loop, a submersible bilge pump (RULE 370) continuously collected large volumes of water, approximately 12 L min^{-1}, an average 1 m below the water surface. The aqueous phase ^{222}Rn in collected water samples was simultaneously isolated from water samples through two spray nozzles (WL-4) in the air-water equilibrium chamber. Each internal air pump in the three RAD7s allowed gas phase ^{222}Rn to reach each RAD7 chamber with about 1 L min^{-1} of airflow rate. A single filter and desiccant chamber eliminated dust or charged α ions and moisture from the gas phase ^{222}Rn respectively. Once the gas phase ^{222}Rn enters the RAD7 chamber, the alpha detector determines ^{222}Rn concentration by collection and measurement of ^{222}Rn daughters, ^{218}Po and ^{214}Po. While operating this continuous system, the boat moved along each transect at about 4 knots or under 5 km hr^{-1}. All ^{222}Rn transect concentration data at equilibrium between the air and water phase were converted to ^{222}Rn in water phase using a ratio of equilibrium determined by the water temperature (Weigel, 1987). In addition, temperature, conductivity, GPS coordinates, water depth and velocity were measured with a CTD-Diver (Schlumberger co.), Global Positioning System (Garmin etrex10), and Sontek FlowTracker acoustic Doppler current meter.

To calculate ^{222}Rn concentration in water using the triple RAD-7 measurement system, the measured ^{222}Rn concentration of air in the closed loop system were corrected to ^{222}Rn concentration in water using an empirical partition coefficient (K) of ^{222}Rn in pure water at a given temperature (°C):

$$Rn_{water} = \frac{Rn_{air}}{Ef} \times 2.22 \times K \qquad \text{Equation 1}$$

where Rn_{air} is ^{222}Rn concentration of air in the closed loop system (cpm), Ef is the efficiency of each RAD-7 (cpm pci^{-1} L^{-1}), 2.22 is for the unit conversion (2.22 dpm = 1 pci), and K is the empirical partition coefficient calculated by an equation 2 (Weigel, 1978):

$$K = 0.105 + 0.405e^{-0.0502T} \qquad \text{Equation 2}$$

where T is the water temperature in °C, which was obtained by measuring the water temperature in situ using a CTD-Diver (Schlumberger co.).

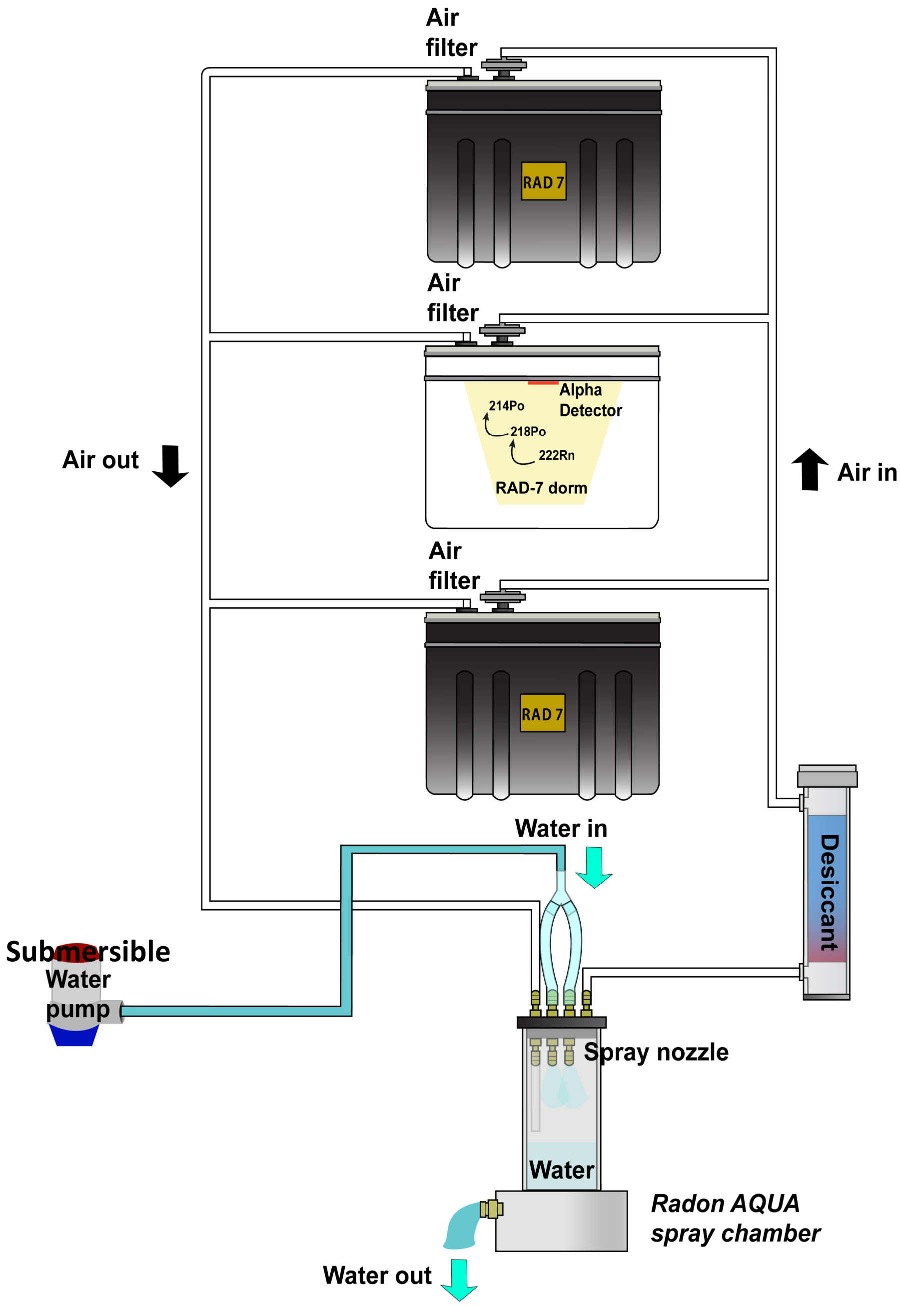

Figure 7. A schematic diagram of ^{222}Rn real-time monitoring system with multiple radon-in-air detectors, RAD-7, is shown.

^{222}*Rn grab sample analysis and Calculation*

In more isolated locations, ^{222}Rn grab samples of water were collected in numerous bayous, wells, and lakes. Water was collected using a peristaltic pump to fill a large plastic bottle. All collected samples were analyzed for ^{222}Rn excess within 36 hours using a single radon analyzer (RAD7) for at least 3 hrs. This single radon analysis system has the same technology described for the transect, however, it uses one detector instead of multiple detectors and does not use the submersible pump and spray chamber [Figure 8]. Instead, helium is pumped directly into the sample collection bottle to de-gas the ^{222}Rn. After counting ^{222}Rn in each water sample, the volume of each sample, V_{water} (m^3), was measured so that the ^{222}Rn concentration in water, C_{water} (dpm m^{-3}), can be calculated using the following equation 3:

$$C_{water} = \frac{C_{air} * V_{air} + K * C_{air} * V_{water}}{V_{water}} \qquad \text{Equation 3}$$

where C_{air} is the ^{222}Rn concentration in air (dpm m^{-3}); V_{air} is the volume of air (m^3) obtained from summation of volume of RAD7 chamber, tubing, bottle headspace, and desiccant air space; K (unitless) is an empirical partition coefficient in pure water at a given temperature (°C) that describes the ^{222}Rn concentration ratio of water to air using a temperature dependent equation 4 (Weigel, 1978):

$$K = {}^{222}\text{Rn(liquid)} / {}^{222}\text{Rn(gas)} = 0.105 + 0.405e^{-0.0502T} \qquad \text{Equation 4}$$

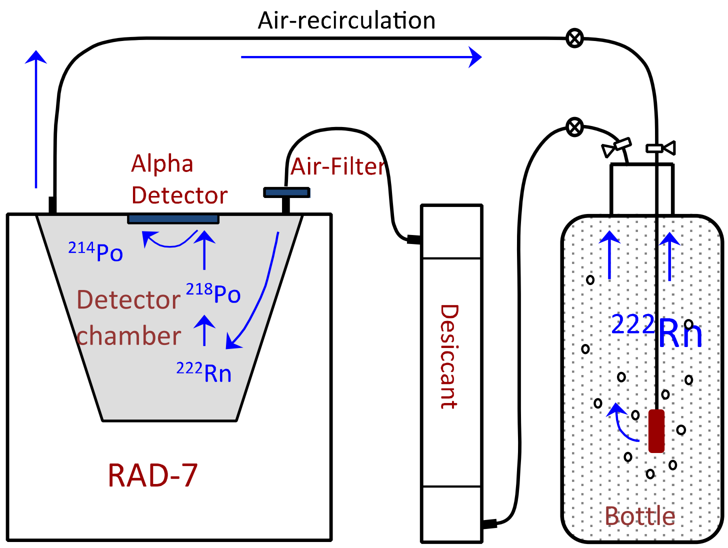

Figure 8. A schematic diagram is shown of ^{222}Rn analysis by RAD7 for discrete water bottle samples.

All radon activities were corrected based on the elapsed time, *t*, between sample collection and sample measurement (hrs):

$$C_t = C_0 * e^{-\lambda t} \qquad \text{Equation 5}$$

where C_t is the concentration of radon at the time of measurement (dpm m^{-3}), C_o is the radon concentration at the time of sample collection (dpm m^{-3}), and λ is the decay constant for ^{222}Rn (0.1809 day^{-1}).

Water and sediment sampling

At each sampling site, physico-chemical properties such as temperature, pH, specific conductivity, dissolved oxygen (DO), and salinity of the water were measured by a YSI probe (Model No. 556). A hand augur was also used for collecting bayou, lake, and wetland surface sediment samples for batch analysis of sediment diffusion.

<u>Laboratory Methods</u>

Sediment ^{222}Rn diffusion batch experiment

To determine the contribution of the excess ^{222}Rn flux from the sediment by diffusion, the pore water ^{222}Rn concentration at equilibrium with solid phase sediments was measured by performing sediment batch experiments on multiple sediment samples collected from lakes, bayous, and the river. All collected wet sediment samples were dried to measure porosity and bulk density. After three days, 50 g of dried sediment sample was sealed in a 1-L glass jar with 500 ml tap water. Once the ^{222}Rn concentration reaches equilibrium with ^{226}Ra after 30 days in the jar, the ^{222}Rn concentrations were measured by a single RAD7 closed loop system described previously for ^{222}Rn grab sample analysis. For every experiment run, a control sample, which was only 500 ml tap water in the jar, was analyzed at the same time for ^{226}Ra to collect background concentrations.

Mass Balance Model

^{222}Rn mass balance model for Bayou Fortier

In a steady state water box model, ^{222}Rn in-flux and out-flux should be equal if there are no supported or diluted ^{222}Rn factors involved. Therefore, any supported or diluted ^{222}Rn factors are calculated with a simple ^{222}Rn mass balance equation if the other terms are known. These kinds of mass balance approaches are useful mechanisms for understanding how chemicals or other constituents respond to different perturbations and to estimate any missing or unknown sources or sinks. A mass balance equation is described in Equation 6 to show how one could explain the behavior of ^{222}Rn in a swamp,

$$J_{adv} = J_{inv} + J_{atm} - J_{diff} \qquad \text{Equation 6}$$

where J_{adv} is the ^{222}Rn flux through the advective processes into the swamp (Bq m^{-2} day^{-1}); J_{inv} is the ^{222}Rn flux based on inventory (Bq m^{-2} day^{-1}); J_{atm} is the flux of ^{222}Rn across the air-water interface (Bq m^{-2} day^{-1}); J_{diff} is ^{222}Rn sediment diffusion flux in the swamp (Bq m^{-2} day^{-1}). J_{adv} is usually combined with large-scale advection, such as groundwater inflow, and small-scale processes, such as tidal pumping or wave set-up. In nature, the main ^{222}Rn contribution process is a large-scale advection process rather than a small-scale process (Burnett and Dulaiova, 2003).

In addition, considering the nature of the research area, which is perfectly surrounded by different kinds of vegetation, the ^{222}Rn loss by the atmospheric evasion of ^{222}Rn can be ignored (Burnett et al., 2010). Therefore, once all terms except J_{adv} are achieved, the groundwater flux can be easily obtained by dividing a calculated ^{222}Rn advective flux by the ^{222}Rn end member (Bq m^{-3}) in the local groundwater.

^{222}Rn inventory calculation

To determine the seasonal variability of ^{222}Rn concentration in the swamp water located in the upper Bayou Fortier, the ^{222}Rn regression approach was applied based on all ^{222}Rn transect results. Based on the results of ^{222}Rn transect data, the trend of each ^{222}Rn concentration in the water mass was decreased with an increase distance from the upper Bayou Fortier. This indicates that there is a high ^{222}Rn source around the swamp in the upper Bayou Fortier and the high ^{222}Rn in the water were exponentially decrease due to the loss factors of ^{222}Rn such as decay, dilution, and air-sea evasion. Therefore, the ^{222}Rn concentration in the swamp water can be determined using the an exponential regression approach equation 7:

$$y = Rn_o \times exp^{-k \cdot x} \qquad \text{Equation 7}$$

where Rn_o is the y intercept of the ^{222}Rn regression curve, k is the exponential loss rate of ^{222}Rn, and x is the distance from the swamp. Rn_o indicates the initial ^{222}Rn concentration of groundwater in the swamp and it decayed by ^{222}Rn loss factors over the water mass transit time [Figure 10].

^{222}Rn input via sediment diffusion

^{222}Rn is naturally produced by the decay of the parent radioisotope ^{226}Ra ($t_{1/2}$ = 1,600 years) from the sediment. Therefore, examining ^{222}Rn diffusion from the bottom sediment is essential for the ^{222}Rn mass balance approach and can be easily determined by various experimental methods. However, since each approach has a different process and analysis, the comparison between the results and uncertainty are significant. In this study, four different sediment ^{222}Rn diffusion approaches were performed and compared to minimize the uncertainty of the sediment diffusion.

A popular method is a depth independent mathematical approach from Martens et al., 1980 [Equation 8]. For this approach, multiple sediment batch experiments were performed and analyzed for sediment properties such as a porosity (∅), bulk sediment density, and sediment grain density. A ^{222}Rn diffusion equation is described in Equation 8:

$$J_{diff} = A_s \cdot \sqrt{\lambda \cdot D_s} \cdot (C_{eq} - C_o) \qquad \text{Equation 8}$$

where A_s is total bottom sediment area (m^2); λ is decay constant for ^{222}Rn (0.1809 day^{-1}); D_s (cm^2 s^{-1}) is the bulk sediment diffusion coefficient for ^{222}Rn after correcting the molecular diffusion coefficient (D_m) (Brocker and Peng, 1974) for water temperature in Kelvin (T_k) and sediment tortuosity (θ); C_{eq} (Bq m^{-3}) is the average ^{222}Rn activity at equilibrium with sediment pore water, which was obtained from a sediment equilibrium experiment (Cable et al., 1996); and C_o (Bq m^{-3}) is the average excess ^{222}Rn activity in the water column for a given station. The bulk sediment diffusion coefficient (D_s) of ^{222}Rn was determined from D_m and the tortuosity (θ) of each sediment sample using Equation 9 (Schulz and Zabel. 2006),

$$D_s = \frac{D_m}{\theta^2}$$ Equation 9

where the ^{222}Rn molecular diffusion coefficient (D_m) is described by a temperature dependence in Equation 10.

$$-logD_m = \left(\frac{980}{T_k}\right) + 1.59$$ Equation 10

In addition, the tortuosity of the sediment (θ) was calculated by a porosity ($\emptyset$) dependent Equation 11 (Boudreau 1997).

$$\theta^2 = 1 - \ln(\emptyset^2)$$ Equation 11

The porosity ($\emptyset$) of each collected sediment sample was calculated using following Equation 12 (Cable et al., 1996),

$$\emptyset = \frac{\frac{m_w}{\rho_f}}{\frac{m_w}{\rho_f} + \frac{m_d}{\rho_g}}$$ Equation 12

where the mass of pore water in wet sediment (m_w) is measured by the difference between the weight of wet and dry sediment and accounting for the pore water density assumed for freshwater($\rho_f \cong 1g\ cm^{-3}$). Also, the sediment dry grain density (ρ_g) was measured by the displacement of volume in water.

The second approach for determining the ^{222}Rn diffusive flux was performed by using an initial ^{222}Rn decay trend from a closed loop sediment batch experiment. The ^{222}Rn activity in air shows a linear growth rate within the first several hours after exposing sediment to the overlying water [Figure 9]. Once the decay of ^{226}Ra and the production of ^{222}Rn reach equilibrium, the slope is then consistent with increasing sediment exposure time. This initial linear slope of ^{222}Rn can be used to determine the sediment ^{222}Rn diffusive flux using the following equation 13(Chanyotha et al., 2014),

$$J_{Diff} = \frac{S \cdot V_{air}}{Area_s} \qquad \text{Equation 13}$$

where S is the ^{222}Rn activity initial trend within approximately 12 hours (Bq m^{-3} hr^{-1}); V_{air} is total volume of air in experiment system (m^3); and $Area_s$ an experiment sediment surface area (m^2). In this study, the total air volume and sediment surface area were 1.84 x 10^{-3} m^3 and 0.005 m^2, respectively.

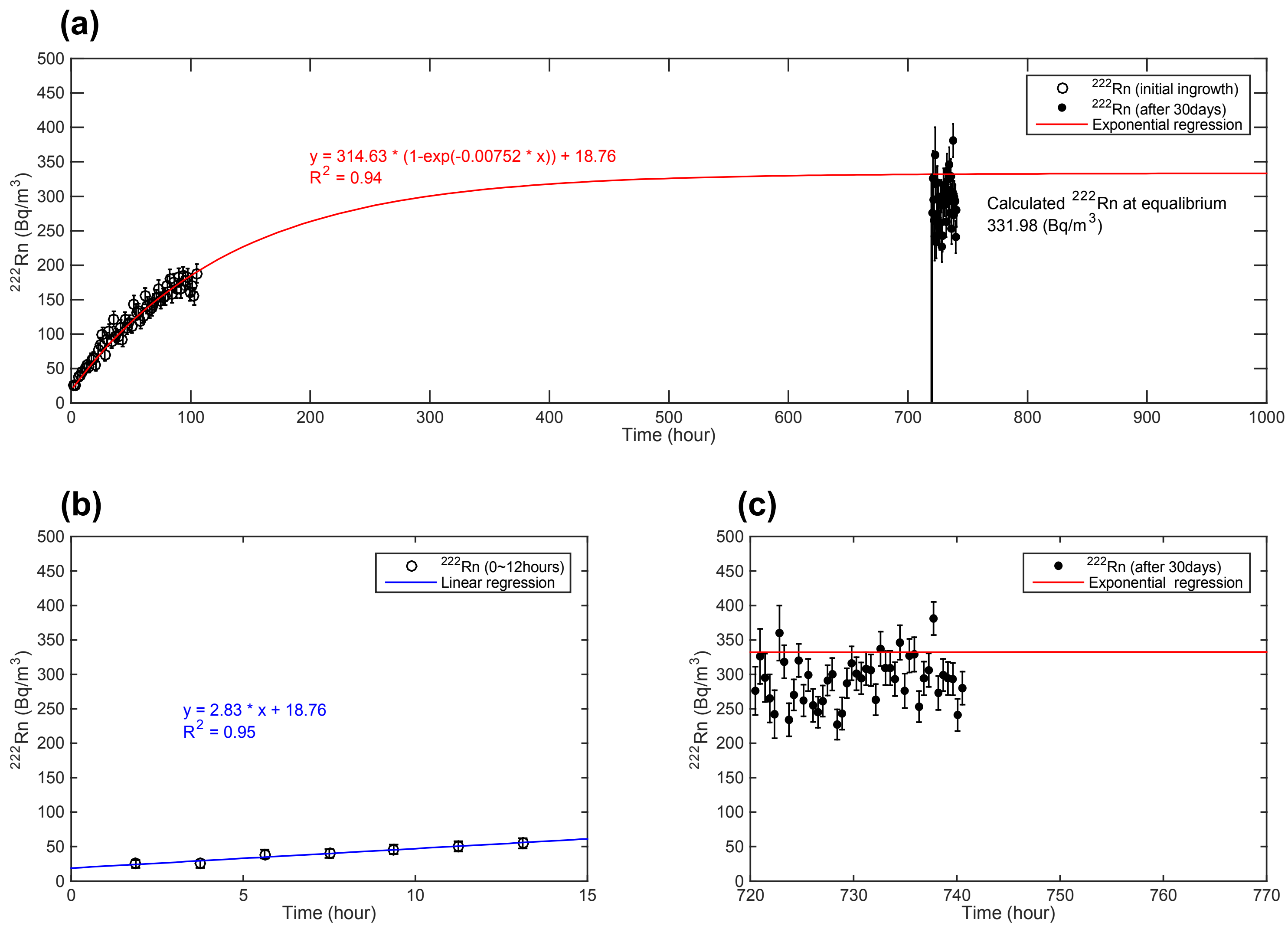

Figure 9. **(a)** ^{222}Rn activity change in the closed air loop during the start of measurement (0~100hours) and at the equilibrium phase (approximately after 30days of ingrowth). The red solid line indicates the best exponential curve fit with ^{222}Rn constant (0.00752 hours^{-1}) based on the first 0~100 hours of ^{222}Rn decay data. **(b)** Initial ^{222}Rn activity change with its linear function fitting. **(c)** Equilibrated ^{222}Rn activity in the sediment batch experiment with its decay and leakage. Note that the difference between a theoretical equilibrium constant (in this case, 331.98 Bq m^{-3}) and ^{222}Rn activity was due to the leakage of the sediment batch experiment.

The equilibrium activity of ^{222}Rn can be calculated by using a theoretical curve fitting method based on ^{222}Rn ingrowth data within the initial 12 hours of sediment exposure,

$$y = y_o + A_{eq}(1 - e^{-\lambda t}) \qquad \text{Equation 14}$$

where y_o is the y-intercept from the initial linear slope approach, which is accumulated ^{222}Rn diffusion concentration in the water after the exposure sediment to the water and before the ^{222}Rn measurement; A_{eq} is the ^{222}Rn concentration when ^{222}Rn production, decay, and leakage reach equilibrium; λ is the decay constant of ^{222}Rn (0.00752 hr^{-1}); and t is ^{222}Rn measurement time in hours. Therefore, if all the parameters are achieved, the ^{222}Rn equilibrium activity can be obtained by adding y_o and A_{eq} after applying an exponential curve fitting [Figure 9]. The equation related to ^{222}Rn sediment diffusion flux and inventory can be used to evaluate the total ^{222}Rn diffusion flux from the sediment (Chanyotha et al., 2014).

$$J_{Diff} = \left(\frac{A_{eq} \cdot V_{air} + A_{water} \cdot V_{water}}{Area_s}\right) \cdot \lambda \qquad \text{Equation 15}$$

In Equation 15, A_{water} is ^{222}Rn activity in the overlying water in the sediment equilibrium experiment (Bq m^{-3}); V_{water} is volume of water in the jar (m^3); $Area_s$ is the surface area of experimental sediment (m^2); and λ is ^{222}Rn decay constant (0.1809 day^{-1}). For this sediment diffusion flux calculation, 5.0×10^{-4} m^3 was used for the water volume and the surface area of sediment was 5.03×10^{-3} m^2.

The last sediment diffusion approach was performed by an empirically defined relationship between ^{226}Ra and the corresponding measured ^{222}Rn diffusion flux (Burnett et al., 2003). All sediment samples that contributed to this empirical equation [Equation 16] were collected from the both marine and fresh water environments of Barataria Basin,

$$J_{Diff} = 495 \cdot A_{^{226}Ra} + 18.2 \qquad \text{Equation 16}$$

where A_{226Ra} is ^{226}Ra activity in the sediment sample (dpm g^{-1}).

^{222}Rn concentration in local groundwater

There are some ways to estimate ^{222}Rn concentrations in local groundwater as an end-member such as monitoring local wells, deploying piezometers, collecting water samples from seepage meters, and measuring ^{222}Rn in pore water (Cable et al., 1996; Taniguchi et al., 2003; Burnett et al., 2007). In this study, groundwater from a total of 5 local wells was sampled and measured for the ^{222}Rn concentration using a simple bottle measurement method described above (Lee and Kim, 2006) [Figure 8].

Groundwater seepage rate calculation

The total advective flux of ^{222}Rn from the bottom sediment (J_{adv}, Bq d^{-1}) can be calculated using the difference between ^{222}Rn input sources (J_{in}, Bq d^{-1} ; J_{diff}, Bq d^{-1} ; J_{prod}, Bq d^{-1}) and the summation of ^{222}Rn output sources (J_{atm}, Bq d^{-1} ; J_{out}, Bq d^{-1}; J_{decay}, Bq d^{-1}) from the water column. Once the total ^{222}Rn flux from advection is determined, the regional groundwater flux GW (m d^{-1}) can be calculated by dividing the ^{222}Rn advective flux by the mean concentration of ^{222}Rn in local groundwater (C_{gw}, Bq m^{-3}) (Burnett and Dulaiova, 2003) [Equation 17].

$$GW = \frac{J_{adv}}{C_{gw}} \qquad \text{Equation 17}$$

Conceptual model for ^{222}Rn transect data

Scientists have long predicted that another source of freshwater was needed to account for the salinities found in Mississippi River deltaic estuaries, particularly Barataria Basin. Reed et al. (1995) showed in a salt balance of the basin that observed salinities were actually lower than what would be predicted based on the tides and precipitation. In a hydrodynamic model of Barataria Basin, Inoue et al. (2008) found that the water balance pointed to a missing freshwater source; they predicted this freshwater was coming from numerous unknown streams flowing into the basin. Kolker et al. (2013) found Mississippi River discharge decreased from Tarbert's Landing to the downstream location at Belle Chasse, thus indicating a net loss of river flow, which they hypothesized was entering the alluvial aquifer and potentially flowing into the surrounding floodplain wetlands as groundwater seepage. Previous research has also shown that groundwater may be a source to Barataria Basin, where a seasonal study of ^{222}Rn in surface waters of the basin indicated a relationship to the Mississippi River stage (Inniss, 2002). These studies all point to the likelihood that freshwater is entering the basin via some unseen path and evidence suggests this path may be through groundwater flow.

Groundwater flow into Barataria Basin would likely enter through buried paleochannels left behind by previous river avulsions, or through the alluvial aquifer. My investigation began with the hypothesis that paleochannels maintain a subsurface connection to the river and these paleochannels are the conduits by which groundwater was driven into the deltaic wetlands. Using ^{222}Rn as a tracer for groundwater inputs to surface waters, multiple surveys were conducted using real-time continuous surveys along bayous and across lakes of Barataria Basin. Most surveys were conducted across Lac des Allemands and into Bayou Fortier, Louisiana. In every case, the ^{222}Rn concentrations interface waters increased within increasing proximity to the Mississippi River [Figure 11]. This trend becomes especially clear when the bayou data isolated from lake data.

To understand groundwater input to Bayou Fortier in the upper Barataria Basin, ^{222}Rn concentrations along the surface water surveys were plotted versus distance along the bayou reach [Figure 10]. Theses data indicate an exponential decrease occurs from the upper bayou to the confluence of the bayou and Lac des Allemands. A conceptual model was developed to describe the behavior of ^{222}Rn along the transect [Figure 10]. Once high concentration of ^{222}Rn in groundwater originating from the point bar around the Mississippi River is released into the nearby swamps, groundwater ^{222}Rn activity exponentially decreases over the transit time due to radioactive decay ($\lambda = 0.1809$ day^{-1}), dilution, and atmospheric evasion across the water surface. Diffusion from the bottom sediments, water column particle re-suspension, and potential groundwater sources result in a concurrent increase of ^{222}Rn activity in the water column. Thus, the difference between the theoretical ^{222}Rn decay curve and a regression curve based on ^{222}Rn transect data indicates ^{222}Rn loss by water dilution and atmospheric evasion during the water transit time [Figure 10]. Furthermore, the ^{222}Rn regression curve contains ^{222}Rn sediment diffusion and excess ^{222}Rn, including ^{222}Rn sources from the potential groundwater and suspended particles in the water column. The evaluation of ^{222}Rn concentrations in the swamp in the upper Bayou Fortier can be made using the ^{222}Rn regression curve based on ^{222}Rn transect results in Bayou Fortier. Once the initial ^{222}Rn concentration in the swamp is determined, the groundwater flux into the Bayou Fortier can be examined using the ^{222}Rn concentration in local groundwater.

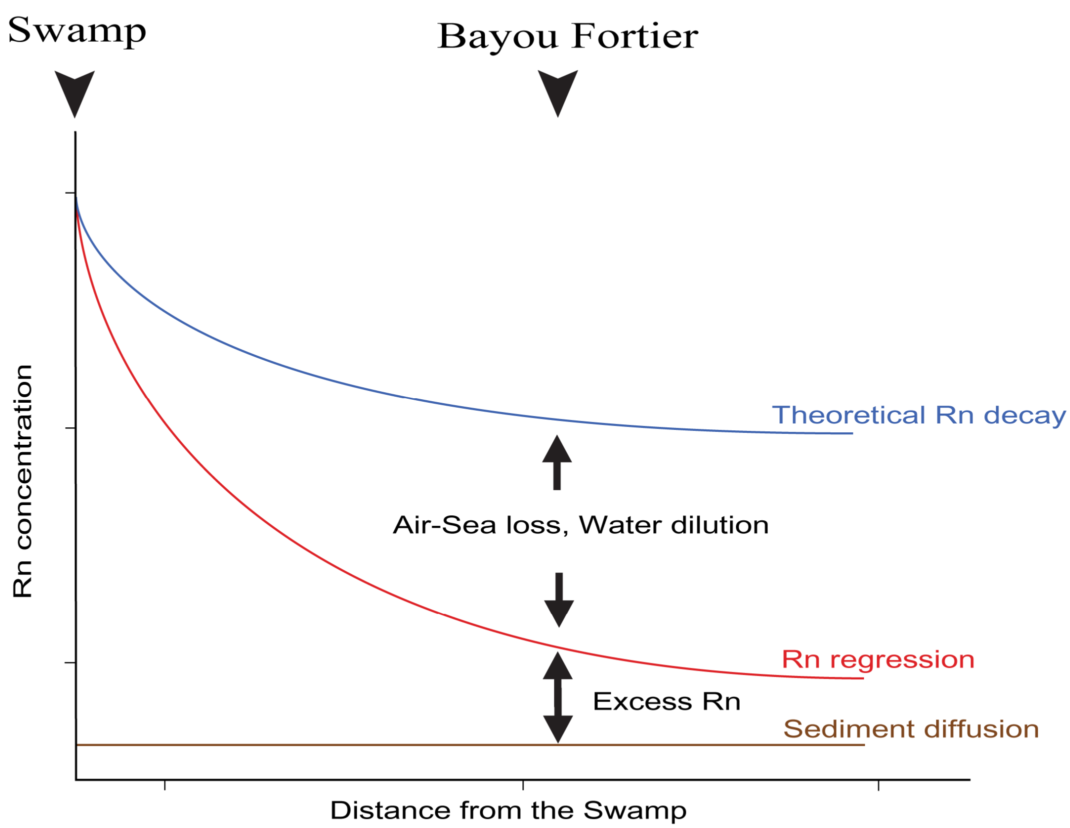

Figure 10. A conceptual model for understanding the change of ^{222}Rn concentration over the distance from the swamp in Bayou Fortier in upper Barataria Basin. A blue line indicates the calculated theoretical ^{222}Rn decay curve based on the decay of an original ^{222}Rn concentration at the swamp during the water transit time. A red line indicates the ^{222}Rn exponential regression curve based on ^{222}Rn transect data and a brown line indicates the ^{222}Rn diffusion flux from the bottom sediment. Note that x-axis is the distance from the swamp, not the Mississippi River.

Results

Geographical ^{222}Rn distribution

A total of 71 bayou and Mississippi River surface water samples were collected from May to July 2013 to elucidate the geographical distribution of ^{222}Rn around Barataria Basin. High ^{222}Rn concentrations were distributed around the upper Barataria Basin close to the main Mississippi River channel with a range from 1.9 to 1415.4 Bq m^{-2} [Figure 11]. Most of the replicate samples collected near the Mississippi River had relatively high ^{222}Rn concentrations regardless of the different sampling dates. Conversely, most coastal surface water samples had 1 to 3 orders of magnitude lower ^{222}Rn activity than the area adjacent to the Mississippi River.

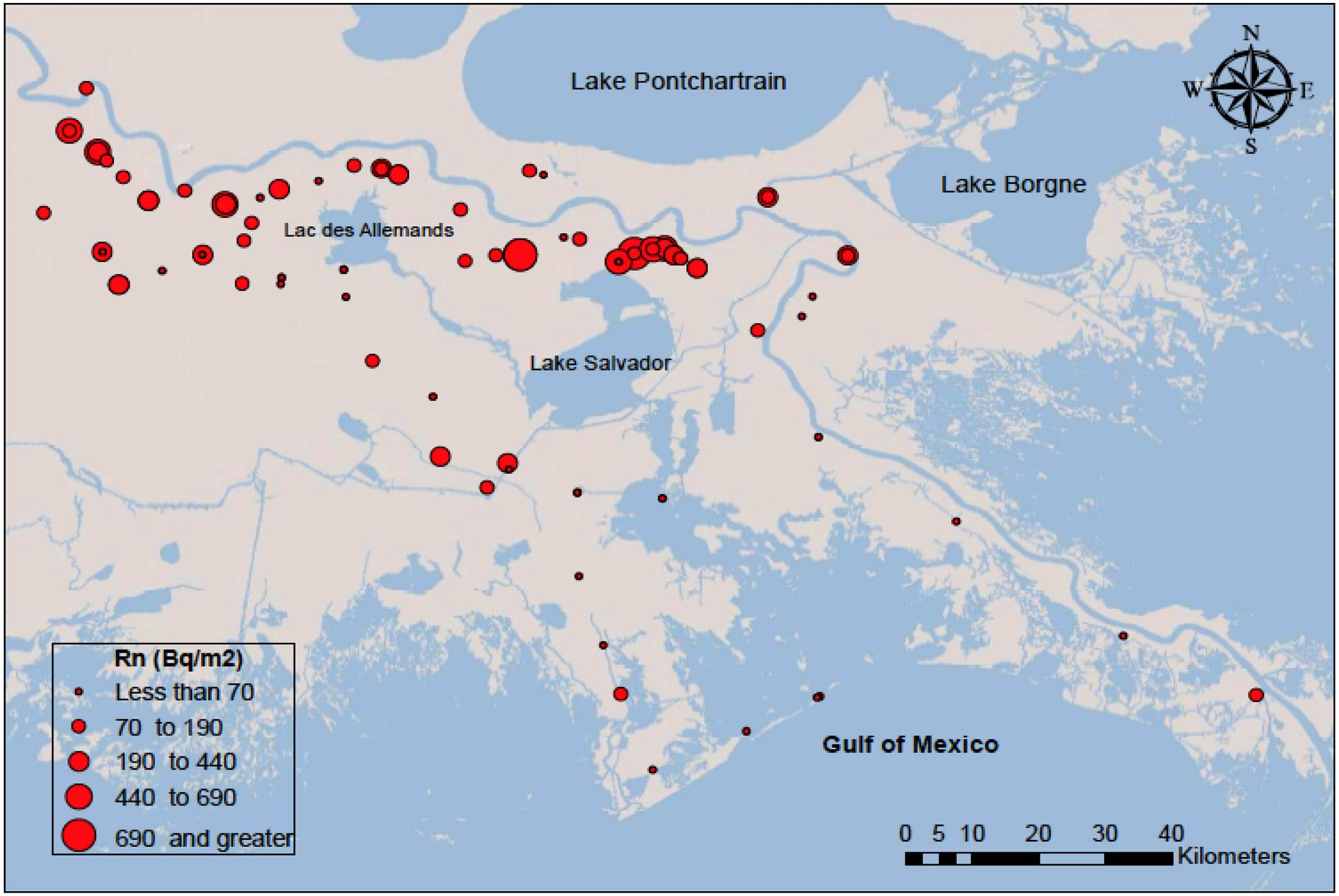

Figure 11. ^{222}Rn inventory distribution in the surface waters in Barataria Basin.
*Overlapping circles indicate replicate samples during different sampling periods.

^{222}Rn transects in Bayou Fortier

At Bayou Fortier, located in the upper area of Barataria Basin, the ^{222}Rn transect was performed from the mouth of the bayou to the upper bayou, (~ 3 km upstream) between April 2013, and September 2014. This ^{222}Rn survey was performed multiple times to capture differences in Mississippi River water stages at various times of the year. The results show a significant decrease in ^{222}Rn concentrations with increasing distance from the Mississippi River [Figure 12]. Most short distances of from the Mississippi River had relatively high ^{222}Rn concentrations during all sampling dates. ^{222}Rn activity measured in Bayou Fortier, between approximately 5 km and 8.5 km from the Mississippi River, exponentially decreased with increasing distance from the Mississippi River [Figure 12].

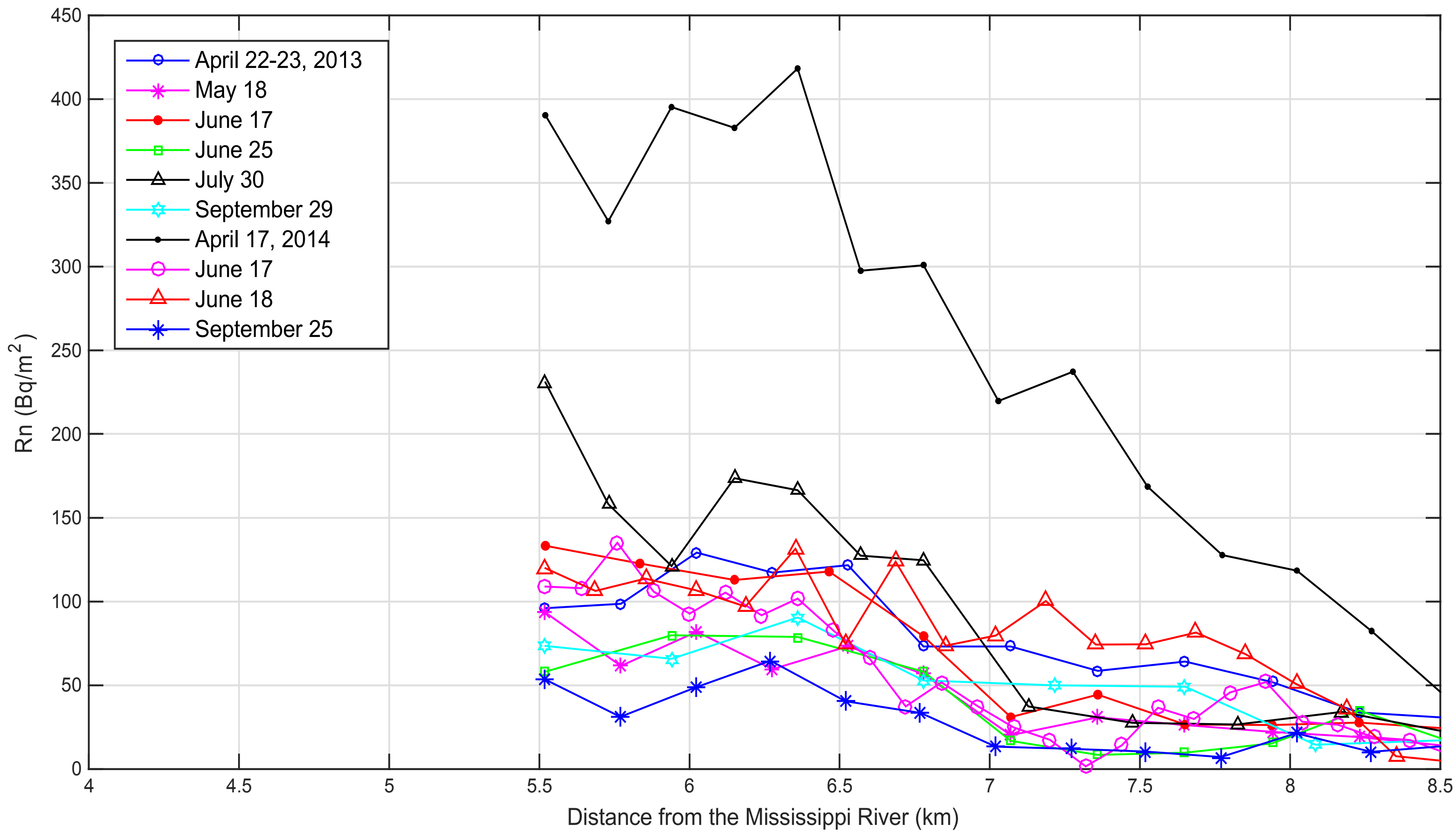

Figure 12. ^{222}Rn transect result at Bayou Fortier during April, 2013 ~ September, 2014.

Experimental comparison for ^{222}Rn sediment diffusion fluxes

Sediment diffusion analysis methods were compared using sediment samples that were collected from two different environments in Barataria Basin. The lower Barataria Basin is a brackish coastal environment (salinity ranges from 4 to 20) and the upper Barataria Basin is mostly a fresh wetland environment (salinity < 1). After performing four different sediment diffusion experiments, the sediment diffusion flux results were compared to reference values from Inniss et al., 2002 (Lower Barataria Basin: 1.9 ± 1.2 (Bq m^{-2} day^{-1}), n=2; Upper Barataria Basin: 27.6 ± 7.6 (Bq m^{-2} day^{-1}), n=2). The result of the ^{222}Rn influx of sediment diffusion was 1.10×10^{7} Bq day^{-1} with a range of 3 to 24% of total ^{222}Rn flux on each of the ^{222}Rn survey dates. Sediment samples from the lower and upper Barataria Basin show varied ^{222}Rn sediment diffusion flux values based on the method used and the sampling location [Figure 13]. The lower Barataria Basin sediment samples had more variance than the upper Barataria Basin ^{222}Rn sediment diffusion flux. However, the upper Barataria Basin samples show relatively similar sediment diffusion values among the different sediment diffusion experiment results, with the exception of the results obtained from the empirical equation method using ^{226}Ra concentrations in the sediment [Figure 13]. This is because the empirical method relies on a limited data set from a few environmental systems (Burnett et al., 2003). Other parameters, such as temperature, grain-size distribution, and the location of radium atoms, might significantly impact the ^{222}Rn sediment diffusion process (Nazaroff et al., 1988). Thus, the determination of ^{222}Rn sediment diffusion using an empirical method may not be efficient without considering sediment properties. On the other hand, the equilibrium method, defined as a ^{222}Rn theoretical decay curve based on the sediment batch experiments, shows the most relevant values compared to other method results. According to Chanyotha et al., 2014, the equilibrium method provides better precision with lower uncertainties (less than 10%). Therefore, in this study, the equilibrium method was used to determine the sediment diffusion flux.

In addition to the methodological comparison, the spatial variability of sediment diffusion flux in the Mississippi River Delta was examined. For this approach, a total of 22 sediment samples were collected from different environments in the Mississippi River Delta and analyzed for sediment diffusion flux using the equilibrium method from Chanyotha et al., 2014 [Figure 14]. As a result, the sediment samples collected from near Lake Salvador (group C) showed the highest sediment diffusion flux with 43.8 ± 6.2 Bq m^{-2} day^{-1}. Lac des Allemands (group B) was found to have a relatively similar flux (25.2 ± 2.6 Bq m^{-2} day^{-1}; n = 6) when compared to previously published results (27.6 ± 7.6 Bq m^{-2} day^{-1}; n = 2) (Inniss et al., 2002). Most sediment samples collected from the salt marsh area (group E) are highly variable (25.9 ± 8.1 Bq m^{-2} day^{-1}) compared to the reference sediment diffusion flux value (15.9 ± 3.5 Bq m^{-2} day^{-1}).

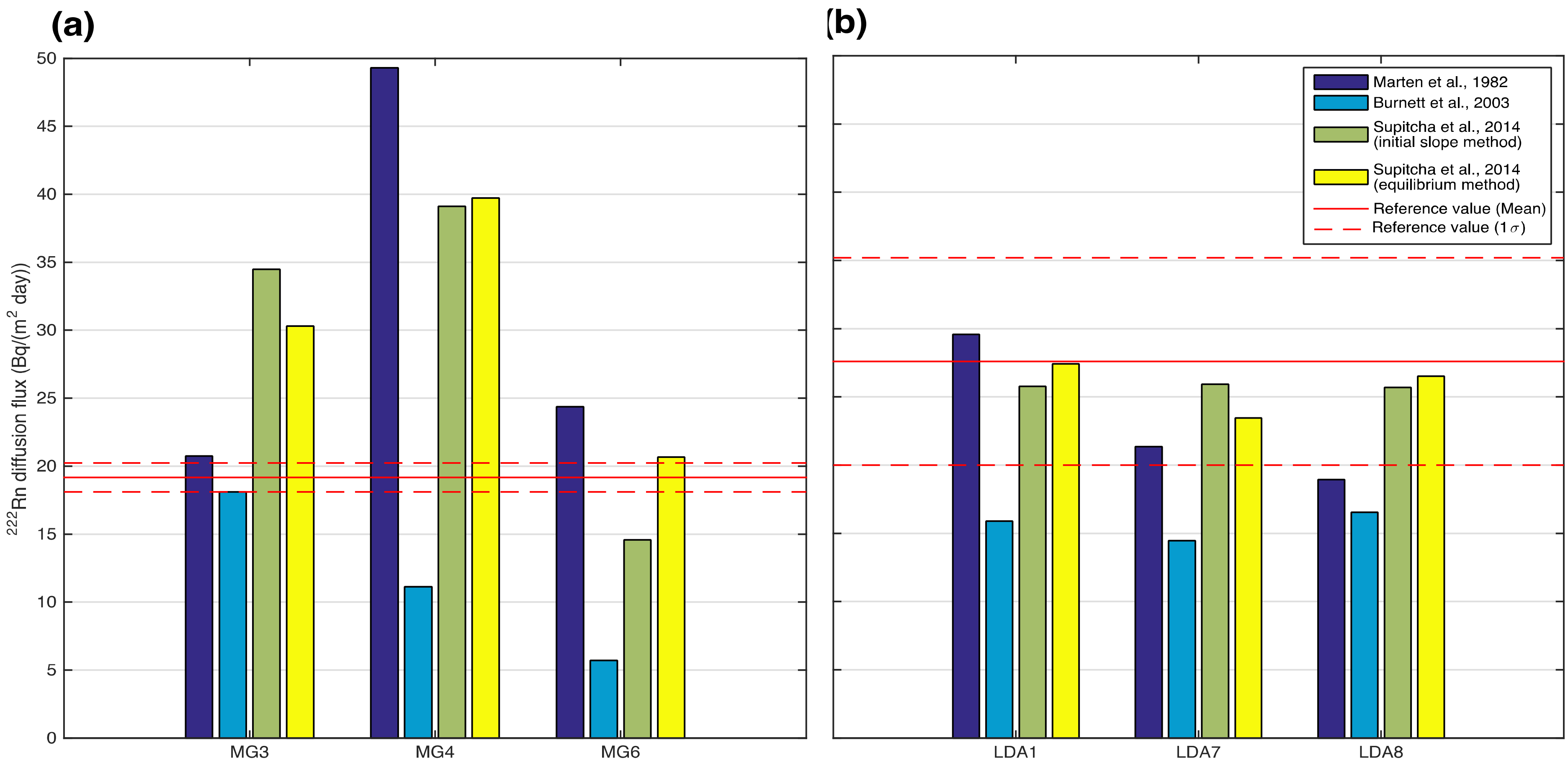

Figure 13. The comparison results from among four different ^{222}Rn sediment diffusion experiment methods for each sediment sample collected from the lower Barataria basin **(a)** and the upper Barataria basin (around Lac des Allemand) **(b)**. Each solid and dashed red line indicates a reference sediment diffusion average and a standard deviation (n=4) (Inniss, 2002).

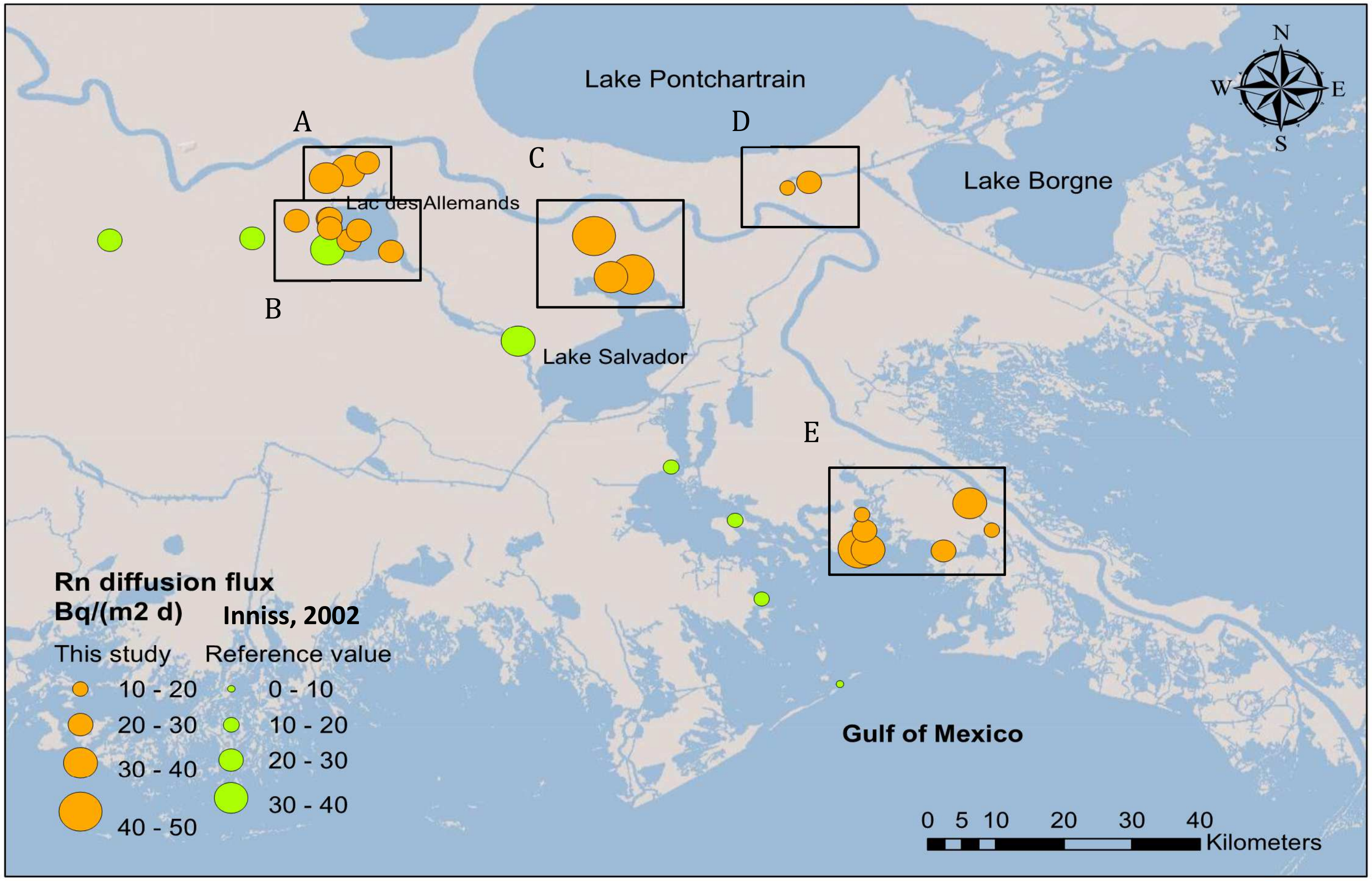

Figure 14. The distribution of ^{222}Rn sediment diffusion fluxes in Barataria Basin. Green points indicate reference values from Inniss, 2002 (n=8) and orange points are from this study (n=22). Note that all results in this study were evaluated by the equilibrium method from Chanyotha et al., 2014 and the reference values were determined by using a depth-independent equation from Martens et al., 1982. **A**: Bayou sediment samples (Bayous around Lac des Allemands), **B**: Lake sediment samples (Lac Des Allemands), **C**: Channel sediment samples (Lake Cataouatche), **D**: Bayou sediment samples (Bayou Bienvenue Marina), **E**: Salt marsh sediment samples (Mytle Grove).

^{222}Rn concentration in groundwater

As a result of ^{222}Rn concentration in local groundwater samples, the mean ^{222}Rn concentration was 3109.7 Bq m^{-3} and was lower than the ^{222}Rn concentrations in different depth monitoring wells located around the lower Barataria Basin (McCoy et al., 2007) (10450 ± 650 Bq m^{-3}, well depth range: 55 – 73 m; 7416.7 ± 533.3 Bq m^{-3}, well depth range: 91 – 131 m). In addition, the evaluated average ^{222}Rn concentration in the local groundwater was higher than the ^{222}Rn concentration in the middle of Barataria Basin at Jean Lafitte National Park (1666.7 Bq m^{-3}) (Inniss, 2002). The spatial variance of ^{222}Rn concentration in the local groundwater in the Mississippi River Delta may be due to the highly heterogeneous subsurface sediment layer consisting of a complex sediment composition (Martin and Whiteman, 1999).

Discussion

Groundwater inputs to swamps in Barataria Basin

Barataria Basin is covered by 95% of open water area with numerous swamp-forests and salt and freshwater marshes (Louisiana Department of Wildlife and Fisheries, 1988). Most swamps in the upper Barataria Basin are distributed nearby the Mississippi River natural levee (Chabreck and Linscombe, 1988). In order to investigate regional groundwater inputs to these various aquatic areas in the Barataria Basin, a total of 86 surface water samples were collected from bayous, swamps, and lakes in the Barataria Basin from May 2013 to April 2014 [Table 1]. Since most sampling areas were very well sheltered by the vegetation, ^{222}Rn atmosphere evasion was ignored for the ^{222}Rn box model approach (Burnett et al., 2010). In addition, the local ^{222}Rn sediment diffusion flux was determined for ^{222}Rn mass balance approach using a total of 21 sediment samples from five different regions in Barataria Basin [Figure 14]. After applying ^{222}Rn mass balance approach using input and output ^{222}Rn fluxes [Table 1], the spatial distribution of groundwater was plotted on the map [Figure 15]. Interestingly, most of the high groundwater discharge areas were located around the Mississippi River main channel with an average 2.1 cm day^{-1} groundwater seepage rate. The highest groundwater seepage rate was located in the upper Lake Salvador. According to USGS groundwater atlas (2010), the direction of subsurface groundwater around the New Orleans area is toward to the upper Lake Salvador area from the Mississippi River main channel. In addition, a groundwater study in the upper Lake Salvador has reported a relatively high groundwater seepage rate (maximum ~10 cm day^{-1}) compared to other research areas in Barataria Basin (Inniss, 2002). The few high groundwater seepage rates were also overlap with the distribution of abandoned courses and distributaries in the Mississippi River Delta [Figure 1]. However, most of high groundwater seepage rates were distributed along the Mississippi River main channel and the abandoned river channel and distributaries were rarely found. According to Louisiana Geological Survey (1973), the sandy subsurface point bar is distributed between the Mississippi River and the nearby swamps and the edge of the point bar is jointed to the nearby swamps. The maximum depth of the point bar is approximately 60 m below mean sea level and the thickness is decreased with increase of the distance from the Mississippi River main channel (Louisiana Geology Survey, 1972). Thus, this sandy subsurface sediment might play a role as a groundwater pathway between the Mississippi River and the swamps. Therefore, considering the distribution of the sandy aquifer, point bar, and its connection with bottom of numerous bayous and swamps around the upper Bayou Fortier, most of groundwater discharge might occur in the upper area of the Bayou Fortier by the high permeable sandy sediment layers near by the Mississippi River main channel. In addition, considering the distribution of high regional groundwater seepage rates based on the grab water samples data, the groundwater discharge might occur in these swamp areas along the Mississippi River natural levee. The average of groundwater seepage rate was 3.3 cm day^{-1} along the Mississippi River levee based on 42 grab water samples. This is equal to approximately 2.04×10^7 m^3 day^{-1} groundwater fluxes into the swamp area in the upper Barataria Basin. In addition, other potential influxes of groundwater in the lower part of Barataria Basin might make the total groundwater fluxes over the whole Barataria Basin increased.

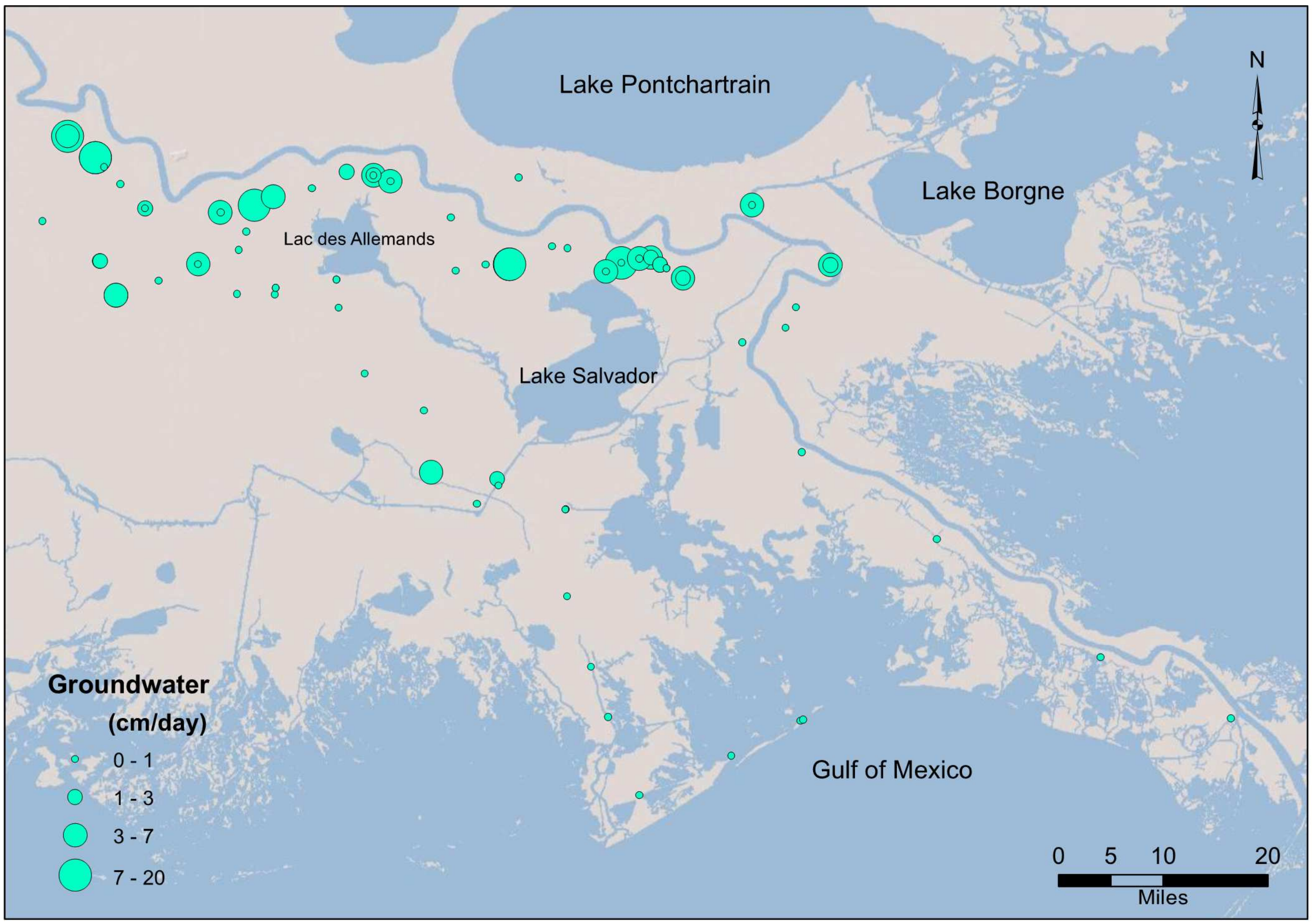

Figure 15. The distribution of local groundwater seepage rate in the Barataria basin in Mississippi River Delta (n=86). All surface water samples were collected from May 30, 2013 to April 15, 2014.

Table. 1 The parameters for the spatial groundwater calculation in Barataria basin.

Sample date	Sample ID	Latitude	Longitude	^{222}Rn Bq/m^3	^{222}Rn inventory Bq/(m^2 day)	Local sediment diffusion Bq/(m^2 day)	Local GW ^{222}Rn Bq/m^3	SGD input cm/day
5/30/13	ST. 1	-90.5939	29.8703	27.9	5.0	26.4	1193.6	0.0
5/30/13	ST. 2	-90.6778	29.8588	55.6	10.1	26.4	1193.6	0.0
5/30/13	ST. 3	-90.7289	29.9110	117.3	21.2	26.4	1193.6	0.0
5/30/13	ST. 4	-90.7189	29.9360	128.3	23.2	26.4	1193.6	0.0
5/30/13	ST. 5	-90.6816	29.9842	523.1	94.6	26.4	1193.6	5.7
5/30/13	ST. 6	-90.6285	29.9956	93.7	17.0	26.4	1193.6	0.0
5/30/13	ST. 7	-90.5801	30.0182	230.8	41.8	26.4	1193.6	1.3
5/30/13	ST. 8	-90.5431	30.0139	183.7	33.2	26.4	1193.6	0.6
5/30/13	ST. 9	-90.5195	30.0050	362.8	65.6	26.4	1193.6	3.3
5/30/13	ST. 10	-90.4363	29.9553	101.5	18.4	26.4	1193.6	0.0
6/3/13	ST. 8	-90.5431	30.0139	260.1	47.0	26.4	1193.6	1.7
6/3/13	ST. 11	-90.2747	29.9137	117.5	21.2	43.8	1816.7	0.0
6/3/13	ST. 12	-90.1596	29.9002	885.7	160.2	43.8	1816.7	6.4
6/6/13	ST. 1	-90.4300	29.8821	131.2	23.7	43.8	1816.7	0.0
6/6/13	ST. 2	-90.3882	29.8906	211.2	38.2	43.8	1816.7	0.0
6/6/13	ST. 3	-90.3549	29.8910	1464.1	264.9	43.8	1816.7	12.2
6/6/13	ST. 4	-90.2965	29.9158	69.3	12.5	43.8	1816.7	0.0
6/6/13	ST. 5	-90.2219	29.8813	939.5	169.9	43.8	1816.7	6.9
6/6/13	ST. 6	-90.2004	29.8931	2206.8	399.2	43.8	1816.7	19.6
6/6/13	ST. 7	-90.1760	29.8988	824.2	149.1	43.8	1816.7	5.8
6/6/13	ST. 8	-90.1470	29.8909	362.7	65.6	43.8	1816.7	1.2
6/6/13	ST. 9	-90.1379	29.8860	129.3	23.4	43.8	1816.7	0.0
6/6/13	ST. 10	-90.1155	29.8718	576.2	104.2	43.8	1816.7	3.3
6/10/13	VNO. 1	-89.3587	29.2650	146.0	26.4	25.9	2251.6	0.0
6/10/13	VNO. 2	-89.5385	29.3490	21.6	3.9	25.9	2251.6	0.0
6/10/13	VNO. 3	-89.7649	29.5121	20.0	3.6	25.9	2251.6	0.0
6/10/13	VNO. 4	-89.9517	29.6320	40.9	7.4	25.9	2251.6	0.0
6/10/13	VNO. 5	-90.0338	29.7840	154.5	28.0	25.9	2251.6	0.1
6/10/13	VNO. 6	-89.9117	29.8901	537.5	97.2	25.9	2251.6	3.2
6/10/13	VNO. 7	-90.0200	29.9731	217.1	39.3	25.9	2251.6	0.6
6/10/13	VNO. 8	-89.9736	29.8037	53.5	9.7	25.9	2251.6	0.0
6/10/13	VNO. 9	-89.9593	29.8316	82.6	14.9	25.9	2251.6	0.0
6/22/13	ST. 1	-90.4736	29.6888	39.6	7.2	26.4	1193.6	0.0
6/22/13	ST. 2	-90.5548	29.7406	129.8	23.5	26.4	1193.6	0.0
6/22/13	ST. 3	-90.5913	29.8313	40.3	7.3	26.4	1193.6	0.0
6/22/13	ST. 4	-90.5939	29.8703	79.0	14.3	26.4	1193.6	0.0

6/22/13	ST. 5	-90.6778	29.8588	92.8	16.8	26.4	1193.6	0.0
6/22/13	ST. 6	-90.6792	29.8499	66.6	12.0	26.4	1193.6	0.0
6/22/13	ST. 7	-90.7312	29.8507	140.0	25.3	26.4	1193.6	0.0
6/22/13	ST. 8	-90.7851	29.8912	396.2	71.7	26.4	1193.6	3.8
6/22/13	ST. 9	-90.8403	29.8684	70.4	12.7	26.4	1193.6	0.0
6/22/13	ST. 10	-90.8987	29.8486	355.7	64.3	26.4	1193.6	3.2
6/23/13	ST. 1	-90.9208	29.8953	317.4	57.4	26.4	1193.6	2.6
6/23/13	ST. 2	-91.0001	29.9504	207.3	37.5	26.4	1193.6	0.9
6/23/13	ST. 3	-90.9655	30.0674	1181.9	213.8	26.4	1193.6	15.7
6/23/13	ST. 4	-90.9271	30.0375	1040.4	188.2	26.4	1193.6	13.6
6/23/13	ST. 5	-90.9152	30.0249	195.4	35.3	26.4	1193.6	0.7
6/23/13	ST. 6	-90.8930	30.0018	165.6	29.9	26.4	1193.6	0.3
6/23/13	ST. 7	-90.8584	29.9678	148.9	26.9	26.4	1193.6	0.0
6/23/13	ST. 8	-90.7545	29.9624	404.2	73.1	26.4	1193.6	3.9
6/23/13	ST. 9	-90.8092	29.9818	56.2	10.2	26.4	1193.6	0.0
6/23/13	ST. 10	-90.9425	30.1283	64.6	11.7	26.4	1193.6	0.0
7/9/13	ST. 1	-90.4634	29.6044	527.5	95.4	25.9	2251.6	3.1
7/9/13	ST. 2	-90.3703	29.5859	27.6	5.0	25.9	2251.6	0.0
7/9/13	ST. 4	-90.2754	29.4332	193.1	34.9	25.9	2251.6	0.4
7/9/13	ST. 5	-90.2427	29.3355	25.6	4.6	25.9	2251.6	0.0
7/9/13	ST. 6	-90.2191	29.2668	47.4	8.6	25.9	2251.6	0.0
7/9/13	ST. 7	-90.1757	29.1589	45.2	8.2	25.9	2251.6	0.0
7/9/13	ST. 8	-90.0484	29.2136	3.1	0.6	25.9	2251.6	0.0
7/9/13	ST. 9	-89.9495	29.2633	64.3	11.6	25.9	2251.6	0.0
7/9/13	ST. 10	-89.9535	29.2616	90.3	16.3	25.9	2251.6	0.0
7/9/13	ST. 3	-90.2776	29.5530	6.5	1.2	25.9	2251.6	0.0
7/9/13	ST. 3-1	-90.2772	29.5532	33.5	6.1	25.9	2251.6	0.0
7/14/13	ST. 1	-90.7852	29.8913	86.5	15.6	26.4	1193.6	0.0
7/14/13	ST. 2	-90.8987	29.8486	475.4	86.0	26.4	1193.6	5.0
7/14/13	ST. 4	-90.9655	30.0674	577.0	104.4	26.4	1193.6	6.5
7/14/13	ST. 5	-90.9271	30.0375	609.7	110.3	26.4	1193.6	7.0
7/14/13	ST. 6	-90.8584	29.9678	340.1	61.5	26.4	1193.6	2.9
7/14/13	ST. 7	-90.7545	29.9624	106.5	19.3	26.4	1193.6	0.0
7/14/13	ST. 8	-90.7073	29.9721	650.0	117.6	26.4	1193.6	7.6
7/14/13	ST. 9	-90.5430	30.0138	403.7	73.0	26.4	1193.6	3.9
7/14/13	ST. 10	-90.5195	30.0049	32.5	5.9	26.4	1193.6	0.0
7/14/13	ST. 3	-90.9207	29.8953	287.7	52.0	26.4	1193.6	2.1
7/19/13	ST. 1	-90.3550	29.8911	1528.8	276.6	43.8	1816.7	12.8
7/19/13	ST. 2	-90.2219	29.8813	68.9	12.5	43.8	1816.7	0.0
7/19/13	ST. 3	-90.2004	29.8931	131.7	23.8	43.8	1816.7	0.0
7/19/13	ST. 4	-90.1759	29.8988	137.2	24.8	43.8	1816.7	0.0
7/19/13	ST. 5	-90.1595	29.9004	408.8	73.9	43.8	1816.7	1.7
7/19/13	ST. 6	-90.1470	29.8908	370.2	67.0	43.8	1816.7	1.3

7/19/13	ST. 7	-90.1380	29.8860	241.5	43.7	43.8	1816.7	0.0
7/19/13	ST. 8	-90.1156	29.8718	402.6	72.8	43.8	1816.7	1.6
7/19/13	ST. 9	-89.9117	29.8901	204.1	36.9	18.7	1816.7	1.0
7/19/13	ST. 10	-90.0200	29.9731	505.9	91.5	18.7	1816.7	4.0
4/15/14	st.1	-90.3425	30.0105	303.1	54.8	43.8	1816.7	0.6
4/15/14	st.2	-90.3721	29.5947	342.7	62.0	25.9	2251.6	1.6
4/15/14	st.3	-90.4002	29.5605	148.5	26.9	25.9	2251.6	0.0

Temporal ^{222}Rn signal variation in swamp & Bayou Fortier

To understand groundwater input to Bayou Fortier in the upper Barataria Basin, ^{222}Rn concentrations along the surface water surveys were plotted versus distance along the bayou reach [Figure 16]. Theses data indicate an exponential decrease occurs from the upper bayou to the confluence of the bayou and Lac des Allemands. Once high concentration of ^{222}Rn in groundwater originating from the point bar around the Mississippi River is released into the nearby swamps, groundwater ^{222}Rn activity exponentially decreases over the transit time due to radioactive decay (λ = 0.1809 day^{-1}), dilution, and atmospheric evasion across the water surface. Diffusion from the bottom sediments, water column particle re-suspension, and potential groundwater sources result in a concurrent increase of ^{222}Rn activity in the water column. Thus, the difference between the theoretical ^{222}Rn decay curve and a regression curve based on ^{222}Rn transect data indicates ^{222}Rn loss by water dilution and atmospheric evasion during the water transit time [Figure 16]. Furthermore, the ^{222}Rn regression curve contains ^{222}Rn sediment diffusion and excess ^{222}Rn, including ^{222}Rn sources from the potential groundwater and suspended particles in the water column. The evaluation of ^{222}Rn concentrations in the swamp in the upper Bayou Fortier can be made using the ^{222}Rn regression curve based on ^{222}Rn transect results in Bayou Fortier. Therefore, once the initial ^{222}Rn concentration in the swamp is determined, the groundwater flux into the Bayou Fortier can be examined using the ^{222}Rn concentration in local groundwater.

Although ^{222}Rn transect data collected in the 2013 to 2014 survey period in Bayou Fortier had a different seasonal variation of ^{222}Rn concentration, all ^{222}Rn concentrations exponentially decreased with increasing distance from the Mississippi River [Figure 16]. In addition, the trend of exponential ^{222}Rn concentration curves fluctuated depending on the ^{222}Rn measurement dates in Bayou Fortier. Based on the ^{222}Rn survey in Bayou Fortier, there is a significant groundwater discharge around the upper Bayou Fortier rather than the lower part of the bayou [Figure 16]. Most ^{222}Rn sources in the lower Bayou Fortier might come originally from the upper Bayou Fortier. In addition, Y-intercept of the each evaluated ^{222}Rn regression curve, which is corresponding to original ^{222}Rn concentration in the swamp, was different depending on the survey date. Considering the nature of the swamp area in the upper Bayou Fortier, which is very well sheltered by vegetation from the wind and connected to the subsurface point bar, the temporal fluctuations of ^{222}Rn concentration in the swamp might be related to the groundwater input controlled by the seasonal change of the Mississippi River water stage. In particular, groundwater seepage rate in a swamp located near upper Bayou Fortier has a very similar value (1.9 cm day^{-1}) compare to estimated ^{222}Rn groundwater seepage rate in the swamp located in the upper Bayou Fortier using a ^{222}Rn regression curve (2.1 cm day^{-1}). This indicates that the applying ^{222}Rn regression curve is a reliable approach to evaluate the temporal change of original ^{222}Rn source in the swamp. Therefore, the relationship between the change of ^{222}Rn concentration and the Mississippi River water stage can be explained using the regression curve approach.

The groundwater discharge flux into one of the swamps in Barataria Basin was calculated using the average local groundwater ^{222}Rn concentration (1193.6 Bq m^{-3}). As a result, the highest groundwater seepage rate was 14.6 cm day^{-1} on April 17, 2014. The smallest groundwater flux was on September 29, 2014 with 0.4 cm day^{-1}. The average groundwater seepage rates in 2013 and 2014 were 4.5 cm day^{-1}. This groundwater seepage rate is same to previous results of 4.5 cm day^{-1} at a Barataria preserve, Jean Lafitte National Park (Inniss, 2002). According to a Louisiana

Geological Society report (1989), the groundwater seepage rate through the upper sand sediment layer in the lower Louisiana aquifer system is 10.8 cm day^{-1}. Considering the range of groundwater seepage rate based on the two years data, our result well reflects the regional groundwater seepage rate in Barataria Basin.

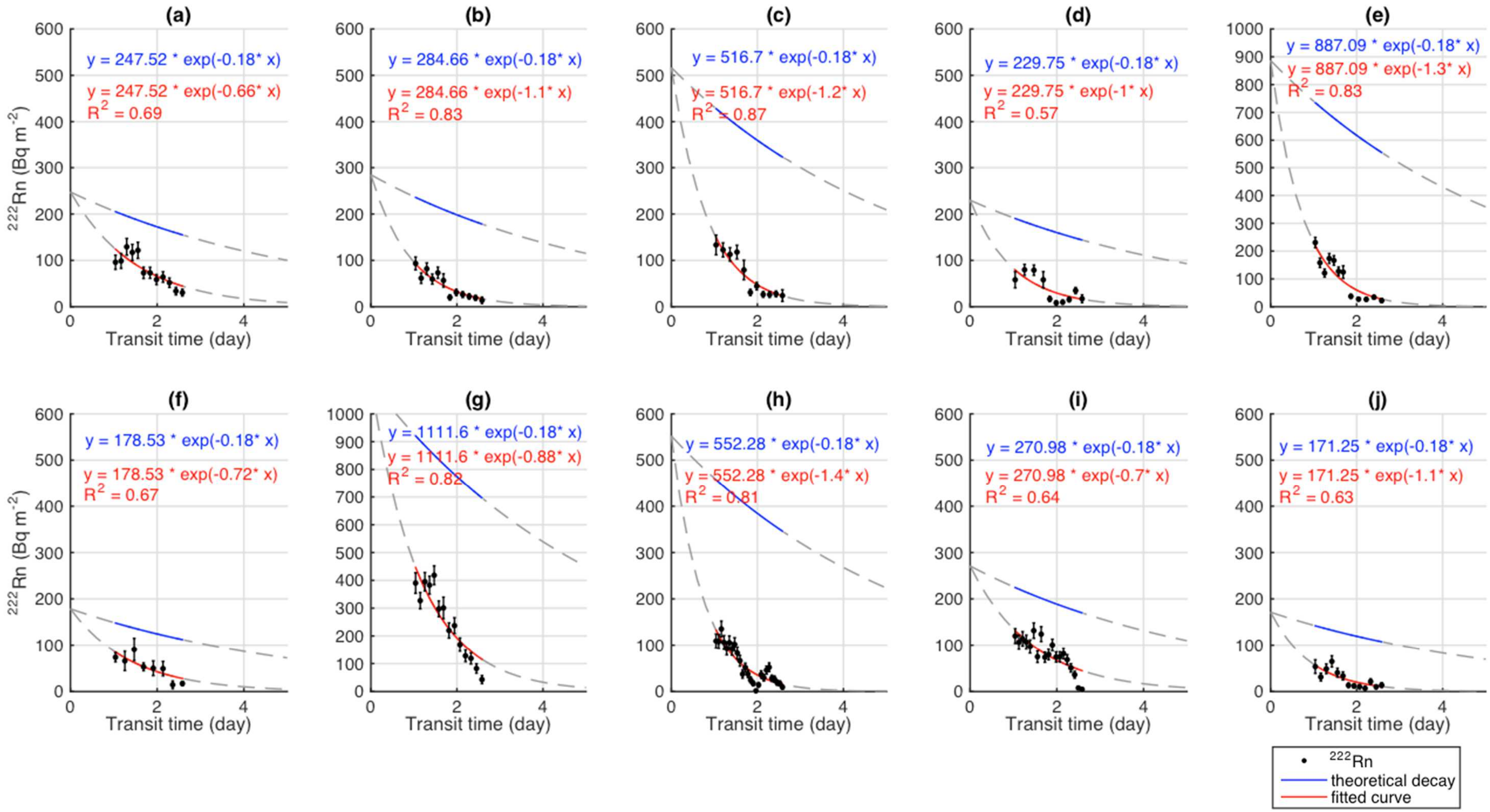

Figure 16. ^{222}Rn activity trends in Bayou Fortier versus water transit time during April, 2013 ~ September, 2014 ^{222}Rn survey. The solid blue curve represents ^{222}Rn theoretical decay (^{222}Rn decay constant 0.18 day^{-1} used for exponential regression curve fitting) as a function of water transit time and the red line indicates an exponential fitting curve based on ^{222}Rn survey data as a function of water transit time. An average water velocity of 2.25 cm sec^{-1} (n=6, June 2014) was used for the ^{222}Rn flux calculation.
(a): April 23, 2013 **(b)**: May 18, 2013 **(c)**: June 17, 2013 **(d)**: June 25, 2013 **(e)**: July 30, 2013 **(f)**: September 29, 2013 **(g)**: April 17, 2014 **(h)**: June 17, 2014 **(i)**: June 18, 2014 **(j)**: September 25, 2014.

Table 2. The parameters for groundwater calculation in the upper swamp using Y-intercept of evaluated ^{222}Rn regression curves.

Sample date	Latitude	Longitude	Y-intercept of ^{222}Rn regression curve	^{222}Rn inventory	*Local sediment diffusion	**Local GW ^{222}Rn	SGD input
			Bq/m²	*Bq/(m² day)*	*Bq/(m² day)*	*Bq/m³*	*cm/day*
4/23/13	-90.5376	30.0103	247.5	44.8	26.4	1193.6	1.5
5/18/13	-90.5376	30.0103	284.7	51.5	26.4	1193.6	2.1
6/17/13	-90.5376	30.0103	516.7	93.5	26.4	1193.6	5.6
6/25/13	-90.5376	30.0103	229.8	41.6	26.4	1193.6	1.3
7/30/13	-90.5376	30.0103	887.1	160.5	26.4	1193.6	11.2
9/29/13	-90.5376	30.0103	178.5	32.3	26.4	1193.6	0.5
4/17/14	-90.5376	30.0103	1111.6	201.1	26.4	1193.6	14.6
6/17/14	-90.5376	30.0103	552.3	99.9	26.4	1193.6	6.2
6/18/14	-90.5376	30.0103	271.0	49.0	26.4	1193.6	1.9
9/25/14	-90.5376	30.0103	171.3	31.0	26.4	1193.6	0.4

* The average of ^{222}Rn sediment diffusion flux from total ten sediment samples from the Lac des Allemands.

** Total 5 local groundwater samples were analyzed and averaged.

Control factors of groundwater fluxes

Typically, Mississippi River water stage increases annually during the spring and decreases during late summer (Milliman and Mead, 1983). During the ^{222}Rn survey periods, the Mississippi River water stage exhibited a typical annual pattern [Figure 17]. The groundwater elevation in the wells located along the Mississippi River natural levees has been reported a relationship between seasonal groundwater elevation change and the Mississippi River water stage change (Louisiana Geological Survey, 1972, 1973; USGS technical report, 2010). Additionally, the distribution of high groundwater seepage rate and an increasing trend of ^{222}Rn concentration around the upper Bayou Fortier indicate the local groundwater inputs in the swamp areas around the upper Bayou Fortier. Considering the ^{222}Rn concentration in groundwater, 3 - 4 orders of magnitude higher than the surface water, the seasonal variation of ^{222}Rn concentration in the swamp water might be related to the local groundwater input (Cable et al., 1996; Corbett et al., 1997; Burnett and Dulaiova, 2003; Burnett et al., 2010). The groundwater fluxes in the swamp based on ^{222}Rn mass balance calculations showed slightly delayed responses to changes of the Mississippi River water stage and the hydraulic head in two local farmland USGS wells [Figure 17]. This lag response time of groundwater between the seasonal change of groundwater seepage rate in the swamp and the seasonal change of Mississippi River water stage might be explained by the distance between the Mississippi River main channel and the nearby swamps (approximately 3 km). Therefore, the local groundwater discharge in the swamp in the upper Bayou Fortier is potentially related to the Mississippi River water change with a delayed response time.

The hydraulic mechanism of this research area, Baratarian Basin, might be explained two different scenarios based on the geological nature of the Mississippi River Delta. The first possible scenario is the numerous relic river channels in the Mississippi River Delta. The Mississippi River delta has been formed by main river channel avulsions and contained numerous abandoned relic river channels with sandy sediment layers [Figure 1]. Considering the distribution of buried sandy sediment layers and its role as a connection between the Mississippi River channel and nearby aquatic environment such as swamp, bayou, and marshes in the Baratarian Basin, the relic river channel might a potential groundwater conduit in the Mississippi River Delta. The second possible scenario is a shallow aquifer, point bar. According to the Louisiana Geological Survey 1972, a shallow aquifer, point bar, is located beneath the Mississippi River main channel containing a fresh groundwater [Figure 18]. In addition, the seasonal hydraulic head change of groundwater elevation in the local wells is clearly response to the change of the Mississippi river water stage (Louisiana Geological Survey, 1973). Thus, this high permeable sediment layer, point bar, might be another potential groundwater pass way between the Mississippi River main channel and nearby swamps [Figure 18].

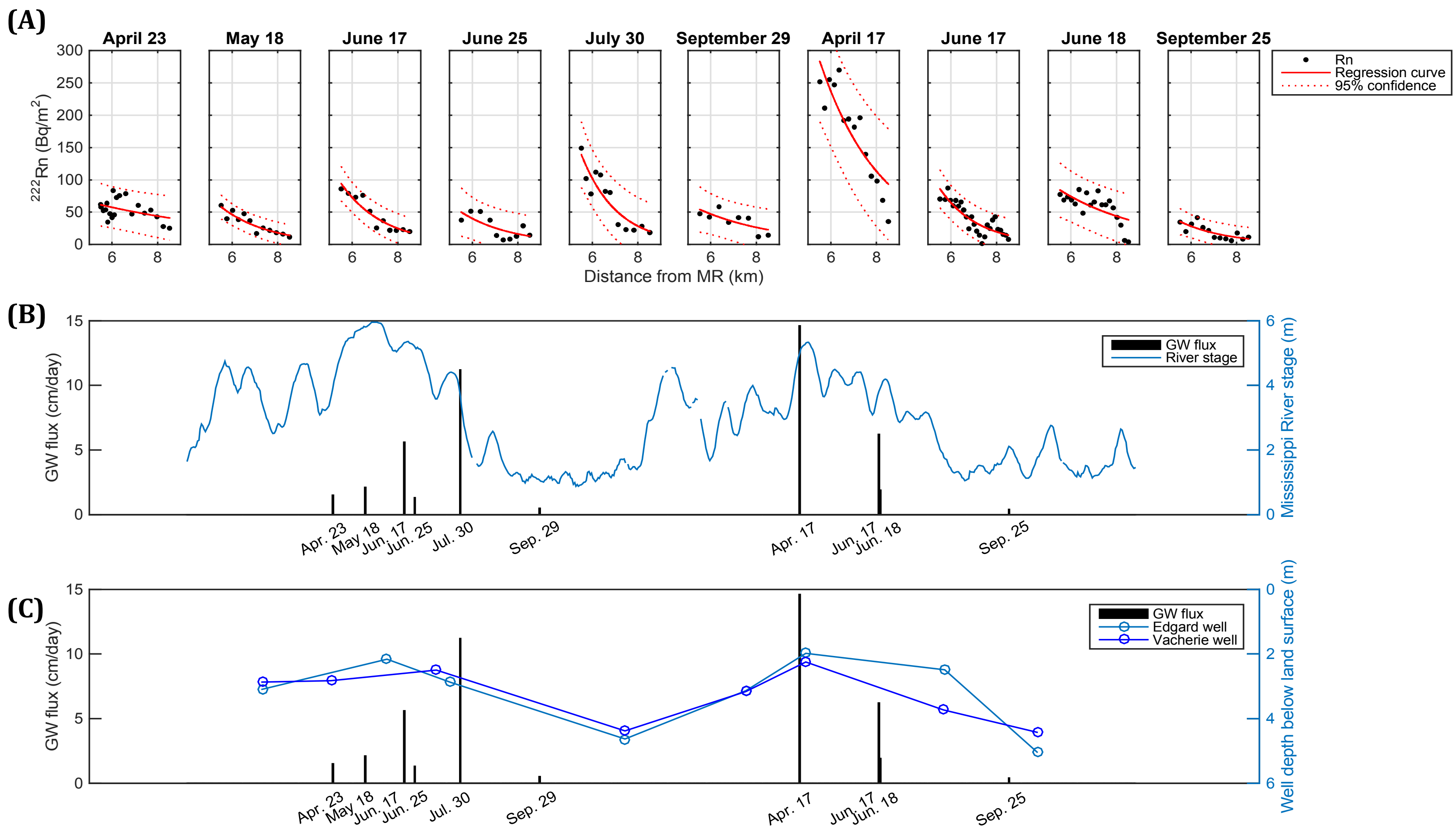

Figure 17. **(A)** A ^{222}Rn inventory trend as a function of distance from the Mississippi River, **(B)** a comparison between calculated groundwater seepage rates at each survey date and the Mississippi River stage change, and **(C)** a hydraulic head change in farmland well versus calculated groundwater seepage rates using ^{222}Rn mass balance. *Groundwater elevation data from USGS (Edgard well - Latitude: 30°02’34” Longitude: 90°39’03”; Vacherie well - Latitude: 30°00’24” Longitude: 90°43’35”, www.waterdate.usgs.gov)

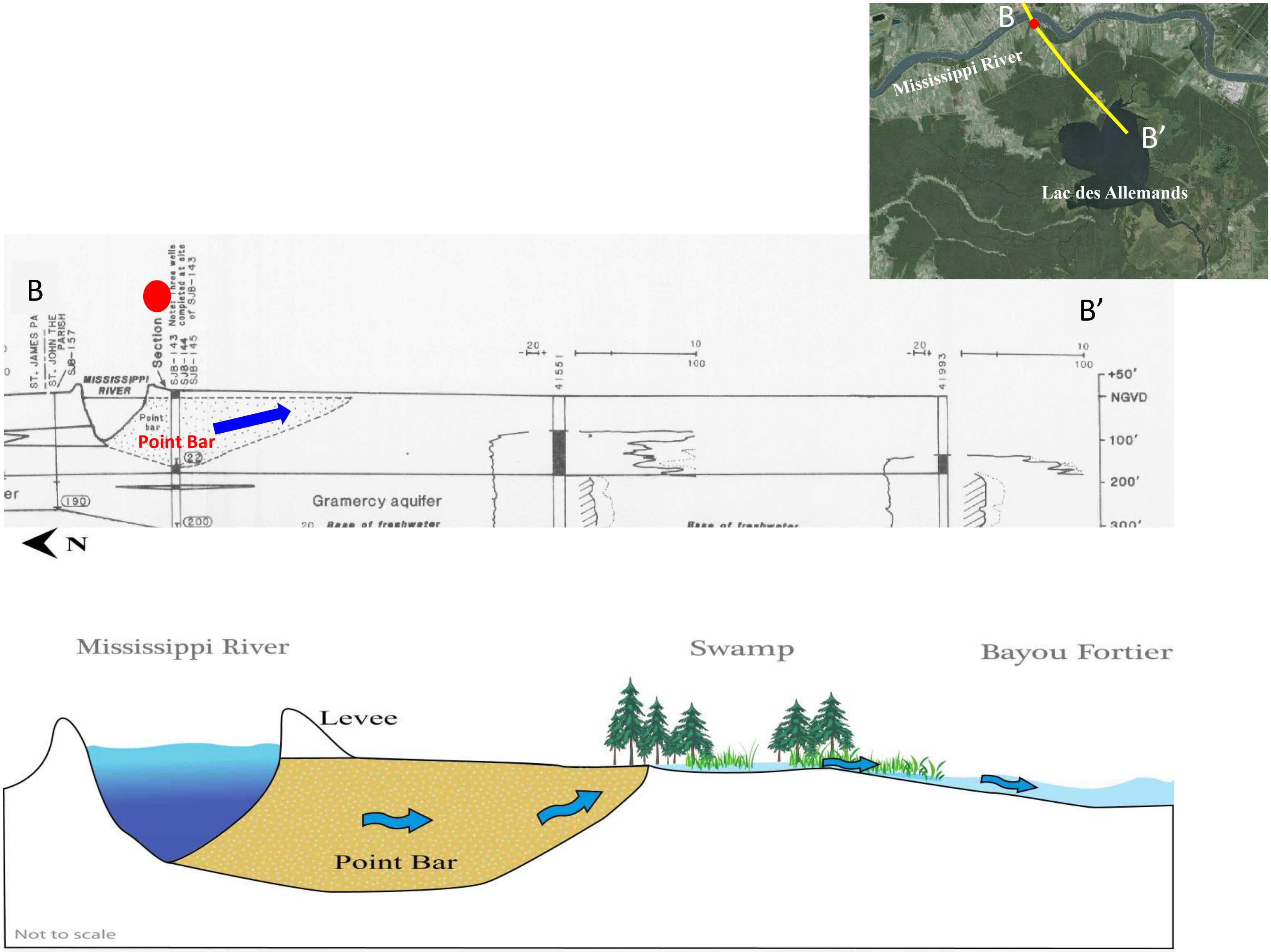

Figure 18. A cross section in the upper Baratarian Basin (USGS, 1980) and a diagram of hydraulic connection between the Mississippi River and nearby swamps. Note that each blue arrow indicates a possible groundwater flow from the Mississippi River to the swamp.

Comparison with other research areas

Previous studies in other areas around Gulf of Mexico indicate slightly different groundwater seepage rates depending on research locations [Table 3]. For discussion purposes, previous studies are subdivided into four zones: east of Gulf of Mexico (Florida Bay), northeast of Gulf of Mexico (Turkey Point FL), north of Gulf of Mexico (Mississippi River Delta), and northwest of Gulf of Mexico (southern part of Texas Bay). Corbett et al. (1999) reported the groundwater seepage rate in Florida Bay along the Keys, the north coast, and the mid-bay, using seepage meter. Their results for each area have slightly different groundwater seepage rates of 21.2 ± 5.2 ml m^{-2} min^{-1} (n=17), 7.2 ± 2.5 ml m^{-2} min^{-1} (n=6), and 13.4 ± 2.3 ml m^{-2} min^{-1} (n=10), respectively. However, after correcting these seepage rates to velocity units, the range of groundwater velocity, 1 to 3 cm day^{-1}, was very similar with a groundwater velocity, 1.2 to 1.7 cm day^{-1}, evaluated by ^{222}Rn tracer (Top et al., 2001). The groundwater seepage rates in the northeast of the Gulf of Mexico coastal area were highly variable with ranging from 1.4 to 50 cm day^{-1} and strongly influenced by tides [Table 3]. The groundwater seepage rates in the southern part of Texas Bay including Nueces Bay, Copano Bay, and Baffin Bay were examined by using ^{226}Ra and ^{228}Ra. The range of groundwater seepage rates, 0.2 to 0.4 cm day^{-1}, was at maximum two orders of magnitude lower than a groundwater seepage rate in the north east coast of Gulf of Mexico. This might be due to the difference of geological sediment distribution between the northeast coast and northwest of Gulf of Mexico. Interestingly, previous studies in the Mississippi River Delta area have slightly different groundwater seepage rates between offshore and onshore of the Mississippi River Delta [Table 3]. The range of groundwater seepage rates in coastal areas along the Mississippi River Delta was from 0.1 to 2.5 cm day^{-1} and the groundwater seepage rates in the landward Mississippi River Delta was from 4.5 cm day^{-1}. This might be related with the heterogeneity and high porosities of subsurface sandy sediment layer distributions onshore of the Mississippi River Delta. Overall, even though the groundwater seepage rates in the coastal area of the Gulf of Mexico were highly variable depending on their locations, the regional groundwater seepage rates show a very similar range of groundwater velocities. Therefore, the geological subsurface sediment distribution and local hydrological system might play a significant role in the groundwater discharge along the Gulf of Mexico coastal zones.

Table 3. A comparison between the groundwater seepage rates in Mississippi River Delta with other estuaries.

Location	**Groundwater seepage rate**	**Method**	**Reference**
	cm day^{-1}		
Florida Bay	1-3	Seepage meter	Corbett et al., 1999
	1.2-1.7	^{222}Rn	Top et al., 2001
Northeast Gulf of Mexico (FSU marine Lab)	1.4-11.5	CH_4	Bugna et al., 1996
	2-10	^{222}Rn	Cable et al., 1996a
	5-50	^{222}Rn	Lambert and Burnett 2003
Nueces Bay, Texas	0.4	^{226}Ra, ^{228}Ra	Breier and Edmonds 2007
Copano Bay, Texas	0.3	^{226}Ra, ^{228}Ra	Breier et al., 2010
Baffin Bay, Texas	0.2	^{226}Ra, ^{228}Ra	Breier et al., 2010
Louisiana Continental shelf (MR and AR)	1	^{226}Ra, ^{228}Ra	Krest et al., 1999
Continental shelf of MR-BFD	2.5	^{223}Ra, ^{224}Ra	Moore and Krest 2004
Continental shelf west of MR	0.1	H/He, ^{222}Rn	McCoy et al., 2007b
JL National Park swamp	4.5	^{222}Rn	Inniss. 2002
Lac des Allemands marsh	0.003-1.9	Darcy's value	Breaux, *in prep.*
Barataria Basin	**2.1**		
Bayou Fortier swamp	**0.4 – 14.6**	**^{222}Rn**	**This study**
Swamps along the MR	**3.3**		

Conclusions

Over the last two decades, submarine groundwater discharge (SGD) has been recognized as a significant coastal process that transports terrestrial freshwater, nutrients, and anthropogenic contaminants to the ocean (Burnett, 1999). Globally, total influxes of terrestrial SGD to the ocean are equal to 5 to 10 % of the annual global river water discharge into the ocean (Burnett et al., 2001, 2003, 2006; Moore, 1999, 2010; Zekster and Loaiciga, 1993). According to Bokuniewicz (1980) and Bokuniewicz and Pavlik (1990), the subsurface groundwater discharge in the Great South Bay, New York is greater than 20% of the surface freshwater inputs to the bay. Furthermore, a myriad of SGD research has reported the biogeochemical transport of SGD and its ecological impacts on the aquatic systems. For example, Valiela et al., (1978, 1992, 2002) suggested that groundwater nutrient inputs to salt marches are critical to the overall nutrient composition in the salt march area. The SGD nutrient inputs into eastern Florida Bay was equal to the nutrient inputs via surface freshwater runoffs (Corbett et al., 1999, 2000). These rich nutrient supplies via SGD to the ocean might create a possible scenario, in which SGD cause harmful algae blooms in the ocean (Laroche et al., 1997; Hwang et al., 2005). However, most of the previous SGD studies were performed in confined coastal zones, rather than deltaic areas. According to Roberts (1997), deltas are a center for terrestrial sediment deposition. The consecutive transportation via river water runoffs develops complex sediment layers in the subsurface of the delta and directly exports terrestrial nutrients and carbon to the ocean (Michalopoulos and Aller, 1995; Burdige, 2005). In particular, several recent SGD studies have reported large volume of SGD inputs through the deltaic area (Basu et al., 2001; Peterson et al., 2009).

This research shows that groundwater discharge to the Bayou Fortier, a sub-bayou in the Mississippi River Delta, has a range from 0.4 to 14.6 cm day^{-1} using a radon mass balance. For this seepage rate, I estimate an average daily groundwater fluxes to the Bayou Fortier is approximately 2.2×10^4 m^3 day^{-1}. When I compare this flux to the entire upper Barataria Basin estimates based on surface water sampled along the Mississippi River, the average groundwater seepage rate is 3.3 cm day^{-1} and the total groundwater flux is 2.0×10^7 m^3 day^{-1}. In addition, the groundwater seepage rate in the entire Barataria Basin averaged 2.1 cm day^{-1} based on total 86 grab water samples and the daily groundwater fluxes to the entire Barataria Basin is 1.3×10^8 m^3 day^{-1}. The seasonal fluctuation of groundwater discharge into the Bayou Fortier is mostly controlled by the seasonal Mississippi River water stage with a lag time.

APPENDIX 1: DISTRIUBUTION OF DOC AND TN

Preparation of water sampling for DOC & TN

All surface water samples were collected using 500 ml Nalgene bottles for dissolved organic carbon (DOC) and total nitrogen (TN) analysis. Bottles were prepared by rinsing with DI water and nanopure (18.1 MΩ ionic purity) water in the laboratory prior to sample collection. Surface water was also collected using a peristaltic pump (Geo Tech®) into glass scintillation vials (20 ml) for later analysis of the stable isotopes $\delta^{18}O$ and δD. To reduce the air space in the sampling vial, each water sample was gently overflowed and then capped simultaneously. All collected water samples were immediately stored in coolers in the field and later transferred to a refrigerator in the laboratory to reduce any high temperature impact.

Prior to sample collection, all glass vials for DOC and TN samples were prepared by soaking in a bath of 10% HCl solution for at least 24 hours and rinsed 3 times with nanopure water. Vials were then baked at 500°C for 6 hours and capped with baked aluminum foil individually and stored until needed. All collected surface water samples were filtered in the field using a GFF filter, binder free 47 mm glass microfiber, 0.7 μM. Before filtering water samples, all filters were fired in a muffle furnace at 500°C for approximately 6 hours to combust organics. After filtering water samples, each water sample was divided into two amber glass vials (each 40 ml) and two transparent glass vials (each 40 ml) and capped with an acid washed Teflon® sheet and then frozen.

Distribution of DOC and TN

A total of 71 bayou and Mississippi River surface water samples were collected from May to July 2013 to elucidate the geographical distribution of ^{222}Rn, dissolved organic carbon (DOC), and total nitrogen (TN) concentrations around Barataria Basin. The spatial distribution of DOC had a range from 265.5 to 3332.5 μM with the highest DOC concentrations located around urban areas or industrial complexes [Figure 19]. High TN concentrations were also found near urban or farmland areas with a range from 24.2 to 300.6 μM [Figure 19].

Groundwater has been well known to be a source of nutrients and anthropogenic contaminants to the coastal ocean (Krest et al., 2000; Bone et al., 2007; Santos et al., 2009). Recent groundwater studies have reported significant carbon and nitrogen transportation via groundwater into the coastal area such as North Inlet, SC and northeast of Gulf of Mexico (Goñi & Gardner. 2003; Santos et al., 2008; Santos et al., 2009). In this study, all groundwater ^{222}Rn, DOC, and TN of farmland wells, wetland wells, and seepage show a linear relationship ($y = 1.16x - 1.5; R^2 = 0.6$) among all parameters [Figure 20]. Additionally, the groundwater samples collected from the coastal salt marsh wells (Mytle Grove; Figure 20), fresh wetland wells (Lac des Allemands; Figure 20), and farmland wells (Edgard well; Figure 20) contained high concentrations of ^{222}Rn, DOC, and TN. The salt marsh wells had the highest range of DOC (3077.85 ± 1281.17 μM), TN (1362.72 ± 841.71 μM), and ^{222}Rn (3914.46 ± 4229.25 Bq m^{-3}) [Figure 20]. The coastal groundwater samples salinity range was from 4.36 to 16.26, which is higher than the bayou and wetland ground water samples due to seawater intrusion (Day et al., 2000). The groundwater samples from the fresh wetland wells had a relatively large range of DOC and TN. The maximum and minimum DOC were 9770.83 μM and 970.83 μM, respectively, and the maximum and minimum TN were 1298.93 μM and 71.79 μM, respectively. DOC in groundwater samples havs a higher range (581.96 μM to 9770.83 μM) than the Mississippi River water (261.79 μM to 320.38 μM). In addition, these DOC concentrations were considerably higher than Barataria estuary (200 to 300 μM) and marsh creeks in the Terrebonne-Timbalier Bay estuary (500 to 700 μM) (Wysocki et al., 2006; Bianchi et al., 2009). A previous study in the lower Mississippi River and inner Louisiana shelf showed significantly high concentration of nutrients and DOC in the sediment pore water (Sutula et al., 2004). Thus, the groundwater in Barataria Basin not only contains high concentration of ^{222}Rn, DOC and TN, but also transports high concentration of DOC and TN to the subterranean estuary in the Mississippi River Delta.

According to the Louisiana Geology Report (1973), a subsurface sediment layer near by the Mississippi River main channel is directly connected to the main river channel by the point bar. We found visible groundwater seepage on a New Orleans road (4913 N Galvez St., New Orleans, LA 70117; Latitude: 29.97, Longitude: -90.02) located approximately 200 m from the Mississippi River main channel. There we measured for ^{222}Rn, DOC, and TN. As a result, DOC and TN were similar (283.42 ± 11.89 μM for DOC, 275.07 ± 13.1 μM for TN) to Mississippi River water (288.19 ± 10.25 μM for DOC, 290.3 ± 28.1 μM for TN). Additionally, water was also collected from a small natural pond (surface area of approximately 400 m^2; average depth: 1.5 m) located near the main Mississippi River channel (Latitude: 29.89, Longitude: -89.91) to elucidate the connection between the Mississippi River and nearby a natural pond. DOC and TN in the pond water samples were 319 ± 16.72 μM and 223.86 ± 14.11 μM, respectively, and are similar values to the Mississippi River. Therefore, based on physicochemical data, the numerous wetlands distributed near by the Mississippi River main channel may be directly connected with the Mississippi River.

DOC and TN concentrations of Mississippi River Delta groundwater were considerably higher than the DOC and TN concentrations measured in surface water of the bayou water, lake water, and seawater. According to DeLaune et al. (2008), the large area of organic marsh soil and the variety of plant materials are the main sources of DOC in the Mississippi River Delta. Additionally, sediment pore water in the Mississippi River Delta contains high gradients of DOC and TN (Sutula et al., 2004). Therefore, physiochemical processes such as advection or diffusion may be able to transport accumulated high DOC and TN into the surface water.

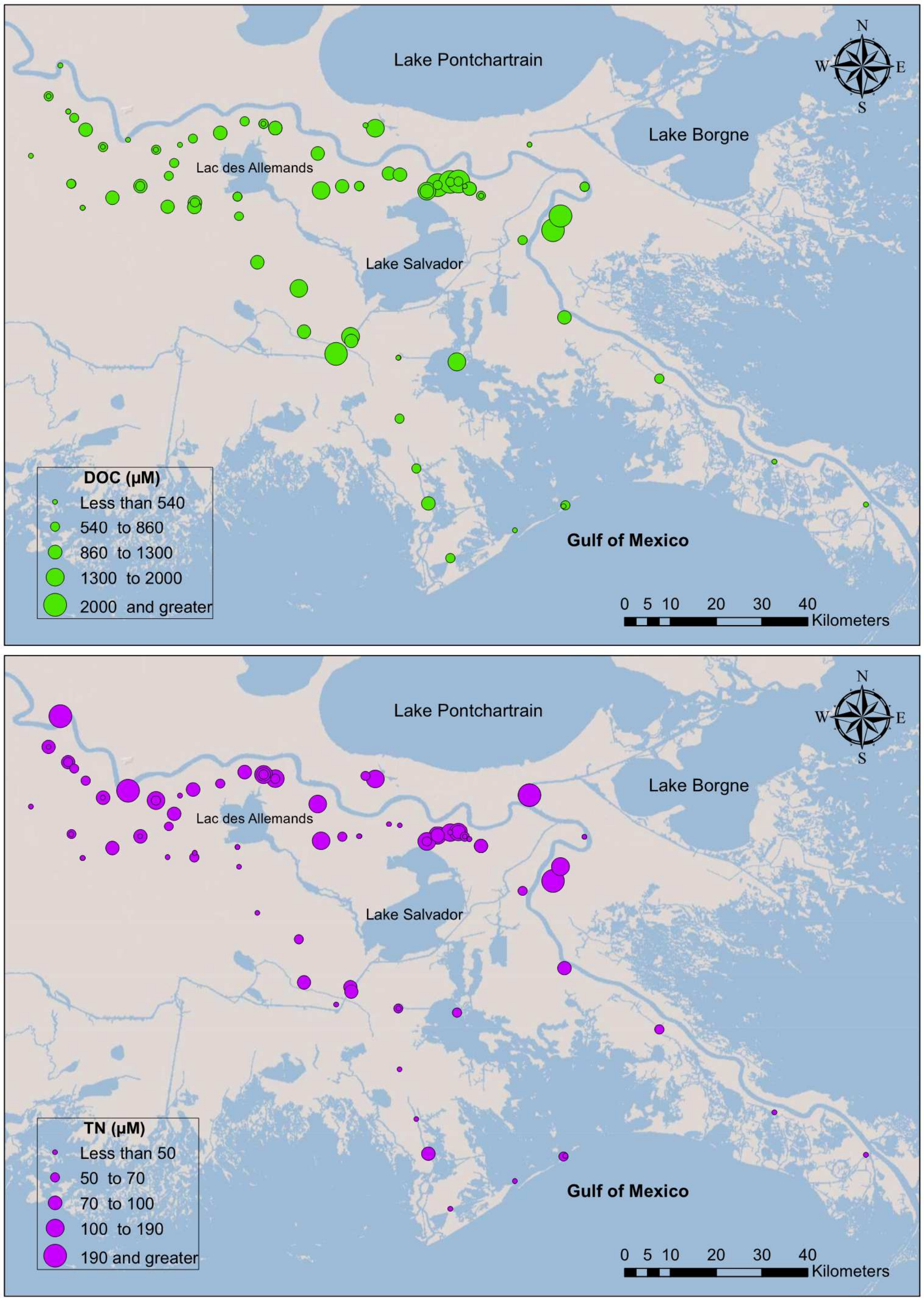

Figure 19. The distribution of dissolved organic carbon and total nitrogen in Barataria Basin. Note that ^{222}Rn distribution is presented in the main thesis.

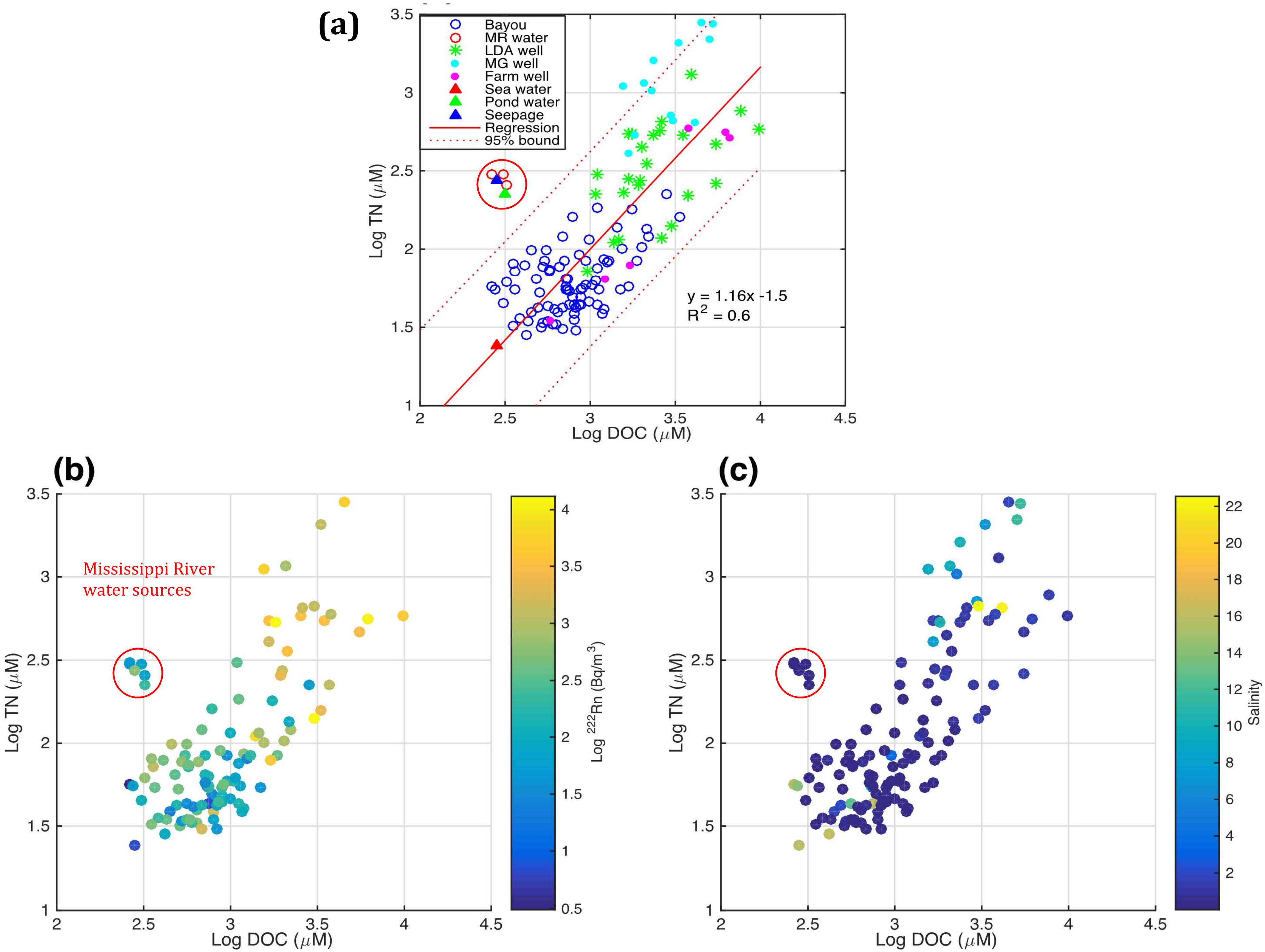

Figure 20. Comparison among ^{222}Rn, DOC, and TN concentration in total water samples including bayou and land groundwater and their relationship with salinity. **(a)** DOC (μM) vs. TN (μM) in bayou, Mississippi River, farm land well, wetland well, pond water, and Gulf of Mexico seawater **(b)** DOC (μM) vs. TN (μM) with change of ^{222}Rn concentration (Bq m^{-3}) **(c)** DOC (μM) vs. TN (μM) with change in salinity. Note that all data were normalized by the log-scale for the comparison except salinity.

APPENDIX 2: DISTRIBUTION OF STABLE ISOTOPES

δ^{18}O, δD, and d-excess distribution in precipitation, surface water, and groundwater

The concentrations of stable isotopes and the salinity of surface water, groundwater, Mississippi River water, precipitation, and Gulf of Mexico seawater are listed in Table 4. A total of 29 lake water samples were collected during three different sampling periods (July and September, 2013 and February, 2014) with salinities of 0.072±0.02, 0.081±0.007, and 0.11±0.02, respectively. Lake water salinity concentration slightly increased, depending on season. The range of δD and δ^{18}O values were from -13 ‰ to 2.9 ‰ (mean: -4.3 ‰) and -2.1 ‰ to 1.3 ‰ (mean: 1.1 ‰), respectively. Although most of δD and δ^{18}O values in the lake water samples followed closely to the Global Meteoric Water Line ($GMWL; \delta D = 8 \cdot \delta^{18}O + 10$) of Craig (1961), the linear model ($\delta D = 4.3 \cdot \delta^{18}O + 0.39;\ R^2 = 0.8$) had a shallower slope than the GMWL slope. Similarly, the linear model of the bayou water samples showed a shallow slope ($\delta D = 3.9 \cdot \delta^{18}O - 0.66;\ R^2 = 0.8$) when compared to GMWL slope.

A total of 22 groundwater samples, which consisted of farmland groundwater (n=4) and wetland (n=18) groundwater, were collected from 2 farmland wells and 9 wetland wells located in Barataria Basin between the Mississippi River and Lac des Allemands. Most δD and δ^{18}O samples of wetland groundwater fall close to and below the GMWL and the linear model has a relatively steep slope ($\delta D = 6.6 \cdot \delta^{18}O - 4.5;\ R^2 = 0.9$). The δD and δ^{18}O data distribution of wetland groundwater were -12.4 ‰ to 3.4 ‰ for δD and -2.5 ‰ to -0.2 ‰ for δ^{18}O. These ranges are relatively higher than the δD and δ^{18}O values measured in farmland groundwater, which were -20.2 ‰ to -11.4 ‰ for δD and -4.3 ‰ to -2.1 ‰ for δ^{18}O.

The average of δD (-7.9 ‰) and δ^{18}O (-2.0 ‰) in the wetlands were higher than the farmland groundwater δD (-17.4 ‰) and δ^{18}O (-3.5 ‰). All precipitation data formed a cear parallel trend to GMWL with only a small gap [Figure 4]. The distribution of δD and $\delta^{18}O$ of the Mississippi River water samples ranged from -43.4 ‰ to -35.7 ‰ and from -6.9 ‰ to -5.6 ‰ with the lowest mean values of δD (-39.8 ‰) and $\delta^{18}O$ (-6.3 ‰), respectively.

Deuterium excess (d-excess) is defined as a deviation between the stable isotope values and the GMWL line [Equation 18] (Dansgaard, 1964). This value is broadly used to identify local moisture sources.

$$d = \delta D - 8 \cdot \delta^{18}O \qquad \text{Equation 18}$$

d is deuterium excess in ‰, δD and $\delta^{18}O$ are the hydrogen-2 and oxygen-18 isotopic compositions. Although the *d* of global meteoric waters is close to 10, it varies between geographic regions (Cappa et al., 2003). The calculated d-excess of precipitation data points proportionally increased with an increase of $\delta^{18}O$ values. However, all water samples including the lake, bayous, wells and river water have an inversely proportional relationship between the deuterium excess and $\delta^{18}O$ [Figure 4]. Each *d* has a different data point depending on the season. In particular, Mississippi River water samples formed an isolated group based on the relationship between d-excess and $\delta^{18}O$ with a range of d-excess (9.5 to 11.7 ‰) and $\delta^{18}O$ (-6.9 to -5.6 ‰). Mississippi River water samples were also split into two different groups depending on the sampling time (June and July 2013). The calculated d-excess of water samples, except the precipitation and the Mississippi River water samples, exhibit a similar inverse relationship with $\delta^{18}O$.

Characteristics of $\delta^{18}O$, δD, and d-excess and their implications

The Global Meteoric Water Line (GMWL) has been well recognized and utilized as a significant indicator to understand the hydrological cycle using $\delta^{18}O$ and δD isotopic composition of water (Craig, 1961; Rozanski et al., 1993). $\delta^{18}O$ and δD relationship with the GMWL also represents the local climatic conditions such as geographical variation (Hoefs, 1996). The $\delta^{18}O$ and δD composition of precipitation is related to several climatic factors such as isotope composition of the vapor source, fractionation due to the intrusion of water vapor into air masses, and the formation of precipitation (Dillon and Chanton, 2008).

In this study, all precipitation samples (n=4) were collected between May and July 2014 during the early summer. As result, the $\delta^{18}O$ and δD compositions of the precipitation samples plotted above the GMWL, which indicates that arid vapor sources contributed for the formation of this precipitation [Figure 4]. This can be attributed to a difference in air temperature. The δD and $\delta^{18}O$ compositions of Mississippi River water were significantly isolated. The average Mississippi River water $\delta^{18}O$ composition was calculated as -6.3 ‰ (July and June 2013), which was heavier than previous measurements of -8.3 ‰ (March 1979), -7.8 ‰ (March 1983), and -6.9 ‰ (March 1988) (Gerard and Paul, 1990) for the Mississippi River in St. Francisville, La. The deviation between this study and previous research values may be due to different seasonal air temperature. Additionally, all surface water samples including lake water, bayou water, and seawater, show enrichment of the heavy isotopes in each sample. This may be due to a high evaporation effect on the water samples (Abass et al., 2010).

Four groundwater samples were collected from two farmland wells, which were located north of Bayou Fortier, Edgard well, and west of Lac des Allemands, Vacherie well. The δD and $\delta^{18}O$ compositions in the groundwater samples varied depending on the sampling date and location. One set of groundwater δD and $\delta^{18}O$ values in the groundwater sample had a similar composition to most bayou surface water, bayou groundwater, and lake water. Other groundwater samples had intermediate isotope values between the precipitation and Mississippi River water [Figure 4 (a)]. This indicates that some local groundwater is possibly a combination of precipitation and the Mississippi River water depending on the well distance from the Mississippi River. Furthermore, based on these stable isotopes data, the regional bayou groundwater contributes to the nearby wetland and lake water body.

The *d* composition of precipitation had a very narrow linear increasing line with a range of 13.96 ‰ to 16.90 ‰ [Figure 4 (b)]. This indicates that the origin of precipitation was high moisture in the air (Abass et al., 2010). Additionally, the groundwater d-excess composition was found to be between Mississippi River and groundwater d-excess. Therefore, the groundwater source might be a mixture of Mississippi River and seasonal precipitation undergoing different degrees of evaporation related to the different stable isotope compositions.

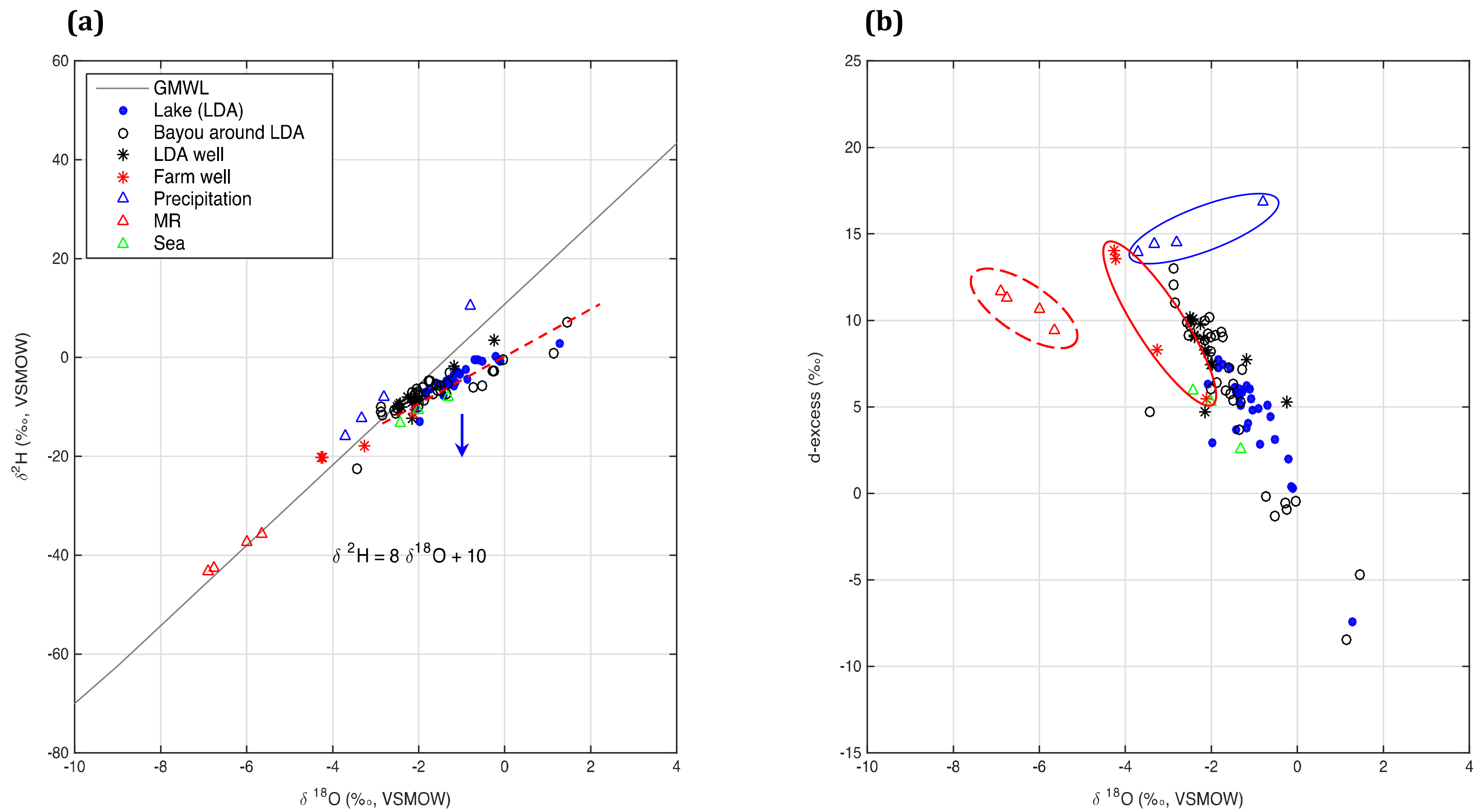

Figure 21. Oxygen-18 and hydrogen-2 isotope distribution in the lake water, bayou water, groundwater in the Barataria Basin, Gulf of Mexico seawater, and the Mississippi River water. **(a)** Oxygen-18 versus hydrogen-2 isotope relationship. Global Meteoric Water Line (GMWL) defined by Craig, 1961. Red solid line denotes the trend of radioisotope concentration in the lake, bayou, and LDA well water samples **(b)** Oxygen-18 isotope versus calculated excess deuterium (d-excess). Red dashed circle denotes the Mississippi River water group and blue solid circle represents local precipitation samples. Red solid circle indicates stable isotope composition in the farmland groundwater.

APPENDIX 3: SUPPLEMENTARY INFORMATION OF SEDIMENT SAMPLES

Sample ID	**Sample location**		**^{222}Rn sediment diffusion flux**
	Latitude	*Longitude*	*Bq/(m^2 d)*
MG1	29° 27' 25.96"	89° 48' 44.02"	22.6
MG2	29° 29' 17.87"	89° 44' 53.93"	18.8
MG3	29° 31' 34.43"	89° 46' 38.70"	30.5
MG4	29° 27' 37.27"	89° 55' 23.45"	40.0
MG5	29° 30' 36.98"	89° 55' 12.01"	18.0
MG6	29° 29' 12.09"	89° 55' 00.03"	20.9
MG7	29° 27' 33.12"	89° 54' 42.38"	30.4
LDA1	29° 53' 23.97"	90° 32' 32.26"	27.9
LDA5	29° 56' 14"	90° 37' 30"	28.1
LDA6	29° 55' 26"	90° 37' 25"	22.1
LDA7	29° 54' 22"	90° 35' 51"	23.4
**LDA8	29° 56' 14.1"	90° 37' 25.4"	26.5
**LDA11	29° 55' 15.7"	90° 35' 06.8"	23.1
LCT3	29° 51' 12.98"	90° 15' 04.45"	37.2
LCT5	29° 51' 25.69"	90° 13' 22.34"	49.4
LCT7	29° 54' 43.58"	90° 16' 27.40"	44.8
BVN3	29° 59' 22.23"	89° 59' 23.13"	25.0
BVN4	29° 58' 54.20"	90° 01' 05.70"	12.5
LDAbayou1	30° 01' 05.09"	90° 34' 25.27"	24.3

LDAbayou2	29° 59' 44.14"	90° 37' 42.74"	30.2
LDAbayou3	29° 56' 05"	90° 40' 02"	26.4
LDAbayou4	30° 00' 23.14"	90° 35' 57.69"	32.4

APPENDIX 4: SUPPLEMENTARY INFORMATION OF STABLE ISOTOPES' SAMPLES

Sample	**Sampling date**	**Location**		**Salinity**	**δ ^{2}H**	**δ ^{18}O**	**d excess**
		Longitude	*Latitude*		‰	‰	‰
Lake water (LDA)	6/17/13	29° 53' 24"	90° 32' 25"	0.06	-4.7	-1.3	6.0
	6/17/13	29° 55' 33"	90° 33' 10"	0.06	-3.3	-1.2	6.2
	6/17/13	29° 57' 6"	90° 33' 40"	0.07	-2.8	-1.1	6.0
	6/17/13	29° 55' 19"	90° 33' 23"	0.07	-2.4	-0.9	4.9
	6/17/13	29° 58' 12"	90° 33' 46"	0.1	-5.5	-1.4	5.9
	6/17/13	29° 59' 1"	90° 33' 10"	0.1	-6.5	-1.7	7.4
	6/17/13	29° 59' 38"	90° 32' 18"	0.07	-3.2	-1.1	5.4
	6/17/13	29° 59' 40"	90° 32' 38"	0.06	-3.5	-1.0	4.8
	6/17/13	29° 56' 27"	90° 37' 37"	0.06	-5.2	-1.2	4.1
	9/29/13	29° 53' 24"	90° 32' 25"	0.07	-0.9	-0.5	3.1
	9/29/13	29° 55' 33"	90° 33' 10"	0.07	0.2	-0.2	2.0
	9/29/13	29° 57' 6"	90° 33' 40"	0.08	-0.5	-0.7	5.1
	9/29/13	29° 58' 12"	90° 33' 46"	0.08	-4.3	-0.9	2.8
	9/29/13	29° 59' 1"	90° 33' 10"	0.09	-10.3	-2.1	6.3
	9/29/13	29° 59' 38"	90° 32' 18"	0.09	-13.0	-2.0	2.9
	9/29/13	29° 59' 40"	90° 32' 38"	0.08	-0.6	-0.1	0.3
	9/29/13	29° 56' 27"	90° 37' 37"	0.08	-0.6	-0.1	0.4
	9/29/13	29° 54' 39"	90° 35' 40"	0.08	2.9	1.3	-7.4
	9/29/13	29° 55' 14"	90° 35' 6"	0.09	-0.5	-0.6	4.5
	2/22/14	29° 51' 53"	90° 30' 53"	0.1	-5.7	-1.5	6.1
	2/22/14	29° 53' 24"	90° 32' 25"	0.08	-5.4	-1.3	5.1
	2/22/14	29° 57' 6"	90° 33' 40"	0.09	-5.6	-1.2	3.8
	2/22/14	29° 58' 12"	90° 33' 46"	0.12	-7.6	-1.4	3.7
	2/22/14	29° 59' 1"	90° 33' 10"	0.13	-7.5	-1.9	7.3
	2/22/14	29° 59' 38"	90° 32' 18"	0.13	-7.0	-1.8	7.8
	2/22/14	29° 59' 40"	90° 32' 38"		-5.2	-1.4	5.6
	2/22/14	29° 56' 27"	90° 37' 37"		-5.3	-1.6	7.3
	2/22/14	29° 54' 39"	90° 35' 40"		-4.5	-1.3	5.9
	2/22/14	29° 55' 14"	90° 35' 6"		-5.0	-1.3	5.7
Bayou water	5/30/13	29° 52' 13"	90° 35' 37"	0.05	-4.9	-1.7	9.1
	5/30/13	29° 51' 31"	90° 40' 40"	0.04	-7.2	-2.1	10.0
	5/30/13	29° 54' 39"	90° 43' 43"	0.05	-7.8	-2.0	8.2
	5/30/13	29° 56' 09"	90° 43' 07"	0.1	-7.0	-2.0	9.1
	5/30/13	29° 59' 03"	90° 40' 53"	0.21	-7.3	-1.7	6.0
	5/30/13	29° 59' 44"	90° 37' 42"	0.06	-3.1	-1.3	7.2
	5/30/13	30° 01' 05"	90° 34' 48"	0.08	-6.7	-1.6	5.7

	5/30/13	30° 00' 49"	90° 32' 35"	0.07	-4.7	-1.8	9.4
	5/30/13	30° 00' 17"	90° 31' 10"	0.24	-6.3	-2.1	10.2
	5/30/13	29° 57' 19"	90° 26' 10"	0.14	-10.1	-2.9	13.0
	6/3/13	30° 00' 49"	90° 32' 35"	0.09	-7.5	-2.1	9.3
	6/22/13	29° 41' 19"	90° 28' 24"	0.05	-11.2	-2.5	9.1
	6/22/13	29° 44' 26"	90° 33' 17"	0.09	-10.5	-2.5	9.9
	6/22/13	29° 49' 52"	90° 35' 28"	0.14	-2.8	-0.2	-0.9
	6/22/13	29° 52' 13"	90° 35' 37"	0.05	-5.5	-1.6	7.3
	6/22/13	29° 51' 31"	90° 40' 40"	0.09	-5.3	-1.3	5.3
	6/22/13	29° 50' 59"	90° 40' 45"	0.09	-8.7	-1.9	6.4
	6/22/13	29° 51' 02"	90° 43' 52"	0.11	-5.6	-0.5	-1.4
	6/22/13	29° 53' 28"	90° 47' 06"	0.05	0.8	1.2	-8.5
	6/22/13	29° 52' 06"	90° 50' 25"	0.08	-6.5	-1.5	5.4
	6/22/13	29° 50' 54"	90° 53' 55"	0.09	-6.0	-0.7	-0.1
	6/23/13	29° 53' 42"	90° 55' 14"	0.13	-0.6	0.0	-0.4
	6/23/13	29° 57' 01"	91° 00' 00"	0.08	7.0	1.5	-4.7
	6/23/13	30° 04' 02"	90° 57' 55"	0.23	-11.7	-2.8	11.0
	6/23/13	30° 02' 14"	90° 55' 37"	0.27	-8.3	-2.1	8.8
	6/23/13	30° 01' 29"	90° 54' 54"	0.12	-10.0	-2.0	6.1
	6/23/13	30° 00' 06"	90° 53' 34"	0.1	-5.6	-1.5	6.3
	6/23/13	29° 58' 04"	90° 51' 30"	0.09	-7.3	-1.4	3.6
	6/23/13	29° 57' 44"	90° 45' 16"	0.19	-22.6	-3.4	4.8
	3/9/14	30° 00' 49"	90° 32' 35"		-11.0	-2.9	12.1
	4/15/14	30 01' 05"	90 34' 25"	0.04	-6.2	-1.9	9.1
	4/15/14	29 59' 46"	90 37' 21"	0.03	-10.3	-2.5	9.7
	4/15/14	29 56' 05"	90 40' 02"	0.46	-2.8	-0.3	-0.5
Precipitation	7/30/13	29° 59' 40"	90° 32' 38"		10.4	-0.8	16.9
	7/14/13	30° 00' 49"	90° 32' 35"		-15.8	-3.7	14.0
	5/28/14	30° 02' 46"	90° 34' 17"		-12.2	-3.3	14.4
	6/1/14	30° 00' 49"	90° 32' 35"		-8.1	-2.8	14.5
Wetland well groundwater	10/10/13	29° 58' 29"	90° 33' 29"	1.15	-9.3	-2.4	10.0
	10/10/13	29° 58' 56"	90° 33' 12"	0.59	-10.1	-2.4	9.0
	10/10/13	29° 59' 40"	90° 32' 40"	1.3	-10.1	-2.4	9.2
	10/10/13	29° 59' 16"	90° 33' 10"	0.81	-9.9	-2.5	10.1
	10/10/13	29° 59' 17"	90° 33' 11"	0.81	-9.8	-2.5	10.0
	4/16/14	29° 58' 27"	90° 33' 29"	0.99	-8.6	-2.1	8.1
	4/16/14	29° 58' 29"	90° 33' 29"	1.08	-8.5	-2.2	9.0
	4/16/14	29° 58' 56"	90° 33' 12"	0.54	-8.3	-2.0	7.4
	4/16/14	29° 59' 40"	90° 32' 40"	1.3	-8.5	-2.0	7.5
	4/16/14	29° 59' 16"	90° 33' 10"	0.82	-8.1	-2.2	9.8
	4/16/14	29° 59' 17"	90° 33' 11"	0.15	-1.9	-1.2	7.7

	4/16/14	29° 58' 34"	90° 33' 30"	1.16	-9.0	-2.2	8.3
	4/16/14	29° 58' 37"	90° 33' 30"	25.22	3.4	-0.2	5.3
	4/16/14	29° 59' 19"	90° 33' 13"	1.19	-12.4	-2.1	4.7
Farmland well groundwater	4/15/14	30 2' 16'	90 34' 17"	0.17	-20.1	-4.3	14.0
	5/30/14	29° 56' 8"	90° 40' 1"	0.5	-11.4	-2.1	5.5
	5/30/14	29° 56' 8"	90° 40' 1"	1.62	-17.9	-3.3	8.3
	5/30/14	30° 02' 46"	90° 34' 17"	0.38	-20.2	-4.2	13.5
Mississippi River water	6/23/13	29° 58' 54"	90° 48' 33"	0.16	-37.3	-6.0	10.7
	6/23/13	30° 07' 41"	90° 56' 32"	0.17	-35.7	-5.6	9.5
	7/23/13	29° 58' 54"	90° 48' 33"	0.17	-42.7	-6.7	11.3
	7/23/13	30° 07' 41"	90° 56' 32"	0.17	-43.4	-6.9	11.7
Gulf of Mexico sea water	6/22/13	28° 45' 60"	90° 14' 02"	19.17	-8.0	-1.3	2.6
	6/22/13	28° 52' 09"	90° 27' 95"	15.78	-13.4	-2.4	5.9
	6/22/13	28° 59' 3"	90° 31' 1"	17.83	-10.7	-2.0	5.3

APPENDIX 5: SUPPLEMENTARY INFORMATINO OF ^{222}Rn, DOC, AND TN

A) Bayou water							
Station ID	**Sampling date**	**Location**		**^{222}Rn**	**DOC**	**TN**	**Salinity**
		Longitude	*Latitude*	*Bq/m^3*	*µM*	*µM*	
Rb1	5/30/13	29° 52' 13.23"	90° 35' 37.87"	27.86	783.67	49.50	0.05
Rb2	5/30/13	29° 51' 31.60"	90° 40' 40.18"	55.62	808.71	43.94	0.04
Rb3	5/30/13	29° 54' 39.63"	90° 43' 43.91"	117.31	716.63	64.57	0.05
Rb4	5/30/13	29° 56' 09.59"	90° 43' 07.91"	128.29	707.92	84.71	0.10
Rb5	5/30/13	29° 59' 03.09"	90° 40' 53.77"	523.05	555.08	98.71	0.21
Rb6	5/30/13	29° 59' 44.21"	90° 37' 42.59"	93.75	944.17	59.42	0.06
Rb7	5/30/13	30° 01' 05.67"	90° 34' 48.53"	230.79	541.58	84.25	0.08
Rb8	5/30/13	30° 00' 49.86"	90° 32' 35.03"	183.74	783.13	160.61	0.07
Rb9	5/30/13	30° 00' 17.82"	90° 31' 10.03"	362.84	1107.42	185.75	0.24
Rb10	5/30/13	29° 57' 19.23"	90° 26' 10.72"	101.51	994.17	116.14	0.14
Rb8	6/3/13	30° 00' 49.86"	90° 32' 35.03"	260.07	747.67	54.49	0.09
RNb11	6/3/13	29° 54' 49.27"	90° 16' 28.78"	117.47	885.83	48.81	0.14
RNb12	6/3/13	29° 54' 00.88"	90° 09' 34.47"	885.72	2025.83	102.46	0.19
LCb1	6/6/13	29° 52' 55.44"	90° 25' 47.87"	131.17	1746.67	178.00	0.14
LCb2	6/6/13	29° 53' 26.31"	90° 23' 17.41"	211.24	890.42	54.75	0.11
LCb3	6/6/13	29° 53' 27.73"	90° 21' 17.72"	1464.11	804.33	38.82	0.12
LCb4	6/6/13	29° 54' 56.88"	90° 17' 47.25"	69.35	990.83	46.48	0.14
LCb5	6/6/13	29° 52' 52.73"	90° 13' 18.84"	939.47	1543.33	100.43	0.26
LCb6	6/6/13	29° 53'	90° 12'	2206.7	3332.50	159.07	0.40

		35.19"	01.41"	7			
LCb7	6/6/13	29° 53' 55.67"	90° 10' 33.45"	824.19	2213.33	119.50	0.37
LCb8	6/6/13	29° 53' 27.08"	90° 08' 49.29"	362.67	511.67	31.85	0.25
LCb9	6/6/13	29° 53' 09.72"	90° 08' 16.57"	129.27	889.17	44.18	0.25
LCb10	6/6/13	29° 52' 18.47"	90° 06' 55.91"	576.19	658.33	76.64	0.60
RSEb1	6/10/13	29° 15' 54.07"	89° 21' 31.19"	145.95	492.08	42.16	2.06
RSEb2	6/10/13	29° 20' 56.37"	89° 32' 18.67"	21.56	448.67	39.13	1.53
RSEb3	6/10/13	29° 30' 43.60"	89° 45' 53.80"	19.97	726.17	55.54	8.93
RSEb4	6/10/13	29° 37' 55.03"	89° 57' 06.05"	40.87	950.83	85.00	3.48
RSEb5	6/10/13	29° 47' 02.44"	90° 02' 01.77"	154.55	740.83	63.85	0.19
RSEb6	6/10/13	29° 53' 24.21"	89° 54' 42.14"	537.52	633.17	33.34	0.11
RSEb8	6/10/13	29° 48' 13.14"	89° 58' 24.91"	53.54	2823.33	225.86	0.98
RSEb9	6/10/13	29° 49' 53.87"	89° 57' 33.53"	82.60	2171.67	134.86	0.63
ELDAb1	6/22/13	29° 41' 19.61"	90° 28' 24.97"	39.63	1500.83	54.71	0.05
ELDAb2	6/22/13	29° 44' 26.28"	90° 33' 17.37"	129.83	1194.17	40.93	0.09
ELDAb3	6/22/13	29° 49' 52.62"	90° 35' 28.74"	40.31	831.88	30.29	0.14
ELDAb4	6/22/13	29° 52' 13.18"	90° 35' 37.88"	79.03	807.13	35.01	0.05
ELDAb5	6/22/13	29° 51' 31.73"	90° 40' 40.12"	92.78	1171.67	38.75	0.09
ELDAb6	6/22/13	29° 50' 59.57"	90° 40' 45.02"	66.59	1127.92	55.40	0.09
ELDAb7	6/22/13	29° 51' 02.51"	90° 43' 52.14"	140.02	1111.25	43.80	0.11
ELDAb8	6/22/13	29° 53' 28.21"	90° 47' 06.33"	396.16	864.58	91.29	0.05
ELDAb9	6/22/13	29° 52' 06.29"	90° 50' 25.06"	70.44	1112.08	76.11	0.08
ELDAb10	6/22/13	29° 50' 54.97"	90° 53' 55.16"	355.71	432.42	34.71	0.09

UpLDAb1	6/23/13	29° 53' 42.95"	90° 55' 14.76"	317.36	643.29	39.69	0.13
UpLDAb2	6/23/13	29° 57' 01.37"	91° 00' 00.20"	207.33	385.79	35.76	0.08
UpLDAb3	6/23/13	30° 04' 02.55"	90° 57' 55.72"	1181.91	359.46	72.71	0.23
UpLDAb4	6/23/13	30° 02' 14.96"	90° 55' 37.72"	1040.40	453.71	98.29	0.27
UpLDAb5	6/23/13	30° 01' 29.64"	90° 54' 54.72"	195.40	743.21	55.65	0.12
UpLDAb6	6/23/13	30° 00' 06.63"	90° 53' 34.85"	165.56	1031.67	58.86	0.10
UpLDAb7	6/23/13	29° 58' 04.20"	90° 51' 30.22"	148.86	828.29	42.51	0.09
UpLDAb8	6/23/13	29° 57' 44.81"	90° 45' 16.33"	404.16	502.33	52.77	0.19
LoMRDb1	7/9/13	29° 36' 15.98"	90° 27' 48.20"	527.47	1195.42	86.46	0.35
LoMRDb2	7/9/13	29° 35' 09.20"	90° 22' 13.14"	27.62	1253.33	81.61	0.41
LoMRDb3	7/9/13	29° 33' 10.88"	90° 16' 39.44"	6.50	749.17	43.66	0.30
LoMRDb3-1	7/9/13	29° 33' 11.62"	90° 16' 37.99"	33.54	565.42	43.56	0.15
LoMRDb4	7/9/13	29° 25' 59.65"	90° 16' 31.46"	193.07	1296.25	84.39	0.57
LoMRDb5	7/9/13	29° 20' 07.96"	90° 14' 33.70"	25.60	616.25	41.20	8.47
LoMRDb6	7/9/13	29° 16' 00.53"	90° 13' 08.74"	47.44	522.83	33.68	15.75
LoMRDb7	7/9/13	29° 09' 31.89"	90° 10' 32.34"	45.24	564.42	34.39	13.92
LoMRDb8	7/9/13	29° 12' 48.82"	90° 02' 54.33"	3.12	265.54	57.15	16.14
LoMRDb9	7/9/13	29° 15' 48.02"	89° 56' 58.34"	64.32	274.92	54.91	16.08
LoMRDb10	7/9/13	29° 15' 41.74"	89° 57' 12.71"	90.30	417.25	28.15	12.54
NRb1	7/14/13	29° 53' 28.78"	90° 47' 06.64"	86.50	826.13	42.58	0.04
NRb2	7/14/13	29° 50' 54.98"	90° 53' 55.16"	475.41	353.58	32.21	0.04
NRb3	7/14/13	29° 53' 42.94"	90° 55' 14.45"	287.67	563.83	34.88	0.11
NRb4	7/14/13	30° 04' 02.60"	90° 57' 55.64"	577.00	319.17	61.34	0.21

NRb5	7/14/13	30° 02' 14.82"	90° 55' 37.72"	609.74	528.71	77.46	0.27
NRb6	7/14/13	29° 58' 04.22"	90° 51' 30.24"	340.12	688.08	121.68	0.07
NRb7	7/14/13	29° 57' 44.77"	90° 45' 16.24"	106.50	310.04	45.47	0.07
NRb8	7/14/13	29° 58' 19.70"	90° 42' 26.38"	649.99	350.25	81.32	0.08
NRb9	7/14/13	30° 00' 49.74"	90° 32' 34.95"	403.72	907.92	56.88	0.11
NRb10	7/14/13	30° 00' 17.81"	90° 31' 10.34"	32.54	721.58	57.70	0.17
NOb1	7/19/13	29° 53' 27.79"	90° 21' 18.16"	1528.80	688.25	30.58	0.10
NOb2	7/19/13	29° 52' 52.75"	90° 13' 18.79"	68.86	1076.67	62.54	0.28
NOb3	7/19/13	29° 53' 35.13"	90° 12' 01.43"	131.71	570.33	72.09	0.62
NOb4	7/19/13	29° 53' 55.69"	90° 10' 33.40"	137.16	682.17	42.53	0.47
NOb5	7/19/13	29° 54' 01.35"	90° 09' 34.25"	408.77	574.25	74.39	0.33
NOb6	7/19/13	29° 53' 27.03"	90° 08' 49.28"	370.24	364.04	54.59	0.13
NOb7	7/19/13	29° 53' 09.71"	90° 08' 16.64"	241.51	862.50	44.58	0.21
NOb8	7/19/13	29° 52' 18.54"	90° 06' 56.01"	402.58	413.88	79.50	0.40
NOb9	7/19/13	29° 53' 24.26"	89° 54' 42.14"	204.12	601.58	33.23	0.12
Fb1	4/15/14	30° 01' 05.09"	90° 34' 25.27	303.11	483.75	64.80	0.04
Fb2	4/15/14	29° 59' 46.7"	90° 37' 21"	342.66	1869.17	84.14	0.03
Rb8	5/24/14	30° 00' 49.86"	90° 32' 35.03"		1454.17	138.36	0.15
RNb11	5/24/14	29° 54' 49.27"	90° 16' 28.78"		1679.58	57.45	0.19
RSEb7_Radio pond	6/10/13	29° 58' 23.21"	90° 01' 12.02"	217.13	319.00	223.86	0.20
NOb10_seegage	7/19/13	29° 58' 23.19"	90° 01' 11.99"	505.91	283.42	275.07	0.21

B) Well water						

Station ID	**Sampling date**	**Location**		**^{222}Rn**	**DOC**	**TN**	**Salinity**
		Longitude	*Latitude*	*Bq/m^3*	*μM*	*μM*	
LDAw1	10/10/13	29° 58' 27"	90° 33' 29"	3133.62	3490.00	541.50	0.88
LDAw2	10/10/13	29° 58' 29"	90° 33' 29"	3416.78	2546.25	577.75	1.15
LDAw3	10/10/13	29° 58' 56"	90° 33' 12"	3131.84	2145.00	355.00	0.59
LDAw4	10/10/13	29° 59' 40	90° 32' 40"	1229.03	3725.42	222.25	1.30
LDAw5	10/10/13	29° 59' 16"	90° 33' 10"	2788.43	5517.50	468.14	0.81
LDAw6	10/10/13	29° 59' 17"	90° 33' 11"	4367.30	9770.83	581.82	0.81
LDAw1	2/24/14	29° 58' 27"	90° 33' 29"		1772.50	546.93	0.58
LDAw3	2/24/14	29° 58' 56"	90° 33' 12"		1067.92	224.07	0.55
LDAw4	2/24/14	29° 59' 40	90° 32' 40"		2637.08	116.75	
LDAw5	2/24/14	29° 59' 16"	90° 33' 10"		1572.08	231.04	0.72
LDAw6	2/24/14	29° 59' 17"	90° 33' 11"		1692.50	281.25	0.77
LDAw1	4/16/14	29° 58' 27"	90° 33' 29"		2374.17	536.79	0.99
LDAw2	4/16/14	29° 58' 29"	90° 33' 29"		3930.42	1298.93	1.08
LDAw3	4/16/14	29° 58' 56"	90° 33' 12"	1425.40	1986.25	275.50	0.54
LDAw4	4/16/14	29° 59' 40	90° 32' 40"	6800.82	1387.50	111.11	1.30
LDAw5	4/16/14	29° 59' 16"	90° 33' 10"		1990.83	452.07	0.82
LDAw6	4/16/14	29° 59' 17"	90° 33' 11"		970.83	71.79	0.15
LDAw7	4/16/14	29° 58' 34"	90° 33' 30"		7635.42	772.50	1.16
LDAw9	4/16/14	29° 59' 19"	90° 33' 13"		5498.33	261.61	1.19
LDAw1	9/26/14	29° 58' 27"	90° 33' 29"	1391.12	2600.83	655.79	0.82
LDAw4	9/26/14	29° 59' 40	90° 32' 40"	13086.86	3004.58	142.11	1.30

LDAw5	9/26/14	29° 59' 16"	90° 33' 10"	328.88	1088.75	303.54	0.78
LDAw6	9/26/14	29° 59' 17"	90° 33' 11"	699.61	1463.33	114.21	0.58
LDAw7	9/26/14	29° 58' 34"	90° 33' 30"	3471.89	1677.08	549.82	1.16
LDAw9	9/26/14	29° 59' 19"	90° 33' 13"	2229.95	1940.83	258.89	1.19
MGw1	4/13/14	29° 29' 04.50"	89° 57' 00.27"		4116.25	647.00	21.98
MGw2	4/13/14	29° 31' 37.91"	89° 57' 01.87"		5024.17	2194.39	11.42
MGw3	4/13/14	29° 32' 19.55"	89° 56' 58.00"		2352.50	1609.54	9.75
MGw4	4/13/14	29° 35' 03.88"	89° 57' 01.72"		2295.42	1033.46	4.64
MGw5	4/13/14	29° 36' 24.82"	89° 56' 18.96"		2973.75	719.32	7.40
MGw1	5/27/14	29° 29' 04.50"	89° 57' 00.27"	1153.94	3060.83	664.50	22.55
MGw2	5/27/14	29° 31' 37.91"	89° 57' 01.87"	111.16	5257.50	2754.14	11.37
MGw3	5/27/14	29° 32' 19.55"	89° 56' 58.00"	1199.11	3303.75	2082.07	7.01
MGw4	5/27/14	29° 35' 03.88"	89° 57' 01.72"	768.96	2067.92	1154.93	9.34
MGw5	5/27/14	29° 36' 24.82"	89° 56' 18.96"	1554.99	1678.75	409.89	7.55
MGw1	9/24/14	29° 29' 04.50"	89° 57' 00.27"	12510.33	1823.33	538.89	10.35
MGw2	9/24/14	29° 31' 37.91"	89° 57' 01.87"	4850.34	4499.17	2803.71	1.73
MGw4	9/24/14	29° 35' 03.88"	89° 57' 01.72"	5363.51	1558.75	1103.50	8.95
VACw2	9/29/14	29° 56' 08"	90° 40' 1"	986.74	3773.75	595.43	1.58
EDGw	5/30/14	30° 02' 46"	90° 34' 17"	4263.12	1709.58	78.79	0.38
VACw2	5/30/14	29° 56' 08"	90° 40' 1"	10943.20	6235.42	561.54	1.62
VACw2	5/24/14	29° 56' 08"	90° 40' 1"		6592.92	515.50	
EDGw	5/24/14	30° 02' 46"	90° 34' 17"		1220.42	64.24	
Farmw	4/15/14	30° 02' 17"	90° 34' 14"	427.84	581.96	34.81	0.17

C) Mississippi River water and Gulf of Mexico sea water							
Station ID	**Sampling date**	**Location**		**^{222}Rn**	**DOC**	**TN**	**Salinity**
		Longitude	*Latitude*	*Bq/m^3*	*µM*	*µM*	
LMR	6/23/13	29° 58' 54.59"	90° 48' 33.18"	56.25	307.50	300.64	0.16
UMR	6/23/13	30° 07' 41.74"	90° 56' 32.84"	64.57	320.38	257.21	0.17
LMR	7/23/13	29° 58' 54.59"	90° 48' 33.18"	55.63	261.79	303.54	0.17
UMR	7/23/13	30° 07' 41.74"	90° 56' 32.84"	45.29	263.08	299.82	0.17
GM2	6/22/13	28° 52' 097"	90° 27' 957"	6.70	279.79	24.24	15.78

APPENDIX 6: SUPPLEMENTARY INFORMATIN OF ^{222}Rn SURVEY

Survey date	**Distance from MR**	**Rn** water	**1σ**
	km	*Bq/m²*	*Bq/m²*
4/23/13	17.2	18.8	7.7
	16.8	23.0	8.1
	16.5	19.6	7.4
	16.1	22.8	8.1
	15.8	46.9	11.7
	15.4	37.7	10.5
	15.1	37.0	10.3
	14.7	30.7	9.3
	14.4	25.8	8.6
	14.0	16.7	6.8
	13.7	20.7	7.8
	13.4	15.6	5.4
	12.9	9.8	4.9
	12.5	12.2	5.5
	12.1	12.2	5.4
	11.6	12.4	5.5
	11.2	7.4	4.3
	10.8	24.3	7.7
	10.4	8.4	5.5
	10.3	6.0	3.5
	10.1	4.0	2.8
	10.0	17.9	6.0
	9.9	12.0	4.9
	9.8	20.1	6.4
	9.7	25.9	7.2
	9.6	37.2	8.8
	9.5	17.9	6.0
	9.4	19.6	6.2
	9.3	43.4	9.5
	9.1	38.0	8.7
	9.0	38.3	8.8
	8.9	40.1	9.0
	8.8	39.3	16.9
	8.5	30.5	7.4
	8.2	33.7	8.2
	7.9	51.9	10.2

	7.7	64.1	11.3
	7.4	58.6	10.9
	7.1	73.2	12.0
	6.8	73.1	12.3
	6.5	121.7	17.4
	6.3	117.2	17.3
	6.0	129.3	18.1
	5.8	98.7	16.0
	5.5	95.9	15.4

Survey date	**Distance from MR**	**Rn** **water**	**1σ**
	km	*Bq/m*^{2}	*Bq/m*^{2}
5/18/13	17.2	15.0	6.8
	16.7	23.6	7.5
	16.3	21.1	7.0
	15.9	16.6	6.3
	15.5	14.4	5.9
	15.0	21.7	7.2
	14.6	9.6	4.8
	14.2	16.8	6.3
	13.8	29.1	8.4
	13.4	16.6	6.6
	12.9	18.2	6.1
	12.4	14.3	5.4
	11.9	9.9	4.4
	11.4	6.0	3.5
	10.9	21.7	6.5
	10.4	12.6	5.7
	10.0	3.3	2.3
	9.6	14.9	5.0
	9.2	14.8	4.9
	8.8	7.4	3.8
	8.7	18.0	4.8
	8.5	13.9	7.0
	8.5	19.1	5.5
	8.5	22.1	5.9
	8.5	26.3	6.4
	8.5	30.9	6.9
	8.5	20.2	5.6
	6.8	56.7	14.4

	6.8	73.3	12.2
	6.8	59.6	10.9
	6.8	81.9	12.8
	6.8	61.6	11.2
	5.5	93.4	14.0

Survey date	**Distance from MR**	**Rn** water	**1σ**
6/17/13	*km*	*Bq/m²*	*Bq/m²*
	17.2	97.7	10.4
	16.6	90.2	13.9
	16.1	83.5	13.4
	15.5	79.4	13.1
	15.0	85.9	13.6
	14.4	103.8	15.0
	13.9	86.3	13.7
	13.4	35.5	7.8
	12.8	55.7	10.2
	12.2	50.4	9.7
	11.6	53.9	10.0
	11.0	67.0	11.2
	10.4	35.3	17.2
	9.9	23.1	6.0
	9.4	18.3	5.3
	9.0	22.8	5.9
	8.5	24.1	12.6
	8.2	27.7	6.4
	7.9	26.3	6.2
	7.7	26.5	6.2
	7.4	44.4	8.1
	7.1	30.9	6.7
	6.8	79.3	21.1
	6.5	117.9	14.9
	6.2	113.0	14.6
	5.8	122.7	15.2
	5.5	133.3	21.3

Survey date	**Distance from MR**	**Rn** water	**1σ**
	km	*Bq/m²*	*Bq/m²*

6/25/13	17.2	88.4	13.5
	16.8	98.2	14.5
	16.5	105.1	14.9
	16.2	85.2	13.4
	15.8	79.2	13.1
	15.5	74.8	13.3
	15.2	72.7	14.2
	14.8	94.7	15.1
	14.5	92.6	15.1
	14.2	111.9	16.4
	13.8	83.4	14.5
	13.5	76.4	14.9
	13.2	121.6	16.2
	12.8	95.0	15.4
	12.5	100.3	14.7
	12.1	76.4	12.4
	11.8	52.9	5.1
	11.3	31.5	7.1
	10.7	33.0	7.5
	10.2	39.1	6.8
	9.6	29.7	6.7
	9.1	26.6	6.9
	8.5	17.2	8.5
	8.2	34.9	6.8
	7.9	15.4	5.0
	7.7	9.8	4.4
	7.4	8.4	4.7
	7.1	16.8	5.7
	6.8	58.2	17.5
	6.4	78.9	11.1
	5.9	79.8	11.8
	5.5	58.2	17.5

Survey date	**Distance from MR**	**Rn** $_{water}$	**1σ**
	km	*Bq/m²*	*Bq/m²*
7/30/13	17.2	24.1	10.3
	16.7	42.9	9.6
	16.3	38.9	9.2
	15.9	36.8	8.9
	15.5	34.5	8.6

	15.0	53.9	10.8
	14.6	58.2	11.2
	14.2	96.4	14.4
	13.8	90.4	14.0
	13.4	78.4	13.6
	13.0	94.7	13.1
	12.6	89.5	12.8
	12.2	79.2	12.1
	11.9	71.7	11.5
	11.5	46.4	9.3
	11.1	35.2	8.1
	10.7	38.2	8.3
	10.4	31.0	8.4
	9.9	33.7	7.2
	9.4	17.0	5.1
	9.0	18.3	5.3
	8.5	22.3	7.6
	8.2	34.2	7.0
	7.8	26.6	6.1
	7.5	27.6	6.2
	7.1	37.4	7.2
	6.8	124.6	22.6
	6.6	127.4	15.3
	6.4	166.4	17.3
	6.2	173.6	17.8
	5.9	121.2	14.6
	5.7	158.2	16.9
	5.5	230.8	18.7

Survey date	**Distance from MR**	**Rn** $_{\text{water}}$	**1σ**
	km	*Bq/m*^{2}	*Bq/m*^{2}
9/29/13	17.2	16.2	5.7
	16.6	14.3	10.1
	16.1	7.2	7.2
	15.5	7.3	7.3
	15.0	7.2	7.2
	14.4	7.2	7.2
	13.9	7.2	7.2
	13.4	9.8	3.5
	8.5	17.2	4.6

	8.1	14.5	8.4
	7.7	49.2	15.5
	7.2	50.0	15.8
	6.8	53.0	8.4
	6.4	90.5	24.2
	5.9	65.7	20.8
	5.5	73.6	9.9

Survey date	**Distance from MR**	**Rn** $_{water}$	**1σ**
	km	*Bq/m²*	*Bq/m²*
4/17/14	17.2	8.2	8.2
	16.9	13.4	6.7
	16.6	23.2	8.8
	16.3	15.9	7.1
	16.0	9.6	5.5
	15.7	15.5	6.9
	15.4	12.8	6.4
	15.1	6.6	4.7
	14.8	9.6	5.5
	14.5	9.4	5.4
	14.2	0.0	0.0
	13.9	3.1	3.1
	13.6	16.2	7.3
	13.4	4.1	5.0
	8.5	42.8	14.6
	8.3	82.4	16.8
	8.0	118.5	20.0
	7.8	127.7	21.0
	7.5	168.6	24.1
	7.3	237.2	28.6
	7.0	219.7	27.5
	6.8	300.9	38.9
	6.6	297.5	28.3
	6.4	418.2	33.8
	6.2	382.8	32.3
	5.9	395.2	33.1
	5.7	327.0	29.4
	5.5	390.3	37.0

Survey date	**Distance from MR**	**Rn** **water**	**1σ**
	km	*Bq/m^2*	*Bq/m^2*
6/17/14	17.2	57.7	12.6
	17.0	57.7	11.8
	16.8	67.7	12.8
	16.6	49.9	10.9
	16.4	36.0	9.3
	16.2	40.7	9.9
	16.1	43.3	10.2
	15.9	47.7	10.7
	15.7	40.7	9.9
	15.5	35.3	9.1
	15.3	21.3	7.1
	15.1	17.0	6.4
	15.0	26.1	7.9
	14.8	14.5	5.9
	14.6	9.7	4.9
	14.4	16.5	6.2
	14.2	9.6	4.8
	14.0	16.7	6.3
	13.9	11.8	5.3
	13.7	7.2	4.2
	13.5	26.6	8.0
	13.3	23.2	7.3
	13.1	28.6	8.3
	12.9	11.8	5.3
	12.8	8.0	4.0
	12.6	2.1	2.1
	12.4	6.2	3.6
	12.2	12.2	5.0
	12.0	7.8	3.9
	11.8	10.0	4.5
	11.6	1.9	1.9
	11.5	8.1	4.1
	11.3	6.2	3.6
	11.1	10.2	4.5
	10.9	7.8	3.9
	10.7	2.1	2.1
	10.5	18.1	6.0
	10.4	4.2	2.9

	10.2	14.0	5.3
	10.0	5.9	3.4
	9.8	18.2	6.1
	9.6	8.2	4.1
	9.4	6.0	3.5
	9.3	6.0	3.5
	9.1	12.1	4.9
	8.9	6.1	3.5
	8.7	9.4	4.2
	8.5	9.4	3.8
	8.4	17.3	5.2
	8.3	18.9	5.5
	8.2	26.5	6.4
	8.0	28.2	6.6
	7.9	52.0	9.0
	7.8	45.8	8.5
	7.7	29.8	7.0
	7.6	36.5	8.0
	7.4	14.2	5.0
	7.3	1.5	1.5
	7.2	17.4	5.2
	7.1	24.8	6.2
	7.0	37.6	7.7
	6.8	51.8	9.0
	6.7	37.4	8.8
	6.6	66.0	11.7
	6.5	82.6	13.1
	6.4	101.7	14.5
	6.2	91.8	13.8
	6.1	105.4	14.8
	6.0	92.7	14.0
	5.9	106.0	15.0
	5.8	135.1	17.0
	5.6	107.9	15.3
	5.5	108.9	15.3

Survey date	**Distance from MR**	**Rn $_{water}$**	**1σ**
	km	*Bq/m²*	*Bq/m²*
6/18/14	11.0	3.8	2.7
	10.7	3.9	2.8

	10.5	4.0	2.9
	10.2	5.9	3.4
	10.0	5.8	3.4
	9.7	11.5	4.7
	9.5	2.0	2.0
	9.3	15.6	5.5
	9.0	3.9	2.8
	8.8	7.5	3.8
	8.5	4.7	2.7
	8.4	7.6	3.4
	8.2	36.1	7.5
	8.0	50.7	9.0
	7.9	68.4	10.6
	7.7	81.5	11.5
	7.5	74.5	11.0
	7.4	74.3	11.0
	7.2	100.3	12.7
	7.0	79.6	11.4
	6.9	73.6	11.0
	6.7	123.9	16.1
	6.5	74.7	12.5
	6.4	131.5	16.7
	6.2	96.9	14.3
	6.0	106.7	15.1
	5.9	113.7	15.6
	5.7	106.3	15.2
	5.5	119.8	16.0

Survey date	**Distance from MR**	**Rn** $_{water}$	**1σ**
	km	*Bq/m²*	*Bq/m²*
9/25/14	17.2	23.9	17.9
	16.7	15.6	6.4
	16.3	33.5	9.3
	15.9	23.0	7.7
	15.5	30.9	8.9
	15.0	15.3	6.2
	14.6	25.4	8.1
	14.2	23.1	7.7
	13.8	10.6	5.3
	13.4	8.9	5.0

	13.1	8.8	4.4
	12.9	8.5	4.2
	12.7	8.7	4.3
	12.4	11.1	5.0
	12.2	8.6	4.3
	12.0	8.7	4.3
	11.7	13.5	5.5
	11.5	13.2	5.4
	11.3	0.0	0.0
	11.1	11.3	4.6
	10.8	3.6	2.6
	10.6	7.3	3.7
	10.4	13.0	4.9
	10.1	5.4	3.1
	9.9	11.0	4.5
	9.7	7.5	3.7
	9.4	3.6	2.5
	9.2	9.2	4.1
	9.0	9.0	4.0
	8.7	10.6	4.3
	8.5	13.7	5.2
	8.3	10.1	4.1
	8.0	21.3	6.2
	7.8	7.0	3.5
	7.5	10.4	4.2
	7.3	12.0	4.5
	7.0	13.4	4.7
	6.8	33.5	8.6
	6.5	40.5	9.6
	6.3	64.6	12.0
	6.0	48.7	10.4
	5.8	31.1	8.3
	5.5	53.5	14.7

REFERENCES

Abass, G., Osae, S., Akiti, T., Adomako, D., Ganyaglo, S., Bam, E., Hadisu, A., 2010. Origin of dissolve ions in groundwaters in the Northern Densu River Basin of Ghana using stable isotopes of 18O and 2H. *Journal of water resource and protection*, 2, 1010-1019.

Basu, A.R., Jacobsen, S.B., Poreda, R.J., Dowling, C.B., Aggarwal, P.K., 2001. Large Groundwater Strontium Flux to the Oceans from the Bengal Basin and the Marine Strontium Isotope Record. *Science*, 293: 1470-1473.

Bianchi, T.S., DiMarco, S., Smith, R., Schreiner, K., 2009. A gradient of dissolved organic carbon and lignin from Terrebonne–Timbalier Bay estuary to the Louisiana shelf (USA). *Marine chemistry*, 117:32-41.

Bokuniewicz, H. and Pavlik, B., 1990. Groundwater seepage along a barrier island. *Biogeochemistry*, 10: 257-276.

Bone, S.E., Charette, M., Lamborg, C., Gonneea, M., 2007. Has Submarine Groundwater Discharge Been Overlooked as a Source of Mercury to Coastal Waters?. *Environmental science & Technology*, 41(9): 3090-3095.

Boudreau, B.U., 1997. Digenetic models and their implication; modeling transport and reactions in aquatic sediments. *Springer Verlag.*.

Breier, J., and Edmonds, H., 2007. High ^{226}Ra and ^{228}Ra activities in Nueces Bay, Texas indicate large submarine saline discharges. *Marine chemistry*, 103(1-2): 131-145.

Breier, J., Breier, C., Edmonds, H., 2010. Seasonal dynamics of dissolved Ra isotopes in the semi-arid bays of south Texas. *Marine chemistry*, 122(1-4): 39-50.

Brocker S. W. and Peng H. T., 1974. Gas exchange rates between air and sea. *Tellus,* 26, 21.

Bugna, G.C., Chanton, J., Cable, J., Burnett, W., Cable, P., 1996. The importance of groundwater discharge to the methane budgets of nearshore and continental shelf waters of the northeastern Gulf of Mexico. *Geochimica et Cosmochimica Acta,* 60(23): 4735-4746.

Burdige, D.J., 2005. Burial of terrestrial organic matter in marine sediments: A re-assessment. *Global Biogeochemical Cycles,* 19: GB4011.

Burnett, W.C., Taniguchi, M., Oberdorfer, J.A., 2001. Measurement and significance of the direct discharge of groundwater into the coastal zone. *Journal of Sea Research*, 46: 109-116.

Burnett, W., H. Bokuniewicz., M. Huettel., W.S. Moore., M. Taniguchi., 2003. Groundwater and pore water inputs to the coastal zone. *Biogeochemistry*, 66, 3-33.

Burnett, W.C., Dulaiova, H., 2003. Estimating the dynamics of groundwater input into the coastal zone via continuous radon-222 measurements. *Journal of Environmental Radioactivity*, 69-1: 21-35.

Burnett, W.C., Aggarwal, P.K., Aureli, A., Bokuniewicz, H., Cable, J.E., Charette, M.A., Kontar, E., Krupa, S., Kulkarni, K.M., Loveless. A., Moore, W.S., Oberdorfer, J.A., Oliveira, J., Ozyurt, N., Povinec, P., Privitera, A.M.G., Rajar, R., Ramessur, R.T., Scholten, J., Stieglits, T., Taniguchi, M., Turner, J.V., 2006. Quantifying submarine groundwater discharge in the coastal zone via multiple methods. *Science of the Total Environment*, 367: 498-543.

Burnet, W.C., Peterson, R.N., Santos, I.R., Hicks, R.W., 2010. Use of automated radon measurements for rapid assessment of groundwater flow into Florida streams. *Journal of Hydrology*, 380-3: 298-304.

Cable, J., Bugna, G., Burnett, W., Chanton, J., 1996a. Application of ^{222}Rn and CH_4 for assessment of groundwater discharge to the ocean. *Limnology and Oceanography*, 41: 1347-1353.

Cable, J., Burnett, W., Chanton, J., Weatherly, G., 1996b. Estimating groundwater discharge into the northeastern Gulf of Mexico using ^{222}Rn. *Earth and Planetary Science Letters*, 144: 591-604.

Cable, E.J., Burnett, W.C., Chanton, J.P., Weatherly, G. L., 1996. Estimating groundwater discharge into the northeastern Gulf of Mexico using radon-222. *Earth and Planetary Science Letters*, 144-3: 591-604.

Cappa, C., Hendricks, M., Depaolo, D., Cohen, R., 2003. Isotopic fractionation of water during evaporation. *Journal of geophysical research*, 108

Chabreck, R., Linscombe, G., 1988. Vegetative type map of the Louisiana costal marshes.

Chanyotha, S., and Burnett, W., 2014. Assessing diffusive fluxes and pore water radon activities via a single automated experiment. *Journal of radioanalytical and nuclear chemistry*, 301(2): 581-588.

Colman, J.M., and Wright, L.D., 1975. Modern River Deltas: variability of processes and sand bodies. In: Broussard, M.L. (Ed.), Deltas: Models for Exploration. Houston *Geological Society,* Houston, TX, pp. 99-149.

Coleman, J.M., and Prior, D.B., 1980. Deltaic Sand Bodies. *Tulsa*, OK.

Coleman, J.M., 1988. Dynamic changes and processes in the Mississippi River Delta. *Geological Society of American Bulletin,* 100, 999-1015.

Corbett, D.R., Burnett, W.C., Cable, P.H., Clark, S.B., 1997. Radon tracing of groundwater input into Par Pond, Savannah River Site. *Journal of Hydrology*, 203-1: 209-227.

Corbett, D.R., Chanton, J., Burnett, W., Dillon, K., Rutkowski, C., 1999. Patterns of groundwater discharge into Florida Bay. *Limnology Oceanography*, 44(4): 1045-1055.

Corbett, D.R., Dillon, K., Burnett, W., Chanton, J., 2000. Estimating the groundwater contribution into Florida Bay via natural tracers, 222Rn and CH4. *Limnology and Oceanography*, 45(7): 1546-1557.

Craig. H., 1961. Isotopic variations in Meteoric waters. *Sciecne*, 133: 1702-1703.

Dansgaard, W., 1964. Stable isotopes in precipitation. *Tellus*.

Day, J., Shapper, G., Britsch, L., Hawels, S., Reed, D., Cahoon, D., 2000. Pattern and process of land loss in the Mississippi Delta: A Spatial and temporal analysis of wetland habitat change. *Estuaries and coasts*, 23(4): 425-438.

Delaune, R., Lindau, C., Jugsujinda, A., 2008. Indicators for Evaluating the Influence of Diverted Mississippi River Water on Louisiana Coastal Marsh. *Journal of freshwater ecology*, 23(3): 475-477.

Dillon, K. and Chanton, J., 2008. Nitrogen Stable Isotopes of Macrophytes Assess Stormwater Nitrogen Inputs to an Urbanized Estuary. *Estuaries and coasts,* 31(2): 360-370.

Dimova, N.T., and Burnett, W.C., 2011. Evaluation of groundwater discharge into small lakes based on the temporal distribution of radon-222. *Limnology Oceanography* 56(2):486–494.

Dugan, H.A., Gleeson, T., Lamoureux, S.F., Novakowski, K., 2012 Tracing groundwater discharge in a high Arctic lake using radon-222. *Environ Earth Science* 66(5):1385–1392.

Dulaiova, H., Burnett, W.C., Wattayakorn, G., Sojisuporn, P. 2006. Are groundwater inputs into river-dominated areas important? The Chao Phraya River—Gulf of Thailand. *Limnology Oceanography* 51(5):2232–2247.

Dulaiova, H., Bonneea, M.E., Henderson, P.B., Charette, M.A., 2008. Chemical and physical sources of radon variation in a subterranean estuary – Implications for radon groundwater end-member activities in submarine groundwater discharge studies. *Marine Chemistry*, 110: 120-127.

Emad H., Nuttle, W.K., Rivera-M, V.H., Gautam, S., Wang J., Meselhe, E., Twilley, R.R., 2007. Assessing Effects of Data Limitations on Salinity Forecasting in Barataria Basin, Louisiana, with a Bayesian Analysis. *Journal of Coastal Research*, 23-3:749-763.

Freeze, R.A., Witherspoon, P.A., 1967. Theoretical Analysis of Regional Groundwater Flow. 2. Effect of Water-Table Configuration and Subsurface Permeability Variation. *Water Resources Research*, 3-2.

Grubb, H.F., 1998. Summary of hydrology of the regional aquifer systems, Gulf Coastal Plain, south-central United States. *Geological Survey U.S.*, 1416-A.

Goñi, M and Gardner, I., 2003. Seasonal dynamics in dissolved organic carbon concentrations in a coastal water-table aquifer at the forest-marsh interface. *Aquatic geochemistry*, 9(3): 209-232.

Hwang, D., Lee, Y., Kim, G., 2005. Large submarine groundwater discharge and benthic eutrophication in Bangdu Bay on volcanic Jeju Island, Korea. Limnology and Oceanography, 50(5): 1393-1403.

Hoefs, S., 1996. Stable isotopes. *Springer Verlag*.

Hosman, R.L., 1972. Ground-water resources of the Norco area, Louisiana. *Department of conservation, Louisiana Geological Survey, and Louisiana Department of Public Works Water Resources Bulletin* 18, 61.

Inoue, M., Park, D., Justic, D., 2008. A high-resolution integrated hydrology-hydrodynamic model of the Barataria Basin system. *Environmental Modeling and Software*, 23(9): 1122-1132.

Inniss, L.V., 2002. Scientific and management perspectives in wetland groundwater hydrology. Ph.D. dissertation, Louisiana State University.

Kolb, C.R., and Van Lopik, J., 1958. Geology of the Mississippi River Deltaic Plain, Southeastern Louisiana. *U.S. Army Waterways Experiment Station, Tech Report* 3-482.

Kolker S. A., Jaye E. C., Karen H. J., Mead A. A., Lorna V. I., 2013. Pathway and processes associated with the transport of groundwater in deltaic systems. *Journal of Hydrology* 498:319-334.

Krest J.M., and Moore, W.S., 1999. ^{226}Ra and ^{228}Ra in the mixing zones of the Mississippi and Atchafalaya Rivers: indicators of groundwater input. *Marine Chemistry*, 64-3, 129-152.

Krest, J.M., Harvey, J.W., 2000. Using natural distributions of short-lived radium isotopes to quantify groundwater discharge and recharge. *Limnology and Oceanography*, 48(1): 290-298.

Lambert, M., and Burnett, W., 2003. Submarine groundwater discharge estimates at a Florida coastal site based on continuous radon measurements. *Biogeochemistry*, 66(1): 55-73.

Laroche, J., Nuzzi, R., Waters, R., Wyman, K., Falkowski, P., Wallace, D., 1997. Brown Tide blooms in Long Island’s coastal waters linked to interannual variability in groundwater flow. *Global change biology*, 3(5): 397-410.

Lee, J., and Kim, G., 2006. A simple and rapid method for analyzing radon in coastal and ground waters using a radon-in-air monitor. *Journal of environmental radioactivity*, 89(3): 219-228.

Martens, C.S., Kipput, G.W., Klump, J.V., 1980. Sediment-water chemical exchange in the coastal zone traced by in situ Radon-222 flux measurements. *Science* 208: 285-288.

Martin, J., Cable, J., Smith, C., Roy, M., Cherrier, J., 2007. Magnitudes of submarine groundwater discharge from marine and terrestrial sources: Indian River Lagoon, Florida. *Water Resources Research*: W05440.

McCoy, C., Corbett, D., Mckee, Brent., 2007. An evaluation of submarine groundwater discharge along the continental shelf of Louisiana using a multiple tracer approach. Journal or geophysical research, 112(c3)

McCoy, C., Richard, V., Richard, N.P., Susan, L., Brent, L., John, L., George, V., Erik, S., Denise, S., 2011. Radon as an indicator of limited cross-shelf missing of submarine groundwater discharge along an open ocean neach in the South Atlantic Bight during observed hypoxia. *Continental shelf Research,* 31, 12:1306-1317.

McKee, B.A., Aller, R.C., Allison, M.A., Bianchi, T.S., Kineke, G.C., 2004. Transport and transformation of dissolved and particulate materials on continental margins influenced by major rivers: benthic boundary layer and seabed processes. *Continental Shelf Research*, 24: 899-926.

Michalopoulos, P., and Aller, C., 1995. Rapid clay mineral formation of Amazon delta sediments: Reverse weathering and oceanic elemental cycles. Science, 124.

Milliman, and Mead, R.H., 1983. World-wide delivery of sediment to the oceans. *Journal of Geology*, 91: 1-21.

Moore, W.W., 1996. Large groundwater inputs to coastal waters revealed by ^{226}Ra enrichments. *Nature*, 380, 612-614.

Moore, W. S., 1999. The subterranean estuary: A reaction zone of ground water and sea water. *Marine Chemistry*, 65(1-2): 111-125.

Moore, W. S., and Krest J., 2004. Distribution of ^{223}Ra and ^{224}Ra in the plumes of the Mississippi and Atchafalaya Rivers and the Gulf of Mexico. *Marine Chemistry* 86:105-119.

Moore, W.S., 2010. The effect of submarine groundwater discharge on the ocean. *Annual Review of Marine Science*, 2: 59-88.

Nazaroff, W., and Nero, A., 1988. Radon its decay products in indoor air. John Wiley and Sons Inc.,New York, NY.

Peterson, R.N., Santos, I.R., Burnett, W.C., 2010 Groundwater dis- charge to tidal rivers based on Rn-222 measurements and a dual- assumption approach. *Estuarine, Coast Shelf Science* 86(2):165–178.

Reed et al., 1995. Status and Trends of Hydrologic Modification, Reduction in Sediment Availability, and Habitat Loss/Modification in the Barataria-Terrebonne Estuarine System, Barataria-Terrebonne National Estuary Program, Thibodaux, LA.

Robert, H.H., 1997. Dynamic changes of the holocene Mississippi River delta plain: The delta cycle. *Journal of Coastal Research*, 13(3): 605-627.

Rozanski, K., Araguas, L., Gonfiantini, R., 1993. Isotopic Patterns in Modern Global Precipitation. Climate change in continental isotopic records.

Santos, I.R., Burnett, W., Chanton, J., 2008. Nutrient biogeochemistry in a Gulf of Mexico subterranean estuary and groundwater-derived fluxes to the coastal ocean. *Limnology and oceanography*, 53(2): 705-718.

Santos, I.R., Dimova, N., Peterson, R.N., Mwashote, B., Chanton, J.P., Burnett, W.C. 2009. Extended time series measurements of sub- marine groundwater discharge tracers (^{222}Rn and CH4) at a coastal site in Florida. *Marine Chemistry* 113(1–2):137–147.

Sargent, B. P., 2011. Water use in Louisiana, 2010. *Louisiana Department of Transporttaion and Development Water Resources Special Report* 17, 35.

Schulz, H.D., and Zabel, M., 2006. Marine Geochemistry. *Springer.*

Smith G. C., Jaye E. C., Jonathan B. M., Moutusi. R., 2008. Evaluating the source and seasonality of submarine groundwater discharge using a radon-222 water transport model. *Earth and Planetary Science Letters* 273:312-322.

Solis, R.S., and Powell, G.L., 1999. Hydrography, mixing characteristics, and residence times of Gulf of Mexico estuaries. In: Bianchi, T.S., Pennock, J.R., Twilley, R.R. (Eds.), Biogeochemistry of Gulf of Mexico Estuaries, *Willey, New York*, pp. 29-61.

Stone, G.W., Grymes iii, J.M., Dingler, J.R., Pepper, D.A., 1997. Overview and Significance of Hurricanes on the Louisiana Coast, U.S.A. *Journal of Coastal Research*, 13-3: 656-669.

Sutula, M., Bianchi, T., Mckee, B., 2004. Effect of seasonal sediment storage in the lower Mississippi River on the flux of reactive particulate phosphorus to the Gulf of Mexico. *Limnology and oceanography*, 49(6): 2223-2235.

Taniguchi, M., Ishitobi, T., J. Chen., S.-I. Onodera., K. Miyaoka., W.C. Burnett., R. Peterson., D. Liu., and Y. Fukushima., 2008. Submarine groundwater discharge from the Yellow River Delta to the Bohai Sea, China. *Journal of Geophysical Research*, 113: C06025.

Trefry, J.H., Nelsen, T.A., Trogine, R.P., Eadie, B.J., 1994. Transport of particulate Organic Carbon by the Mississippi River and Its Fate in the Gulf of Mexico. *Estuaries*, 17-4: 839-849.

Tomaszewski, D.J., 2003. Groundwater resources along the lower Mississippi River Southeastern Louisiana. *Louisiana Department of Transportation and Development Water Resource Technical Report,* 69, 23.

Top, Z., Brand, L., Corbett, R., Burnett, W., Chanton, J., 2001. Helium and Radon as Tracers of Groundwater Input into Florida Bay. *Coastal research*, 17(4):859-868

USGS Groundwater Atlas of the United States: Arkansas, Louisiana, Mississippi HA 730-F, 1990.

Valiela, I., Teal, J., Volkman, S., Shafer, D., Carpenter, E., 1978. Nutrient and particulate fluxes in a salt marsh ecosystem: Tidal exchanges and inputs by precipitation and groundwater. *Limnology and oceanography*, 23(4): 798-812.

Valiela, I., Foremna, K., LaMontagne, M., Hersh, D., Costa, J., Peckol, P., Anderson, B., Avanzon, C., Babione, M., Sham, c., Brawley, J., Lajtha, K., 1992. Couplings of watersheds and coastal waters: Sources and consequences of nutrient enrichment in Waquoit Bay, Massachusetts. *Estuaries and coasts*, 15(4): 443-457.

Valiela, I., and Cole, M., 2002. Comparative Evidence that Salt Marshes and Mangroves May Protect Seagrass Meadows from Land-derived Nitrogen Loads. *Ecosystems*, 5(1): 92-102.

Weigel, V. F., 1987. Radon. Chemiker Zeitung 102, 287.

Weiss, J.S., 1992. Geohydrologic units of the coastal lowlands aquifer system, south-central United States. *USGS Professional Paper 1416-C,* Reston, Virginia: USGS.

White, V.E., and Prakken, L.B., 2015. Water Resources of St. Charles Parish, Louisiana. *USGS fact sheet* http://dx.doi.org/10.3133/fs20143118.

Wysocki, L.A., Bianchi, T., Powell, R., Reuss, N., 2006. Spatial variability in the coupling of organic carbon, nutrients, and phytoplankton pigments in surface waters and sediments of the Mississippi River plume. Estuarine, coastal and shelf science, 69: 47-63.

Zekster, I.S., and Loaiciga, H.A., 1993. Groundwater fluxes in the global hydrologic cycle: Past, present, and future. *Journal of Hydrology*, 144: 405-427.